Kentucky Geological Survey
James C. Cobb, State Geologist and Director
University of Kentucky, Lexington

A Ground Magnetic Survey of Kimberlite Intrusives in Elliott County, Kentucky

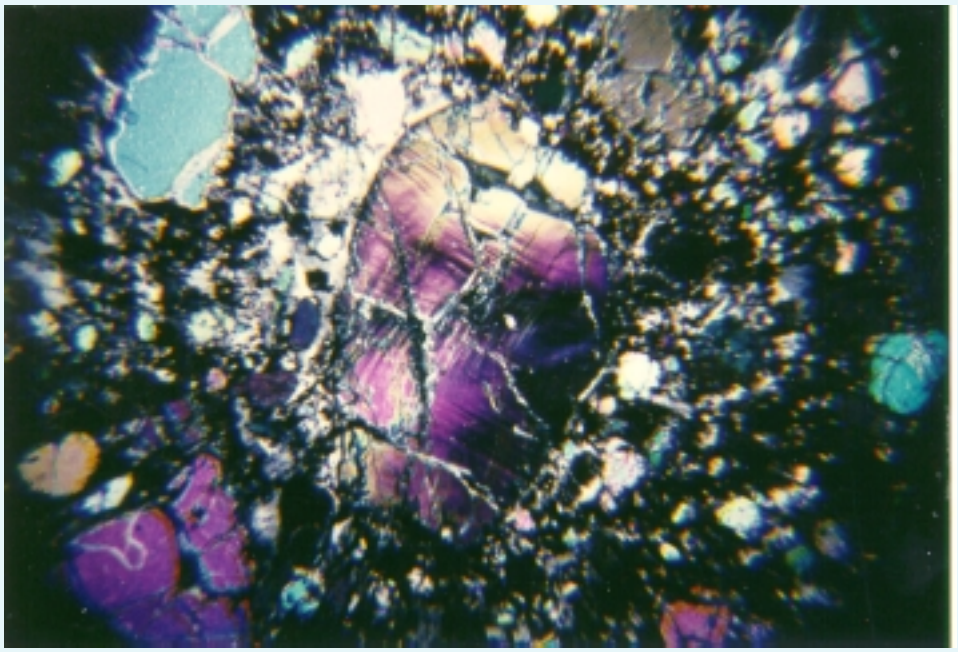

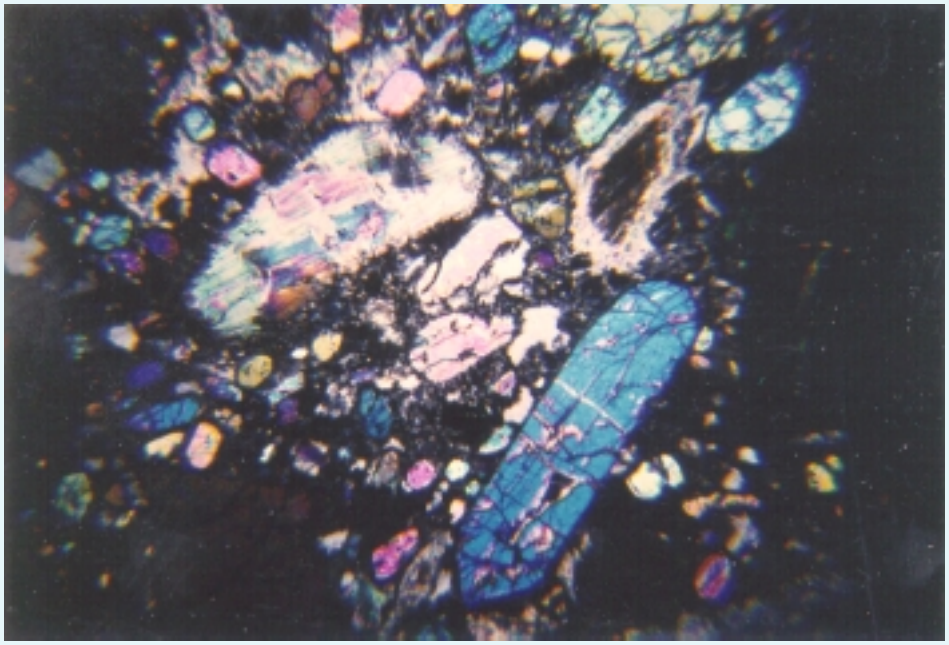

John D. Calandra

Thesis Series 2

Series XII, 2000

Kentucky Geological Survey
James C. Cobb, State Geologist and Director
University of Kentucky, Lexington

A Ground Magnetic Survey of Kimberlite Intrusives in Elliott County, Kentucky

John D. Calandra

On the cover: Photomicrographs of olivine phenocrysts: (top) a stressed first-generation olivine phenocryst and (bottom) a late-stage olivine phenocryst.

Thesis Series 2

Series XII, 2000

UNIVERSITY OF KENTUCKY

Charles T. Wethington Jr., President
Fitzgerald Bramwell, Vice President for Research and Graduate Studies
Jack Supplee, Director, Administrative Affairs, Research and Graduate Studies

KENTUCKY GEOLOGICAL SURVEY ADVISORY BOARD

Henry M. Morgan, Chair, Utica
Ron D. Gilkerson, Vice Chair, Lexington
William W. Bowdy, Fort Thomas
Steve Cawood, Frankfort
Hugh B. Gabbard, Winchester
Kenneth Gibson, Madisonville
Mark E. Gormley, Versailles
Rosanne Kruzich, Louisville
W.A. Mossbarger, Lexington
Jacqueline Swigart, Louisville
John F. Tate, Bonnyman
David A. Zegeer, Lexington
Ralph N. Thomas, Emeritus Member, Owensboro
George H. Warren Jr., Emeritus Member, Owensboro

KENTUCKY GEOLOGICAL SURVEY

James C. Cobb, State Geologist and Director
John D. Kiefer, Assistant State Geologist
Donald C. Haney, State Geologist Emeritus

ADMINISTRATIVE DIVISION

Personnel and Finance Section:
James L. Hamilton, Administrative Staff Officer II
Jackie Silvers, Administrative Staff Officer I

Clerical Section:
Amanda Long, Staff Support Associate II
Jennifer Talley, Staff Support Associate I
Juanita G. Smith, Office Assistant, Henderson office

Office of Communications and Technology Transfer:
Carol L. Ruthven, Manager
Margaret Luther Smath, Geologic Editor III
Douglas W. Reynolds Jr., Geologist II, Communications Coordinator for the Kentucky Board of Registration for Professional Geologists
Terry D. Hounshell, Chief Cartographic Illustrator
Michael L. Murphy, Graphic Design Technician
Collie Rulo, Graphic Design Technician
Shirley Davis Dawson, Staff Support Associate II

Well Sample and Core Library:
Patrick J. Gooding, Manager
Robert R. Daniel, Senior Laboratory Technician

Office of Geologic Information:
Bart Davidson, Manager
Richard A. Smath, Geologist II, Earth Science Information Center Coordinator
William A. Briscoe III, Publication Sales Supervisor
Roger S. Banks, Account Clerk I
Luanne Davis, Staff Support Associate II
Theola L. Evans, Staff Support Associate I

Computer and Laboratory Services Section:
Steven Cordiviola, Head
Richard E. Sergeant, Geologist IV
Joseph B. Dixon, Information Technology Manager I
James M. McElhone, Information Systems Technical Support Specialist IV
Henry E. Francis, Scientist II
Karen Cisler, Scientist I
Jason S. Backus, Research Analyst
Steven R. Mock, Research Analyst
Tracy Sizemore, Research Analyst

GEOLOGICAL DIVISION

Coal and Minerals Section:
Donald R. Chesnut Jr., Head
Garland R. Dever Jr., Geologist V
Cortland F. Eble, Geologist V
Gerald A. Weisenfluh, Geologist V
David A. Williams, Geologist V, Henderson office
Stephen F. Greb, Geologist IV
William M. Andrews Jr., Geologist II
Ernest E. Thacker, Geologist I

Geologic Mapping and Hydrocarbon Resources Section:
James A. Drahovzal, Head
Warren H. Anderson, Geologist IV
David C. Harris, Geologist IV
Brandon C. Nuttall, Geologist IV
Thomas N. Sparks, Geologist III
Douglas C. Curl, Geologist II
John B. Hickman, Geologist II
Steven L. Martin, Geologist II
Jason A. Patton, Geologist II
Mark F. Thompson, Geologist I
Anna E. Watson, Geologist I
Xin-Yue Yang, Post-Doctoral Scholar
R. Shawn Duncan, Geological Technician
Michael P. Solis, Geological Technician

Water Resources Section:
James S. Dinger, Head
Daniel I. Carey, Hydrologist V
R. Stephen Fisher, Hydrogeologist V
David R. Wunsch, Hydrogeologist V
James C. Currens, Hydrogeologist IV
John F. Stickney, Hydrogeologist IV
Alex W. Fogle, Hydrologist III
Robert E. Andrews, Hydrogeologist II
E. Glynn Beck, Hydrogeologist II, Henderson office
Dennis H. Cumbie, Hydrogeologist II
Carlos M. Galcerán Jr., Hydrogeologist II
C. Douglas R. Graham, Hydrogeologist II
Randall L. Paylor, Hydrogeologist II
Ron Counts, Geological Technician, Henderson office
Gregory L. Secrist, Geological Technician
Steven E. Webb, Geological Technician

Geologic Hazards:
Edward W. Woolery, Geologist IV

Contents

FIGURES

FIGURES

(Continued)

PLATES

TABLES

Mission Statement

The Kentucky Geological Survey at the University of Kentucky is a State-mandated organization whose mission is the collection, preservation, and dissemination of information about mineral and water resources and the geology of the Commonwealth. KGS has conducted research on the geology and mineral resources of Kentucky for more than 150 years, and has developed extensive public databases for oil and natural gas, coal, water, and industrial minerals that are used by thousands of citizens each year. The Survey's efforts have resulted in topographic and geologic map coverage for Kentucky that has not been matched by any other state in the Nation.

One of the major goals of the Kentucky Geological Survey is to make the results of basic and applied research easily accessible to the public. This is accomplished through the publication of both technical and nontechnical reports and maps, as well as providing information through open-file reports and public databases.

Reprinted with permission from the author.
For further information contact:
Manager, Office of Communications and Technology Transfer
Kentucky Geological Survey
228 Mining and Mineral Resources Building
University of Kentucky
Lexington, KY 40506-0107

ISSN 0075-5621

A Ground Magnetic Survey of Kimberlite Intrusives in Elliott County, Kentucky

John D. Calandra

Abstract

A ground magnetic survey was performed over an area underlain by kimberlite in the southwestern corner of the Willard 7.5' quadrangle in northeastern Kentucky. The survey area covered approximately 2 square miles (3.2 square km) in which earlier geological mapping had indicated three separate intrusive loci.

A total magnetic intensity contour map was prepared from which nine anomalies were chosen for computer modeling. The largest anomalies are over 1,500 gammas in magnitude, and anomaly widths range from approximately 30 meters to over 300 meters.

Two of the anomalies occur in areas where no kimberlite has previously been reported. Four dikes were modeled which had lengths of 195 to 240 meters and widths of 9 to 29 meters. Modeling indicated that all of the dikes terminated at depths of 180 to 182 meters below the surface. The strikes of the dikes ranged from N8°W to N45°E.

Five pipes having a variety of sizes and shapes were modeled. The largest pipe had an oval surface outline with an average diameter of 106 meters. The smallest pipe was 8 meters in diameter and circular in outline. Four of the five pipes modeled terminated at depths of 180 to 182 meters, and the other at a depth of 136 meters.

Measurements from a massive kimberlite and a kimberlite breccia yielded ratios of remanent magnetic intensity to magnetic susceptibility of 8:1, indicating the dominance of remanence in producing the anomalies. Remanent magnetization directions were N21°W, 21°N (down) for the kimberlite breccia, and N60°E, 14°N (down) for the massive kimberlite.

Acknowledgments

The author would first like to thank Dr. Dewey Sanderson of the Geology Department at Marshall University for being his thesis advisor. The magnetometer used to collect the field data was lent to the author by Dr. Halan Noltimier of Ohio State University, who was also a constant source of support. John LaBrecque of Columbia University's Lamont-Doherty Geophysical Observatory supplied a copy of the magnetics modeling program used in this thesis. Many useful suggestions were given to the author by David Campbell of the United States Geological Survey in Denver, Colorado.

Other members of Marshall's Geology Department which the author wishes to thank include Dr. Richard Bonnett, who helped obtain a grant for the author from the Marshall Foundation. Dr. Protip Ghosh assisted in coordinating the laboratory work for the petrography section, and Dr. Ron Martino took the photographs of the minerals displayed in the petrography section. All of these professors reviewed the first draft of this thesis, and the author is grateful for their time and comments.

The author would also like to thank Rod Mills and Alan Yost of Marshall University's Computer Department. Other help for the data-processing portion of this thesis came from Dr. Gary Anderson (Department of Chemistry) and Dr. Warren Dumke (Department of Physics).

Lastly, a very special thanks goes out to Lloyd and Plina Griffith of Elliott County, Kentucky. Mr. and Mrs. Griffith let the author stay in the guest room of their house while he was collecting field data. At a time when funds were low, their help enabled him to gather the bulk of the field data used in this thesis.

INTRODUCTION

Purpose

The major goal of this study is to interpret the subsurface geometry of kimberlite intrusives in Elliott County, Kentucky. This was accomplished by computer modeling of data from a ground magnetic survey.

Location

The study area is located in Elliott County, Kentucky, between 38°07'10" to 38°8'17" north latitude and 82°57'32" to 83°00'15" west longitude. Most of the survey was conducted between Ison and Hamilton Creeks in the southwest corner of the Willard 7.5' quadrangle (see Figure 1; see Figure 15 for the position of the study area in Elliott County). Collection of regional data extended the survey area into the adjoining corners of the Mazie, Isonville, and Bruin quadrangles.

Geologic Setting

The ultramafic rock type in this study has been interchangeably referred to as peridotite or kimberlite since its discovery. Kimberlite is grouped under the class of peridotites. Bolivar (1972) determined the rock type to be kimberlite based on textural and mineralogical associations. Without further discussion, the rock type will be referred to as kimberlite throughout this report.

Outcrops of kimberlite occur in the valleys of two small north-flowing tributaries of Ison Creek (see Figure 1). The exposures are small and do not form obvious features in the topography. The two outcrops are approximately 1,500 meters apart along an eastward trend. The outcrop to the west is approximately 230 meters southwest of a house presently owned by Willis Ison located on the south side of Route 409. The outcrop has the appearance of three boulders jutting out of the east bank of the stream valley. This kimberlite is a kimberlite breccia. The most noticeable feature of this kimberlite is the great abundance of xenoliths.

The other outcrop is approximately 530 meters southeast of a house presently owned by Lloyd Griffith, which is also on the south side of Route 409. The kimberlite here is a massive kimberlite. It is dark green to black and almost free of xenoliths. This outcrop displayed an irregular set of joints, which were absent at the kimberlite breccia outcrop.

Previous studies (Diller, 1887; Koenig, 1956; Bolivar, 1972) located two other outcrops in the valley of Hamilton Creek. An attempt was made to locate these outcrops since they supposedly fall within the study area. One outcrop was described to occur south of the divide between Ison and Hamilton Creeks. This outcrop is presumed to have been destroyed by the effects of mining and weathering. Mounds of "yellow ground" (oxidized and hydrated kimberlite), kimberlite float, and massive kimberlite boulders were found in this area (see Figure 1). The second outcrop is supposedly in the valley of Hamilton Creek. No evidence of this outcrop was found by geophysical or visual inspection.

One other small exposure of kimberlite is shown on the Willard 7.5' geologic quadrangle (Brown, 1977). The location of this outcrop is approximately 270 meters southeast of the kimberlite breccia outcrop. Visual evidence of this exposure was not found, but geophysical data indicated kimberlite was present.

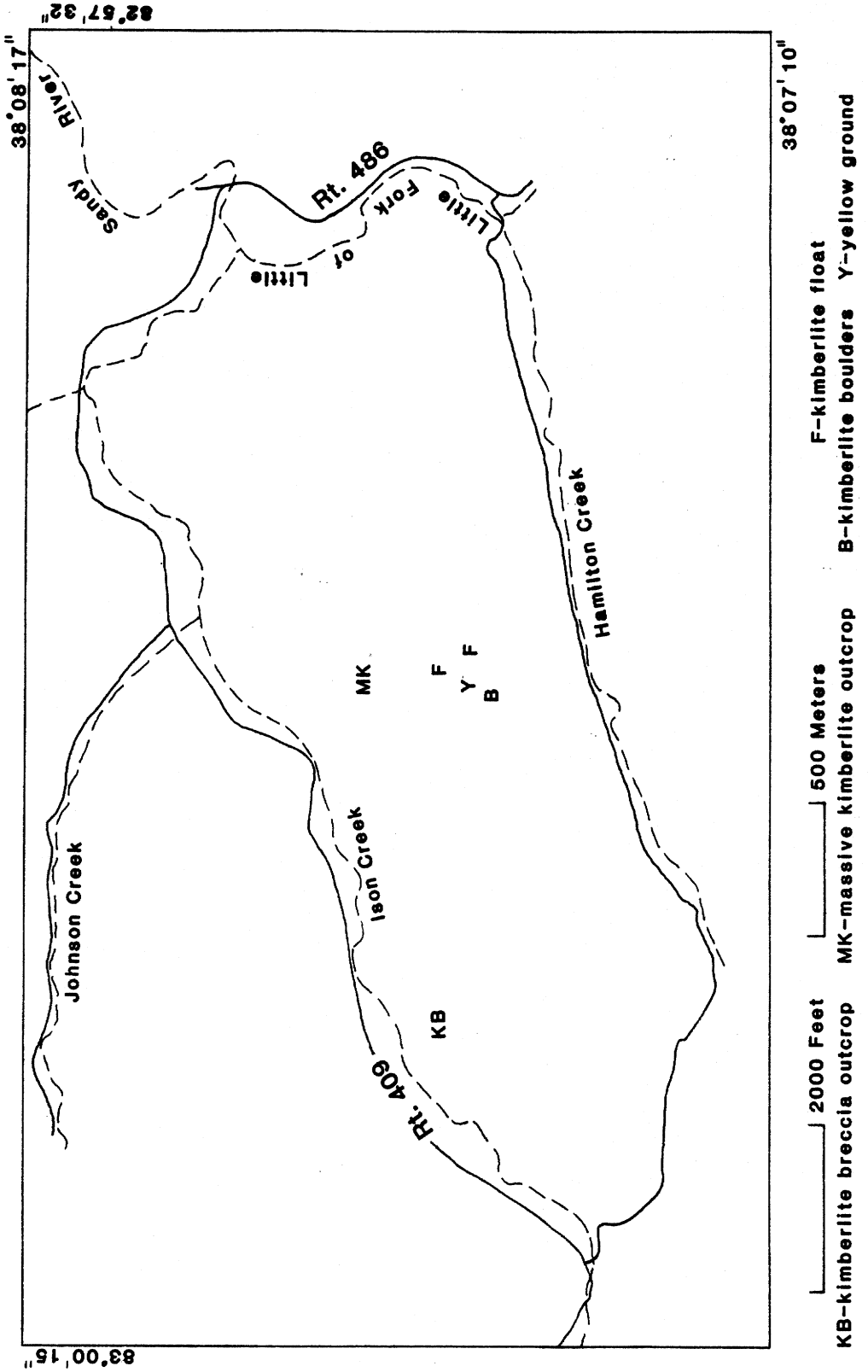

Figure 1. Generalized map of study area.

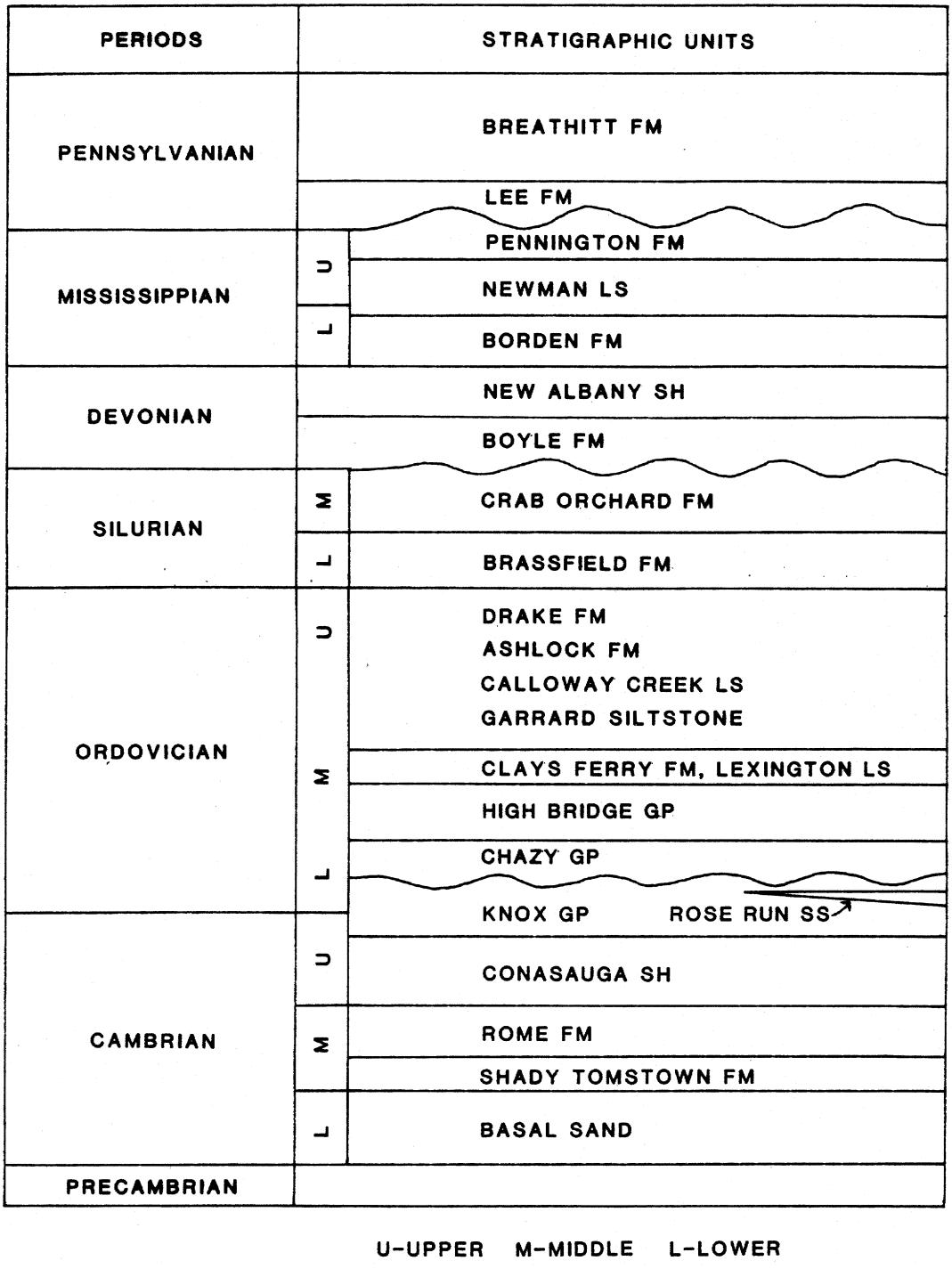

Figure 2. Generalized stratigraphic column for eastern Kentucky (modified from Ammerman and Keller, 1979).

The kimberlites intrude the Lower Pennsylvanian Breathitt Formation. The Breathitt Formation is a coal-bearing sequence and in the study area it consists mostly of sandstone with lesser amounts of siltstone, shale, coal, underclay, and siderite (Brown, 1977). No evidence of doming, extensive fracturing, or contact metamorphism of these strata from intrusion has ever been observed (Diller, 1887; Koenig, 1956).

Pennsylvanian and Mississippian rocks are exposed throughout Elliott County. Minor flexuring of these strata has caused local changes (even reversals) in the direction of dip, which is generally 2 to 3° to the southeast (Diller, 1887). A generalized stratigraphic column for eastern Kentucky is shown in Figure 2.

The study area is located near the western edge of the Cumberland Plateau and has elevations that range from approximately 680 to 1,080 feet (207 to 328 meters). This region is maturely dissected and has a dendritic drainage pattern (McFarlan, 1943).

Approximately a mile to the south of the intrusives is the Little Sandy Fault, a high-angle normal fault trending east–west for almost 12 miles (Koenig, 1956). This fault is considered a surface expression of renewed movement along older faults in the basement (Ammerman and Keller, 1979; Dever, 1980). The intrusives bear no connection to this fault other than being related to the same zones of weakness in the basement (Diller, 1887; Koenig, 1956; Harvey, 1980).

Although occurrences of kimberlite and related rocks are rare, they are widely distributed throughout the United States (Meyer, 1976). The ultrabasic rocks of the Midcontinent and Appalachian regions form an arcuate zone of intrusions which is concave to the northwest (see Koenig, 1956, p. 19). Inclusion of the ultrabasic bodies within this belt is merely based on location, and carries no implications about age, mode of emplacement, or petrography (Koenig, 1956).

Previous Work

Professor A.R. Crandall of the Kentucky Geological Survey is credited for discovering the kimberlites in 1884. He was cited in *Science* (1885) for describing small volcanic dikes intruding the Carboniferous strata of Elliott County.

After a preliminary microscopic investigation, J.S. Diller (1886) of the U.S. Geological Survey outlined the petrology and mineralogy of the kimberlites. He briefly discussed possible origins and decided it was probably a deep-seated eruptive rock type.

Similarities between the Elliott County kimberlites and the South African kimberlites were noted by H.C. Lewis (1886). He mentioned both rocks contained the same accessory minerals and intruded Carboniferous shales. Lewis used the term kimberlite in 1887 to describe the diamond-bearing dikes and diatremes near Kimberley, South Africa.

Both Crandall and Diller followed up their initial accounts with more extensive reports. Most notable of these reports was U.S. Geological Survey Bulletin 38, written by Diller in 1887. This report thoroughly described the mineralogy, petrology, and geochemistry of the Elliott County kimberlites.

Crandall's last report on the kimberlites was published in Kentucky Geological Survey Bulletin 10 (1910). He revised some of his earlier notes about the intrusives and their relation to surrounding geology. Shortly before this report was published, an extensive, but unsuccessful, diamond mining operation was conducted in the study area by A.Q. Miller from Minneapolis, Minnesota. Crandall described this mining effort and new subsurface information on the intrusives yielded by the mining.

The first geophysical information on the kimberlites was published by Warren (1956) from a dip needle survey he did in the vicinity of the intrusives. Warren (1956, p. 17) reported the southeasternmost intrusive had "… an anomaly of about 3.5 degrees deflection with a profile width of about 400 feet," and that three other traverses made across roads supposedly crossing the intrusives did not produce anomalies.

Koenig (1956) studied the composition, texture, and structure of the Elliott County intrusives and the mica peridotites of western Kentucky. Koenig (1956) noted the similarities and differences between

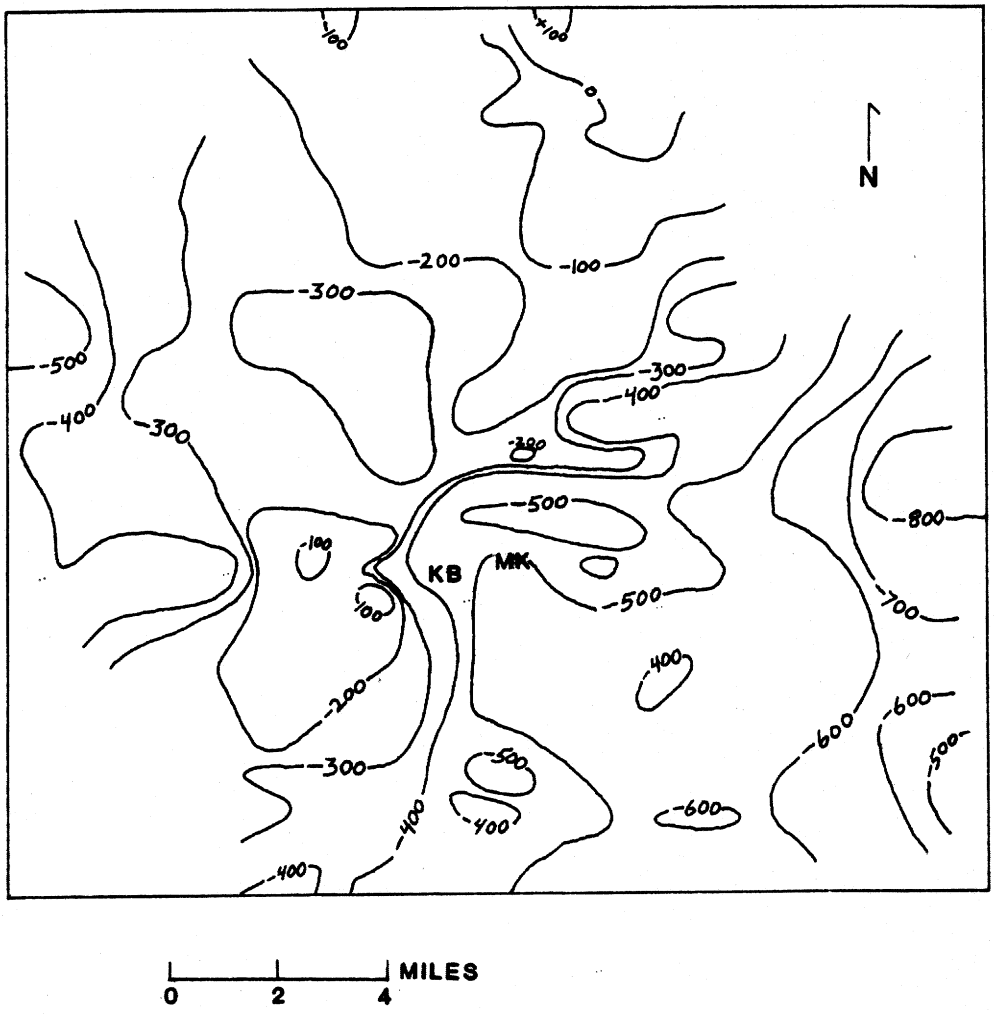

Figure 3. Residual aeromagnetic intensity map in gammas (modified from Harvey, 1980).

the two suites of rocks, and compared them with other ultrabasic intrusions in the Midcontinent and Appalachian regions.

Radiometric dating of alkalic intrusive rocks in the central and eastern United States was carried out by Zartman and others (1967). Their K-Ar and Rb-Sr methods yielded an age of 269 million years for the Elliott County kimberlites.

Haupt (1967) wrote a master's thesis based on the Elliott County kimberlites. The major purpose of his thesis was to remap the intrusives on a scale of 1:6,250 using current topographic maps and aerial photographs. Haupt's map is similar to previous and current maps of the intrusives, with one exception. Haupt claimed not to have found any evidence of the northeasternmost extension shown on Diller's (1887) map of the intrusives, so it was not included. This northeastern extension was mapped by Brown (1977) and is shown on the Willard geologic quadrangle.

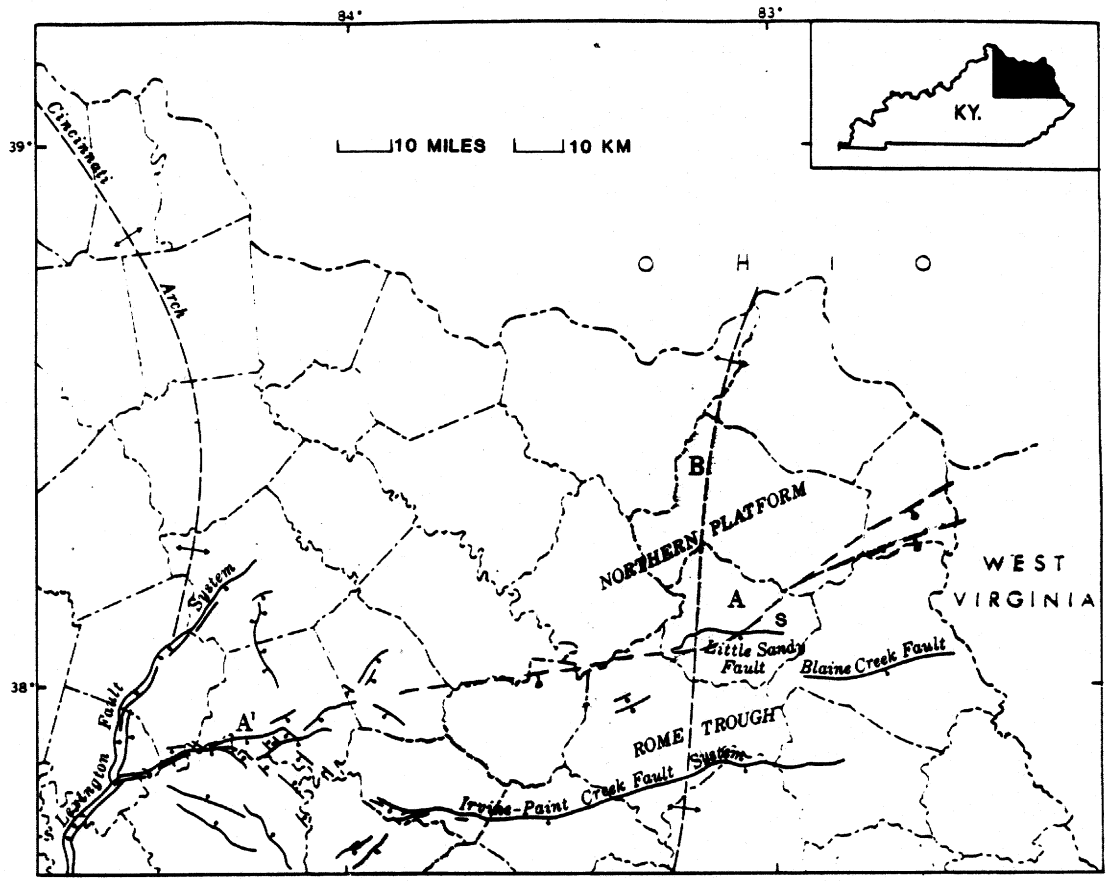

Figure 4. Map showing principal structural features of east-central and northeastern Kentucky (modified from Dever and others, 1977).

Hunt and Bolivar (1972) studied oxygen and carbon isotope ratios in the kimberlites. They concluded the carbonate material in the kimberlites was of primary igneous origin. Bolivar (1972) completed a master's thesis that focused on the geochemistry and mineralogy of the kimberlites. In 1977 Bolivar reported on the Rb-Sr systematics, uranium whole-rock analysis, and microprobe analysis of the kimberlites in his Ph.D. dissertation.

A revised edition of the Willard 7.5' geologic quadrangle was completed by Brown (1977). The intrusives were remapped using outcrops, yellow ground, and areas of soil containing pyrope, ilmenite, and foreign rock fragments. The ground magnetic survey performed for this thesis was based on the location of the three intrusive loci located in the southwest corner of this map.

Harvey (1980) conducted an aeromagnetic survey over the intrusives for her master's thesis. She also performed a paleomagnetic study on a suite of oriented samples from the kimberlite breccia outcrop. Harvey's residual magnetic field contour map is shown in Figure 3.

More detailed petrologic and mineralogic work has been done on the Elliott County kimberlites since 1980 (Garrison and Taylor, 1980; Schulze, 1981, 1982, 1984; Agee and others, 1982). Although the rocks have been extensively explored for diamonds (Crandall, 1910; Creason, 1950; Brown, 1977), there are no documented diamond finds on file with the Kentucky Geological Survey (Garland Dever, personal communication, 1984). The land on which the kimberlite lies is presently under lease, and the precious metal content of the intrusives is being investigated (Frank Ison, personal communication, 1984).

Paleozoic Tectonic History and Principal Structures

During Cambrian and Ordovician time, Kentucky was part of a relatively stable platform. There were transgressions and regressions, mostly due to minor isostatic adjustments. Throughout this period Kentucky received almost continuous deposition of carbonate and clastic sediments (Freeman, 1953).

Deep drilling indicates abrupt thickening of Cambrian–Ordovician units south of an east–west-trending structure. Further drilling and geophysical investigations have revealed the presence of an intracratonic graben extending from northern Pennsylvania into eastern Kentucky (Woodward, 1961). The Kentucky River Fault System is considered a surface extension of the basement faults on the northern side of this structure in eastern Kentucky (Rudman and others, 1964; Ammerman and Keller, 1979; Dever, 1980; Ettensohn, 1980). The kimberlites lie approximately 5 kilometers south of the trace of this fault system (see Figure 4).

This structure is named the Rome Trough (McGuire and Howell, 1963), and it is characterized by asymmetrical block faulting in the basement complex (Harris, 1975; Ammerman and Keller, 1979). Studies of depositional patterns indicate the period of greatest activity along the faults which created the trough was from Middle Cambrian to Early Ordovician time (Webb, 1969; Silberman, 1972; Harris, 1975).

The Waverly Arch extends from north-central Ohio into eastern Kentucky and also became active during this time. Woodward (1961, p. 1653) described the Arch as "… an axis of low and persistent relief (or one of resistance to subsidence) from the late Middle Cambrian through the Early Ordovician." Just before Middle Ordovician time the entire axis of the arch was sharply uplifted (Woodward, 1961). Woodward (1961) defined the position of its axis based on subsurface data provided by Cambrian–Ordovician strata. The axial trace of the arch crosses the Kentucky River Fault System approximately 20 kilometers southwest of the kimberlites (see Figure 4).

In Silurian time, the Cincinnati Arch became a barrier to deposition of clastic sediments across eastern Kentucky. The source area of the sediments was the central craton. The Arch is a major anticlinal structure trending north–south through central Kentucky, and was high enough to be a source area for Devonian deposition (Freeman, 1951).

Previously, Crandall (1910), Koenig (1956), Bolivar (1972), and Harvey (1980) have positioned the structural region of the kimberlites as being on the east limb of the Cincinnati Arch. Recent studies present stratigraphic evidence that the Waverly Arch affected depositional patterns in northeastern Kentucky well into Carboniferous time (Ettensohn and Peppers, 1979; Dever, 1980; Ettensohn, 1980; Sergeant and Haney, 1980). This evidence renders the earlier interpretation incorrect. It is appropriate to locate the kimberlites on the east flank of the Waverly Arch, approximately 17 kilometers east of its axis (see Figure 4).

Additional stratigraphic and structural evidence show that the Kentucky River Fault System was reactivated throughout the Paleozoic. This is an indication of recurrent movements along the basement faults of the Rome Trough (Haney and others, 1975; Haney, 1976; Horne and others, 1976; Dever and others, 1984).

Basement Complex

Literature concerning the basement complex places the study area within the southern extension of the Grenville Province (McLaughlin, 1954; Bass, 1960; Rudman and others, 1964; Ammerman and Keller,

1979). Although two interpretations regarding the position of the western boundary of the Grenville Front were found (see McLaughlin, 1954, and Bass, 1960), the study area lies well to the east of both extensions.

The sources cited above indicate the basement lithology of the Grenville Province is an unusual combination of igneous and metamorphic rocks. The igneous rocks range from granite to rhyolite, anorthosite, and basalt. Metamorphic rocks include amphibolites, metasediments, and granite gneiss. This information came from wells that penetrated the basement (Rudman and others, 1964).

Regional data from an aeromagnetic survey that included a part of eastern Kentucky yielded depth estimates to the basement of 7,500 to 11,500 feet (2.28 to 3.49 km; Johnson, 1960), and detected extremely large magnetic anomalies within the Appalachian Plateau of eastern Kentucky. Gravity data from the same area correlate with the latter findings (King and Zietz, 1960). The anomalies were interpreted as reflections of a large mafic mass in the basement complex of eastern Kentucky (Johnson, 1960; King and Zietz, 1960). Keller and others (1975) suggested that the feature could be an aborted rift system. They noted basalts and rhyolites were encountered in wells drilled to the basement in this area.

The above feature is known as the East Continent Gravity High (Ammerman and Keller, 1979). Gravity and magnetic maps show a right-lateral offset of the Gravity High along the Rome Trough for approximately 80 kilometers (see Figure 5). The Gravity High was interpreted by Lidiak and Zietz (1976) as the signature of the Grenville Front.

Lineament Survey

A three-part lineament survey was conducted to assess the relationship between the local and regional fracture patterns and orientation of the kimberlites. The survey included field mapping of joints, and then tracing of lineaments from air photos and LANDSAT imagery.

Field Study

Data on joints were collected at 25 sites throughout the study area. The sites included outcrops on hills, in streambeds, and roadcuts. A Brunton compass was used to measure strike and dip. At least one to three measurements were made on each set of surfaces showing a common trend at each site. Later, these readings were averaged to establish the orientation of each joint set at the site. The orientations of 75 joint sets were mapped.

Other observations were made to determine the degree of prominence of each joint set. These observations included the nature of the joint surface, density of spacing within 0.5 to 10.0 feet, persistence, regularity, bed thickness, and bed lithology.

The above criteria were used to place the joint sets into one of the following classes:

1. Primary joints: smooth-plane to smooth-curved surfaces, regular spacing within 0.5 to 10.0 feet, good persistence, good regularity.
2. Secondary joints: smooth-plane to smooth-curved surfaces, irregular spacing within 0.5 to 10.0 feet, good to moderate persistence and regularity.
3. Tertiary joints: smooth-curved to irregular surfaces, wide spacing in excess of 10.0 feet, moderate to poor persistence and regularity.

Although the above classes are to be regarded as generalizations (due to inconsistencies and poor exposures at some of the outcrops), they were useful in making certain inferences about the fracture pattern in the study area. The location, orientation, and degree of prominence of the joint sets are shown in Figure 6.

Bed thickness and lithology consisted mainly of massive crossbedded sandstone units, usually thicker than 10.0 feet, and laminated siltstones and shales less than 5.0 feet thick. A weak correlation was noticed between bed thickness, lithology, and joint spacing. In the massive sandstone units the joints were generally spaced farther apart than in the siltstones and shales.

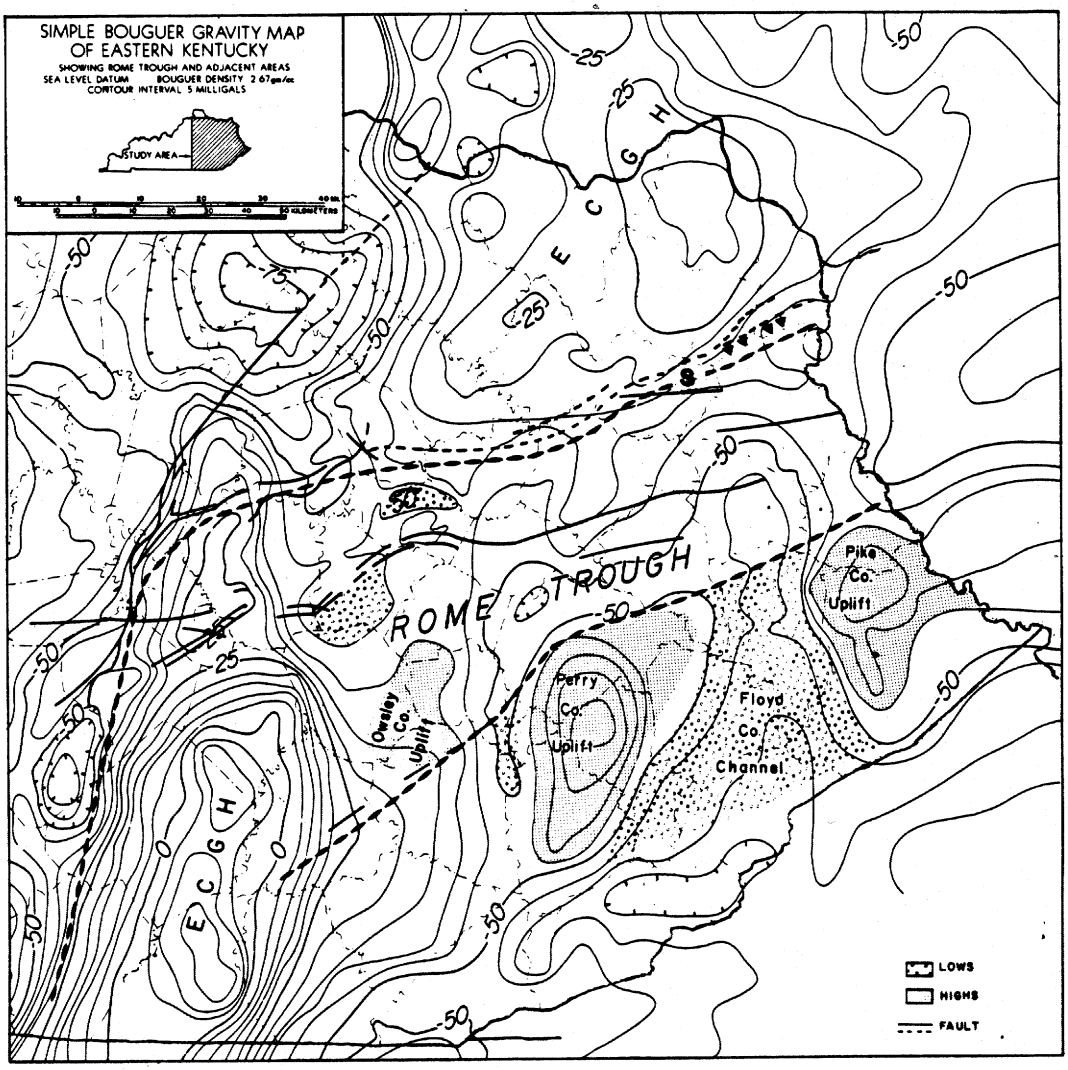

ECGH - East Continent gravity high
S - position of study area

Figure 5. Gravity map for eastern Kentucky (modified from Ammerman and Keller, 1979).

Figure 7 is a contour diagram of the face poles to the 75 joints plotted on Figure 6. The diagram reveals four dominant joint sets interpreted as two orthogonal sets. One set contains the strongest and weakest trends: the northeast and northwest trends, respectively. The second strongest trend, a bipolar NS-NNW trend, and a strong WNW trend, make up the other system. The dips of the joints are generally steeper than 70°.

Observations were also made on which joints terminated other joints. These data were compared with the degree of prominence and the four trends discussed above. The following generalities were noticed:

1. Considering the degree of prominence, the best developed joint set was the WNW set, followed by the NE, NW, and NS-NNW sets.
2. In the orthogonal sets, the NW set almost always terminated against the WNW set. The NS-NNW set terminated against the WNW set slightly more.

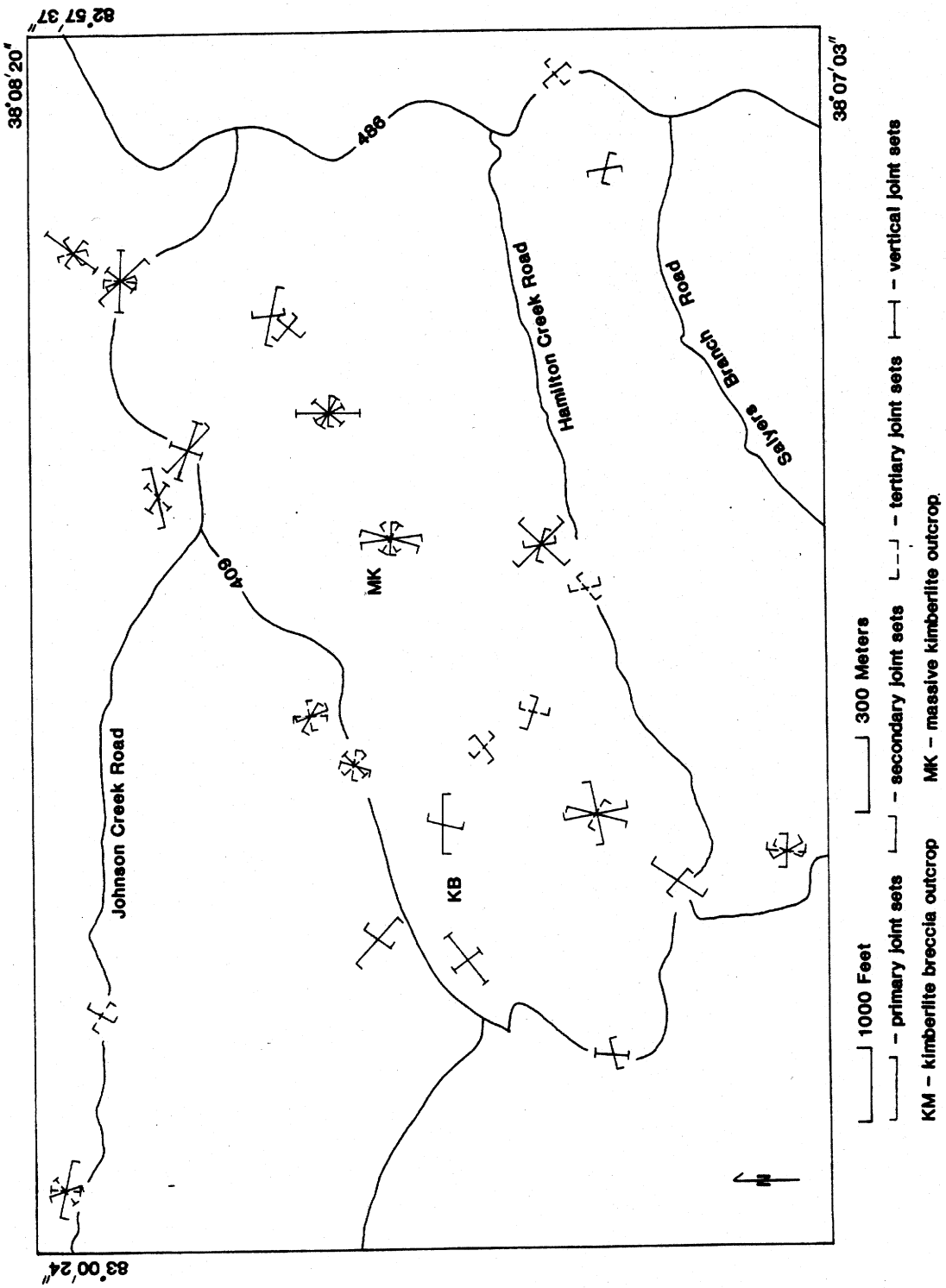

Figure 6. Field sites with joint orientations.

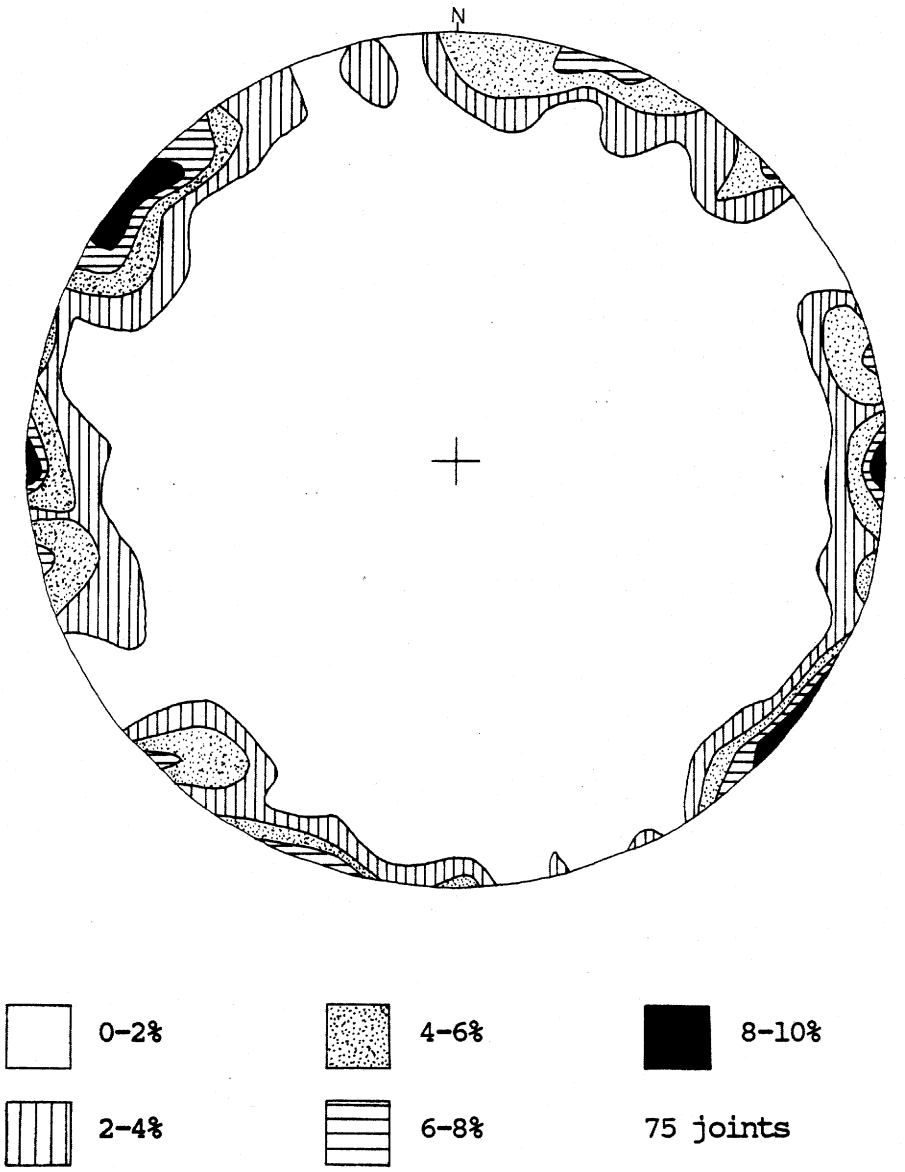

Figure 7. Contour diagram of equal area net showing the orientations of 75 joints in study area.

3. There were insufficient data to determine which orthogonal set terminated the joints of the other more often.

Air Photos

Lineaments were traced from a composite of four air photos (scale 1:26,000) obtained from GRW Aerial Surveys, Lexington, Kentucky. The limits of the area studied and the major structural features within it are shown in Figure 8. Figure 9 shows the location of the 167 lineaments found on the air photos.

An azimuth was recorded for each lineament on Figure 9. Rose and cartesian diagrams were constructed from these data to examine the air photo populations and trends (see Figure 10). Figure 10 clearly shows prominent north–south and east–west trends. The strong northeast trend found in the field study is still discernable but reduced in magnitude.

LANDSAT Imagery

Large-scale lineaments were mapped using two black and white 18.5 cm LANDSAT imagery photos (scale 1:1,000,000). The same methods were used to trace and examine lineament data as were employed for the air photos. The area covered by the LANDSAT imagery and the 112 lineaments found are shown in Figure 11.

Figure 12 shows the rose and cartesian diagrams constructed from the LANDSAT lineament data. Although directions with high percentages of lineaments are scattered, groups occur in north–northeast and west–northwest directions.

Results

The data presented for the three parts of this survey indicate that two orthogonal joint sets, approximately equal in prominence, exist in the study area. In general, the trends of these joint sets are north–south, east–west, northeast, and northwest.

In the field-study portion of this survey, the northeast trend was the strongest, but in the other parts of the survey, it was of lesser prominence. One possible explanation for this is that the air photo and LANDSAT imagery surveys reflect the regional fracture pattern better than the field study, which is more limited in extent. The dominance of the northeast trend observed in the field study may be due to a local variation in the regional pattern.

Discussion

The orientations of the joint sets defined in this survey compare well with the findings of other studies. Bonnett (1975) found very similar joint trends to those found in the field study portion of this survey in the Hurricane and Eighteenmile Creek watersheds northwest of Nitro, West Virginia. In the tri-state region of West Virginia, Kentucky, and Ohio, Sanderson and Duba (1975) identified four sets of vertical joints with orientations of north–south, northeast, east–west, and northwest. Werner (1981) studied the fracture patterns of Silurian and Mississippian rocks in Fleming and Rowan Counties, Kentucky. These two counties lie just to the west of Elliott County. Werner (1981, p. 87) concluded that "… the most prominent directions were found to be N10°E and N45°E (and ones perpendicular to these), and a direction of about N70–80°E is of lesser prominence."

The aforementioned authors offered slightly different views regarding the formation of the fracture sets. Werner (1981) hypothesized that the two sets he identified were caused by tectonic stresses originating from the Appalachian orogeny. Sanderson and Duba (1975) believed the northeast and northwest sets were related to the Appalachian orogeny, but felt the north–south and east–west sets were inherited from structures in the Precambrian basement complex.

This author agrees that the northeast and northwest sets were generated by the Appalachian orogeny. The theory proposed by Sanderson and Duba (1975) seems more appropriate for the north–south and east–west sets. This author believes block faulting in the Rome Trough was the major contributor to

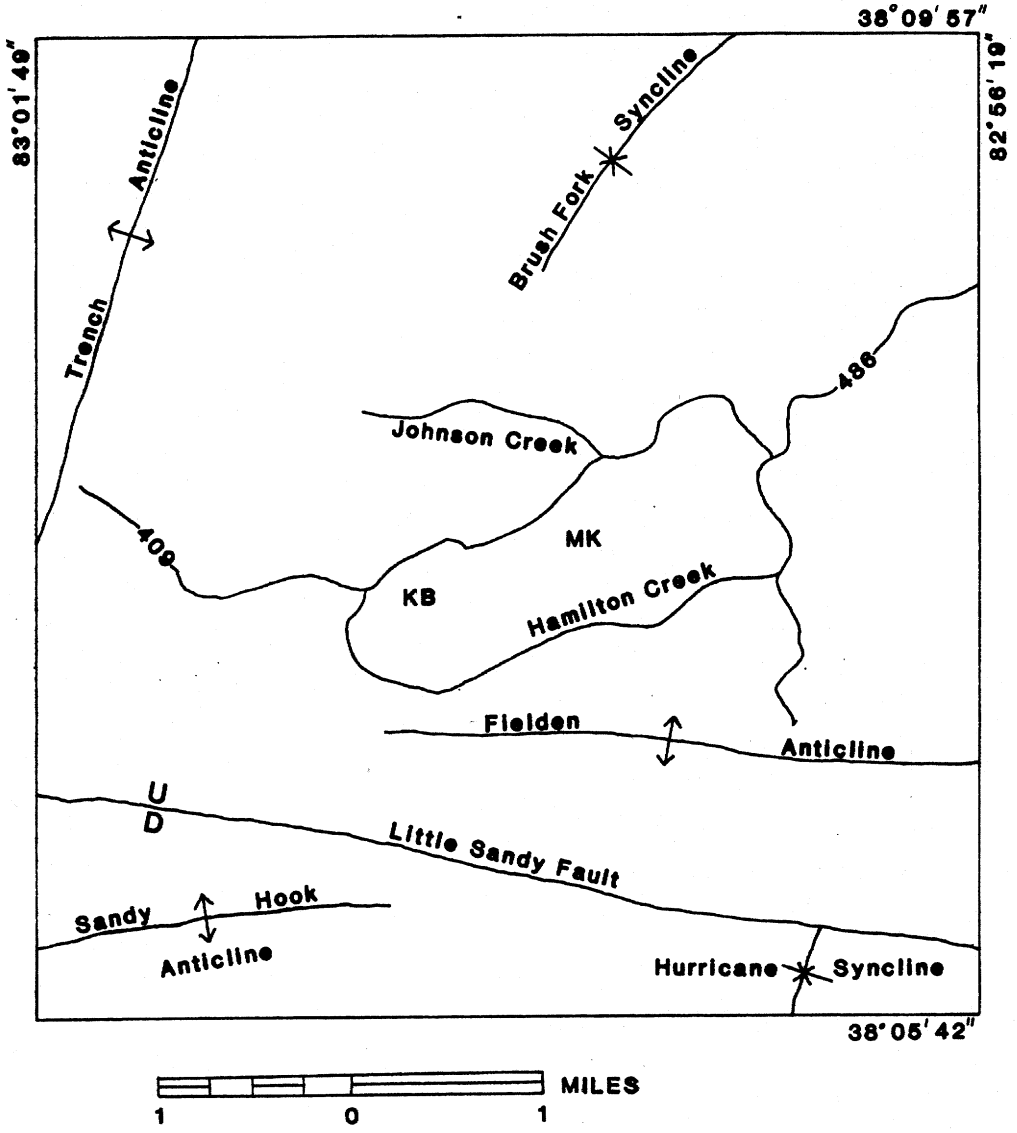

Figure 8. Limits of area studied in aerial photos, and major structural elements within area (modified from Robinson, Hudnall, and Richardson, 1950).

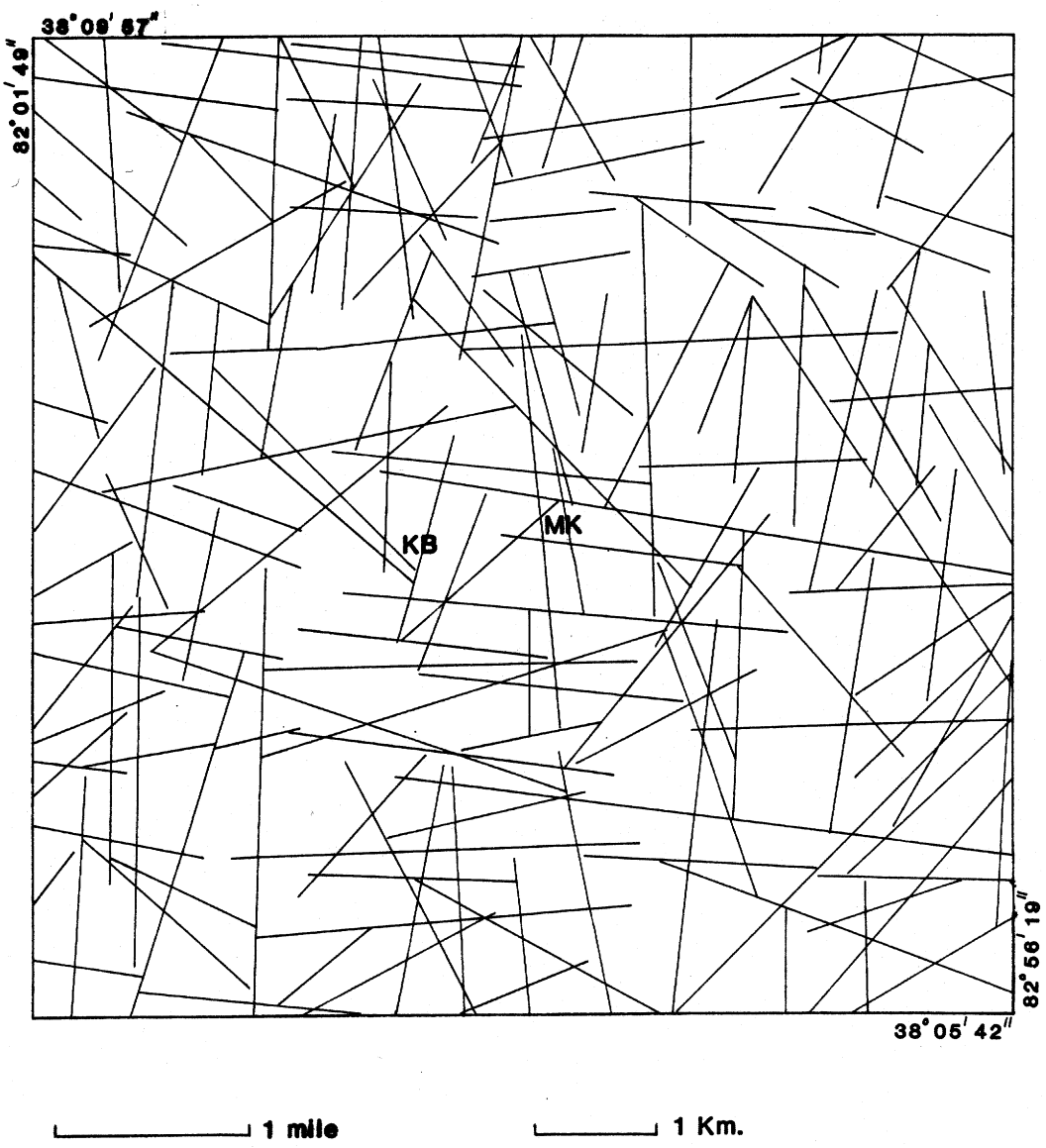

KB - kimberlite breccia outcrop
MK - massive kimberlite outcrop

Figure 9. Lineament traces from air photos.

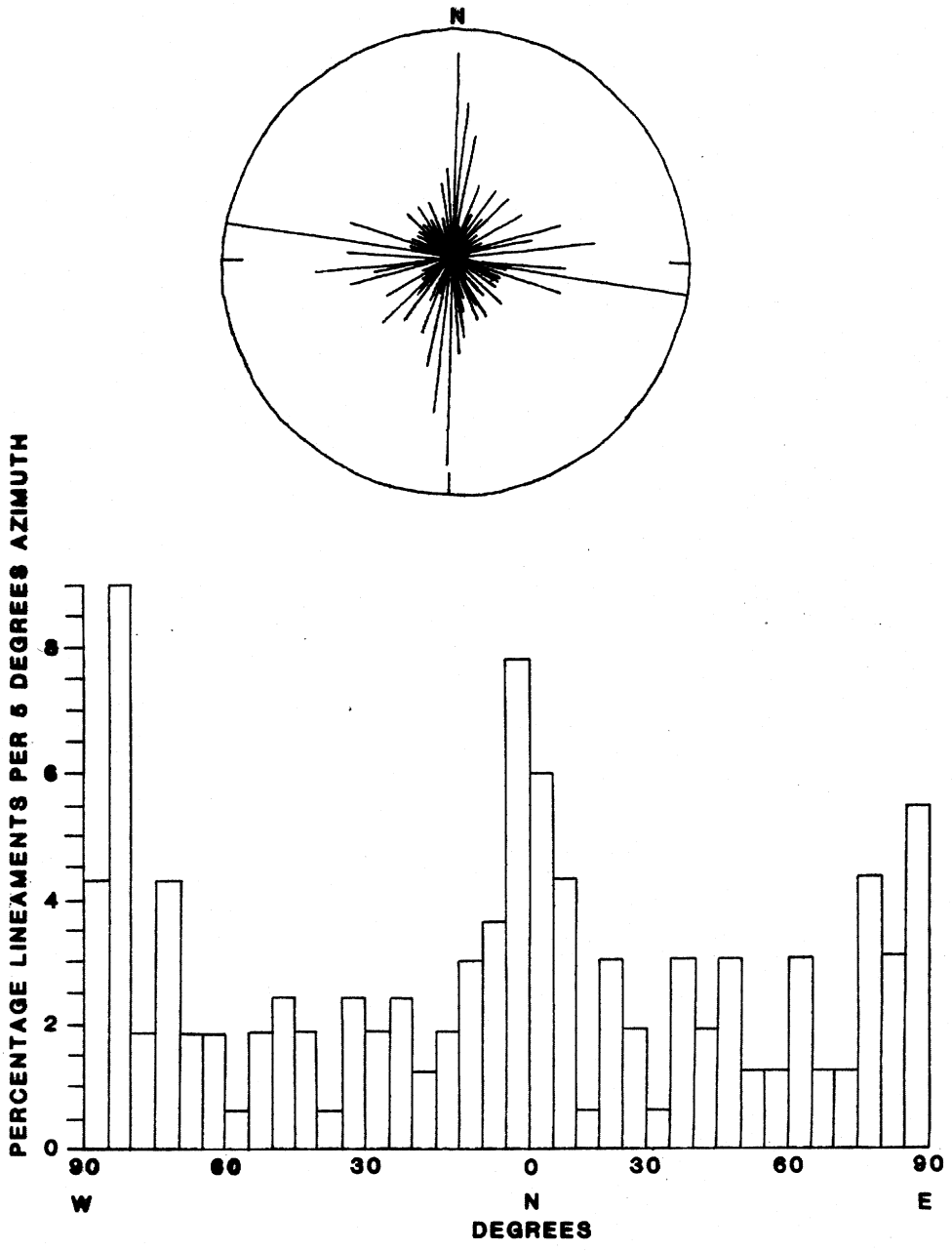

Lengths of lines in rose diagram (above) proportioned to percentages of the total lineament frequency (360°) lying within 5 degrees intervals.

Figure 10. Rose and cartesian diagrams for air photo lineament populations.

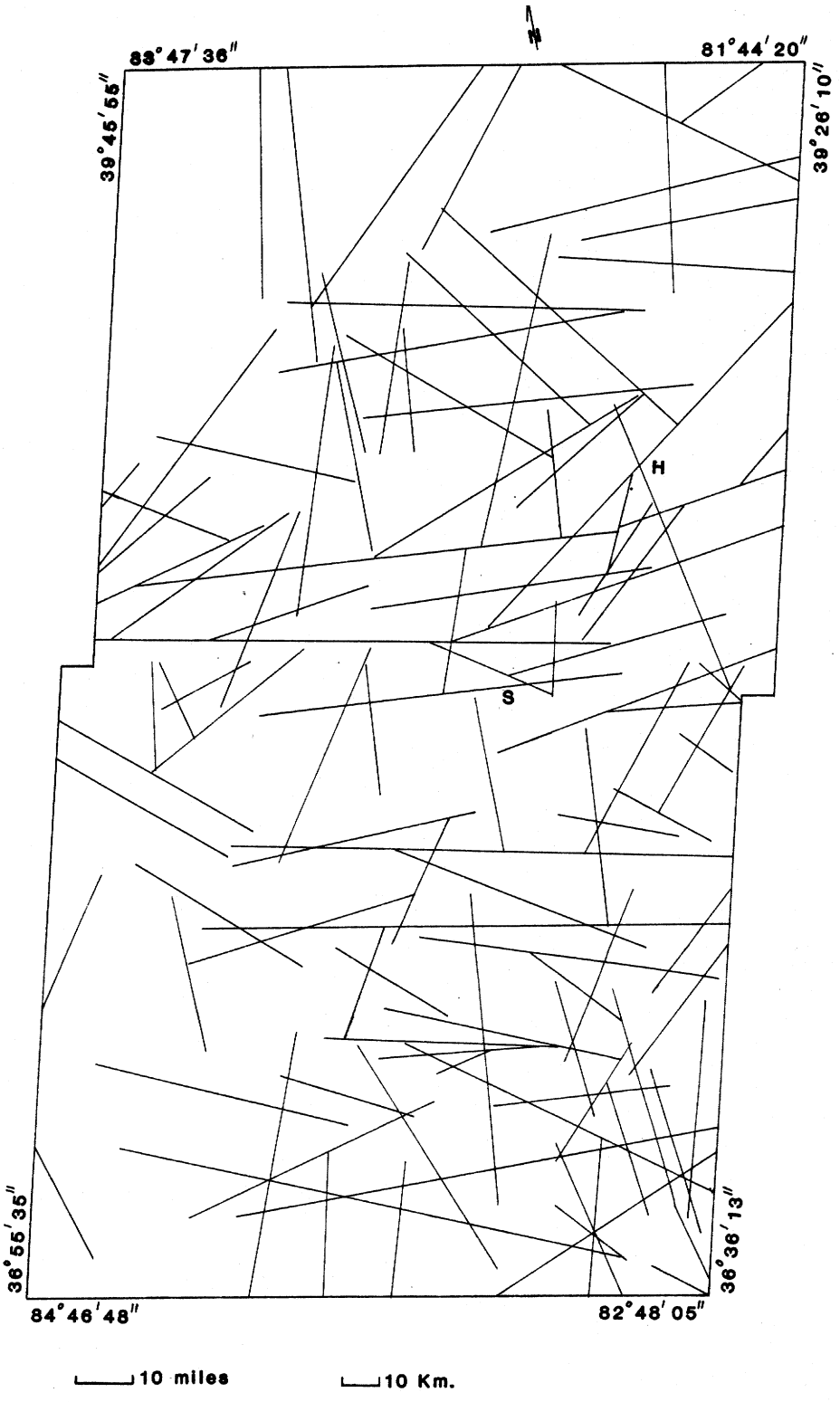

Figure 11. Lineament traces from satellite imagery.

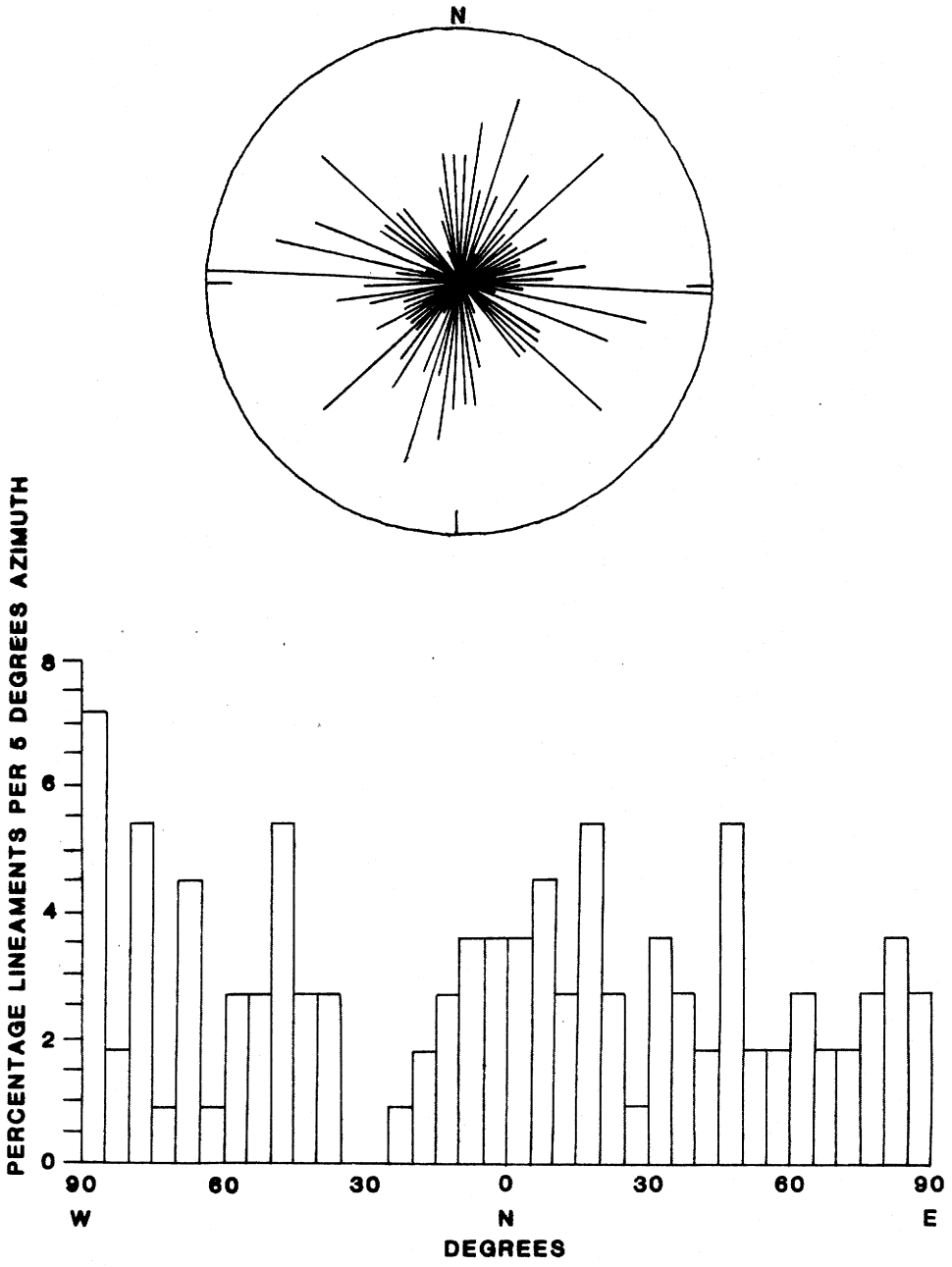

Lengths of lines in rose diagram (above) proportioned to percentages of the total lineament frequency (360°) lying within 5 degrees intervals.

Figure 12. Rose and cartesian diagrams for LANDSAT lineament populations.

the development of the east–west set, and that the north–south set was caused by fold fracturing in the sedimentary column parallel to the axis of the Waverly Arch.

The regional studies discussed above suggest that the two orthogonal joint sets identified in the study area are but a small part of a much larger system, extending at least from northeast Kentucky into western West Virginia.

PETROGRAPHY

The petrography of the Elliott County kimberlites is well documented (see Diller, 1886, 1887; Koenig, 1956; Haupt, 1967; Bolivar, 1972; Harvey, 1980). Field samples were collected from the two outcrops. Thin sections, polished sections, and slabs were prepared for point counting and petrographic analysis.

Hand samples from both localities are porphyritic and have a greenish-black matrix. The matrix is fine to medium grained. The massive kimberlite variety contains abundant olivine phenocrysts, and a lesser amount of ilmenite and garnet phenocrysts. The mineral composition of the massive kimberlite varies little throughout the exposure. Occasionally a xenolith of shale or limestone appears in the groundmass, seldom larger than a centimeter in size.

Much more variability exists in the kimberlite breccia. Xenoliths form up to 50 percent of the whole rock, and some have been reported as large as 45.0 cm in length (Boliver, 1972). The xenoliths are mostly shale, sandstone, limestone, and coal. Xenoliths of syenite and diorite were also observed. Olivine phenocrysts are abundant, but usually more altered than in the massive kimberlite. Ilmenite and garnet phenocrysts are not as plentiful as in the massive variety, but phlogopite phenocrysts were observed in the kimberlite breccia.

Point-Count Analysis

Three polished slabs were point counted megascopically for ilmenite and garnet phenocrysts, and xenoliths. Two slabs of kimberlite breccia were counted because of its variability. Six hundred fifty points were counted on an interval of 1 square millimeter on each kimberlite breccia slab. Representative sections with xenoliths no larger than 100 square centimeters were chosen for counting. One slab of massive kimberlite had 880 point counts on a 1 square millimeter grid. The results are listed in Table 1.

Table 1 shows that the massive kimberlite contains more ilmenite and garnet phenocrysts, but 10 percent fewer xenoliths than the kimberlite breccia. Bolivar (1972) reported the kimberlite breccia having as much as 50 percent xenoliths, with 17 percent being average. These estimates seem appropriate from visual inspection of the outcrop.

Table 1. Summary of slab point-count analysis.

	% ilmenite	*% garnet*	*% xenoliths*	*% other*
kimberlite breccia #1	1.0	0.3	12.0	86.7
kimberlite breccia #2	0.8	0.1	13.3	85.8
avg for breccias	0.9	0.2	12.6	86.3
massive kimberlite	10.2	3.3	2.6	83.9

Eight thin sections were prepared (three from each kimberlite breccia slab, and two from the massive kimberlite slab). One thousand points were counted on one thin section from each kimberlite slab. Care was taken to avoid large xenoliths when preparing the kimberlite breccia slabs so point counting would not be biased. The results of the thin-section point counts are shown in Table 2.

Table 2 presents some differences. The massive kimberlite contains a higher percentage of opaques. The opaques are primarily magnetite and ilmenite, the two minerals responsible for the magnetic properties of the kimberlites.

The xenolith content was higher in the kimberlite breccia, although the percentages encountered were lower than in the slabs. No garnet phenocrysts were counted in the massive variety, and no phlogopite from the breccia, but this is not considered representative because both were observed in hand samples.

Table 2. Summary for thin-section point counts.				
	kb 1	*kb 2*	*kb avg*	*mk*
olivine	39.0	38.2	38.6	39.7
serpentine	29.1	35.8	32.5	27.3
opaques	14.5	13.4	14.0	22.3
garnet	3.4	2.2	2.8	0.0
phlogopite	0.0	0.0	0.0	0.0
pyroxene	0.5	0.0	0.3	0.0
xenoliths	3.1	2.7	2.9	0.7
calcite	7.6	7.4	7.5	9.3
perovskite	1.3	1.0	1.2	0.7
chlorite	1.5	0.4	1.0	0.0

kb 1—kimberlite breccia thin section no. 1
kb 2—kimberlite breccia thin section no. 2
kb avg—average for kimberlite breccia thin sections
mk—massive kimberlite thin section

Percentages represent relative maximums.

Table 3. Summary for polished-section point counts.			
	% ilmenite	*% magnetite*	*% other*
kb	9.0	5.0	86.0
mk	13.0	7.0	80.0

kb—kimberlite breccia polished section
mk—massive kimberlite polished section

Four polished sections were prepared (two from each outcrop). Due to small grain size and the limits of magnification, only 100 points were counted on one polished section from each kimberlite type. This was done to establish the relative percentages of ilmenite and magnetite. The results are listed in Table 3.

The results in Table 3 are not statistically significant because the number of points counted is low, but the data do suggest two things. First, the amount of opaques may be greater in the massive kimberlite. Second, the amount of ilmenite may be greater than the amount of magnetite in both varieties. If these differences are real, important implications exist with regard to the magnetic character of the kimberlites. This will be discussed in the next section.

Petrographic Descriptions

Olivine. Olivine accounts for nearly 40 percent of the composition of both kimberlites. The olivine is mostly forsterite (Haupt, 1967; Bolivar, 1972). Most of the olivine observed in the slabs was 1.0–10.0 mm in length. One grain did measure 15.0 mm across.

Almost all of the olivine is altered to serpentine to some extent. Koenig (1956) described two distinct types of olivine phenocrysts from the kimberlite breccia. Bolivar (1972) claimed as many as five generations could be present, and discussed three in detail. The petrographic observations made in this study support Bolivar's (1972) conclusions.

Bolivar's (1972) first-generation olivine corresponds to the larger type described by Koenig. These phenocrysts are usually 5.0–10.0 mm wide, and are subrounded to rounded in shape or have irregular boundaries. Most of these phenocrysts have cracks healed by serpentine. Undulose extinction and stress-induced twinning were observed in a few of these phenocrysts (see Plate 1).

The larger phenocrysts were interpreted by Bolivar (1972) and Koenig (1956) as

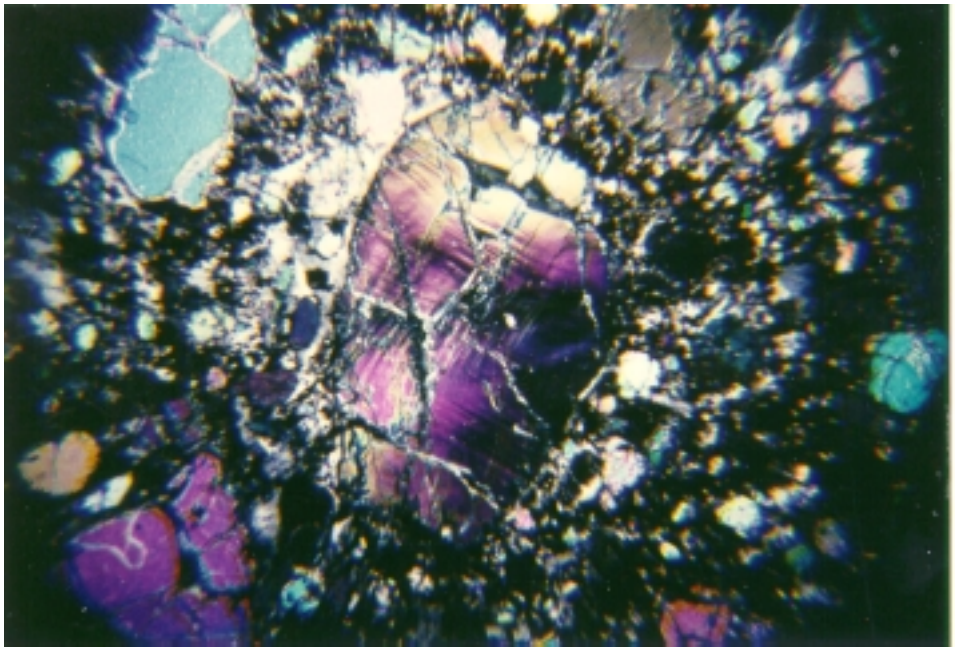

Plate 1. Stressed first-generation olivine phenocryst. Crossed Nicols, 20X.

xenocrysts from the upper mantle transported by a semi-consolidated mush magma. Evidence for this includes twinning, undulose extinction, and a high degree of serpentinization. Bolivar (1972) noted many of these phenocrysts attained heart or oval shapes from abrasion during transport.

The smaller phenocrysts described by Koenig (1956) were referred to as second-generation or late-stage olivines by Bolivar (1972). These phenocrysts are usually 3.0 mm across or less, and often display crystal outlines (see Plate 2). Serpentinization is not as extensive in these phenocrysts, and they are not as abundant as the larger ones.

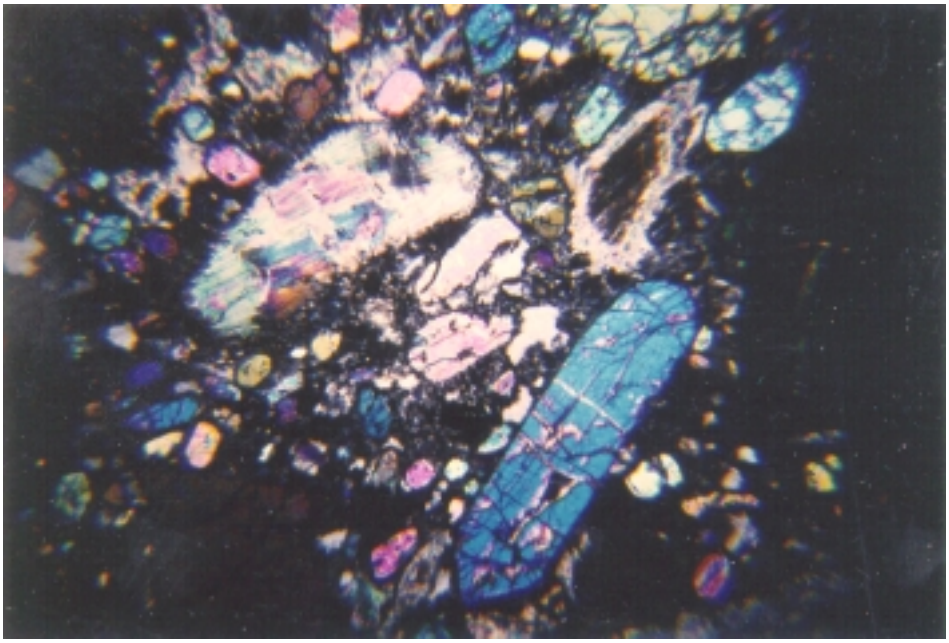

Plate 2. Late-stage olivine phenocryst (blue crystal, lower right). Crossed Nicols, 20X.

Bolivar (1972) described a third generation of olivine in the groundmass, smaller than 0.1 mm in size. He noted most of this olivine was altered to serpentine or chlorite. This third-generation olivine was not easily observed by the present author in thin section.

Ilmenite. Ilmenite occurs as phenocrysts with diameters up to 10.0 mm wide in the groundmass. The larger grains were easily observed in polished section. These grains had rounded irregular boundaries, were pitted, and had partings. In thin section some of the larger grains had alteration rims of perovskite (see Plate 3). A mantle origin for the ilmenite phenocrysts has been interpreted by several authors (Garrison and Taylor, 1980; Agee and others, 1982; Schulze, 1982, 1984).

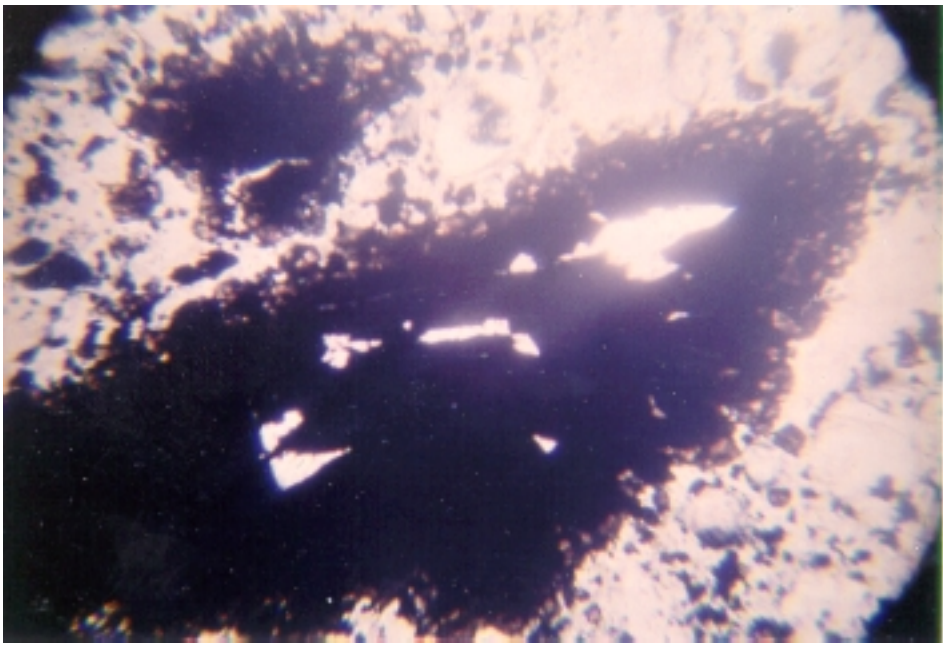

Plate 3. Ilmenite phenocryst with perovskite rim. Plane light, 80X.

Garnet. Garnet was found as red rounded phenocrysts with diameters up to 15.0 mm wide. The garnet is mostly pyrope (Bolivar, 1972). A characteristic feature of these kimberlites is the kelyphitic rims which surround many of the garnet phenocrysts. These alteration rims are a very fine-grained combination of magnetite, chlorite, biotite, and chromite

(Diller, 1887; Harvey, 1980; see Plate 4). Occasionally this alteration extends into fractures running through the phenocrysts. The rounding and kelyphitic rims are evidence that the garnet phenocrysts have undergone transport from the mantle (Koenig, 1956; Bolivar, 1972).

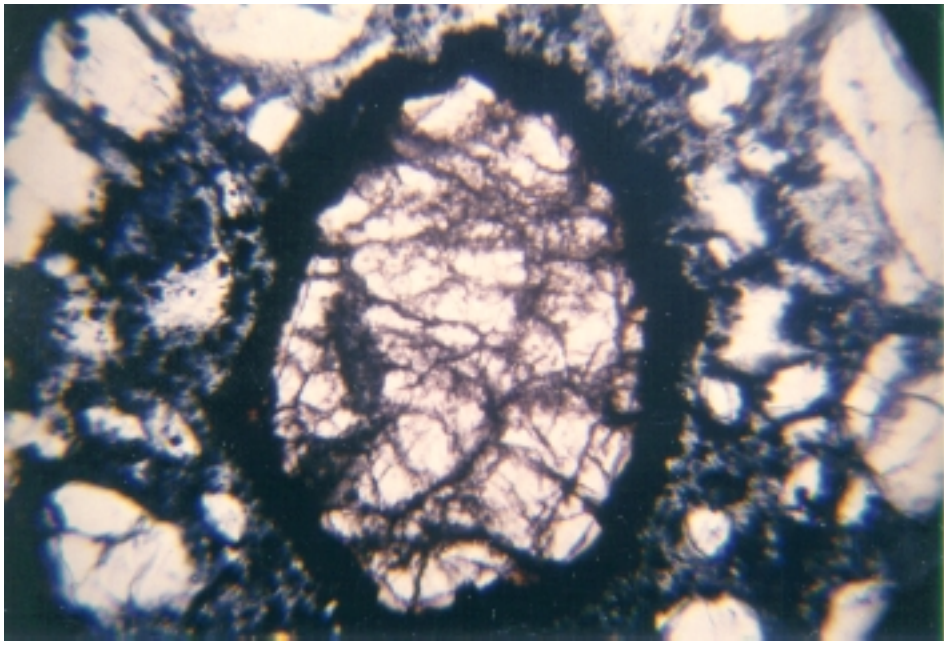

Plate 4. Garnet phenocryst with kelyphitic rim. Plane light, 80X.

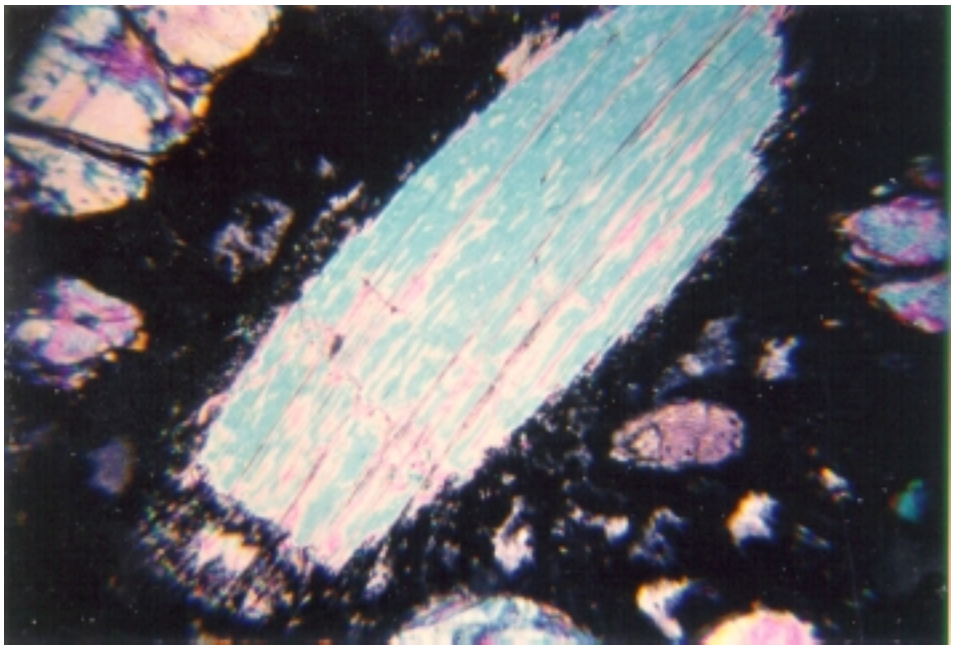

Plate 5. Phlogopite phenocryst. Crossed Nicols, 80X.

Phlogopite. Phlogopite was not encountered during point counting, but it was noticed in hand samples and thin sections. In hand samples it appears as brown flakes up to 15.0 mm across. Phlogopite was observed as oval-shaped grains with alteration rims of vermiculite and opaques in thin section (see Plate 5). Some of the phlogopite grains were bent and exhibited undulose extinction, indicating transport. Schulze (1981) suggested the phlogopite was mantle derived and provided evidence for primary kimberlitic liquids.

Biotite. A trace of biotite was noticed in the massive kimberlite. The largest phenocryst measured was 3.0 mm across. Zartman and others (1967) interpreted the biotite as xenocrysts from the mantle.

Pyroxene. Bolivar (1972) noted pyroxene is not characteristic of kimberlites and was probably brought up from the mantle. A trace of pyroxene was noted in a kimberlite-breccia thin section. The grains are subhedral, usually less than 0.1 mm wide, and have alteration rims (see Plate 6). The pyroxene is primarily enstatite (Schulze, 1984).

Xenoliths. Most of the xenoliths encountered in thin section were derived from sedimentary host rocks. A polished section contained a syenite xenolith, which was checked for magnetic minerals, but

none were found. The xenoliths did not exhibit much alteration, but some had small reaction rims (see Plate 7).

Crandall (1910) mentioned that mining operations uncovered a coal xenolith which showed little evidence of being heated. Sosman (1938) conducted heat experiments on similar inclusions from a dike in Fayette County, Pennsylvania. He concluded the final temperature of intrusion could not have been much more than 500°C (932°F).

The presence of unaltered xenoliths and fractured olivine phenocrysts led to the theory that the kimberlitic magma reached shallow depths in a semi-crystalline state (Diller, 1887; Sosman, 1938; Koenig, 1956; Bolivar, 1972; Harvey, 1980).

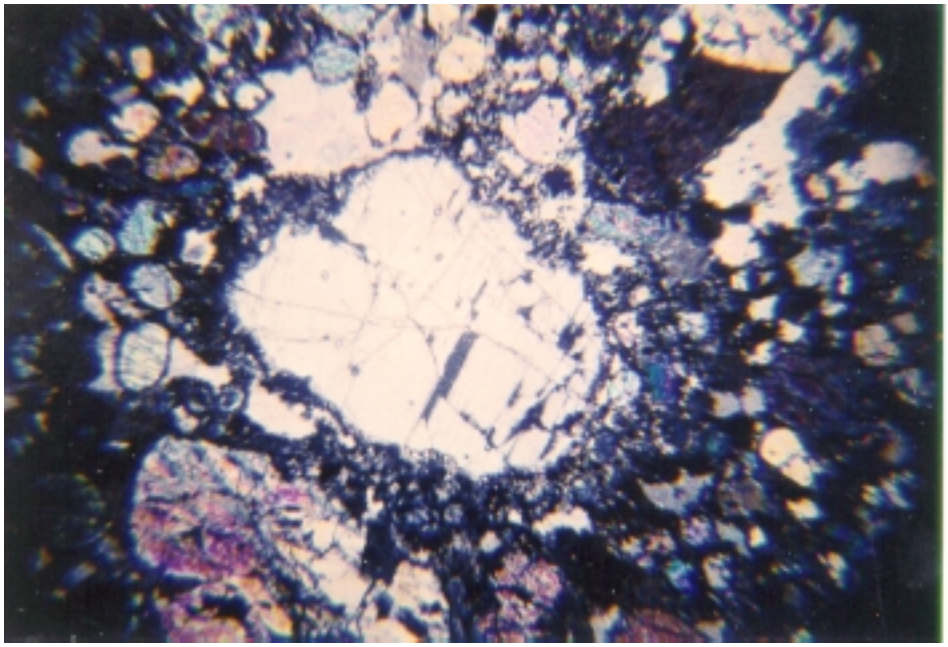

Plate 6. Pyroxene phenocryst. Crossed Nicols, 20X.

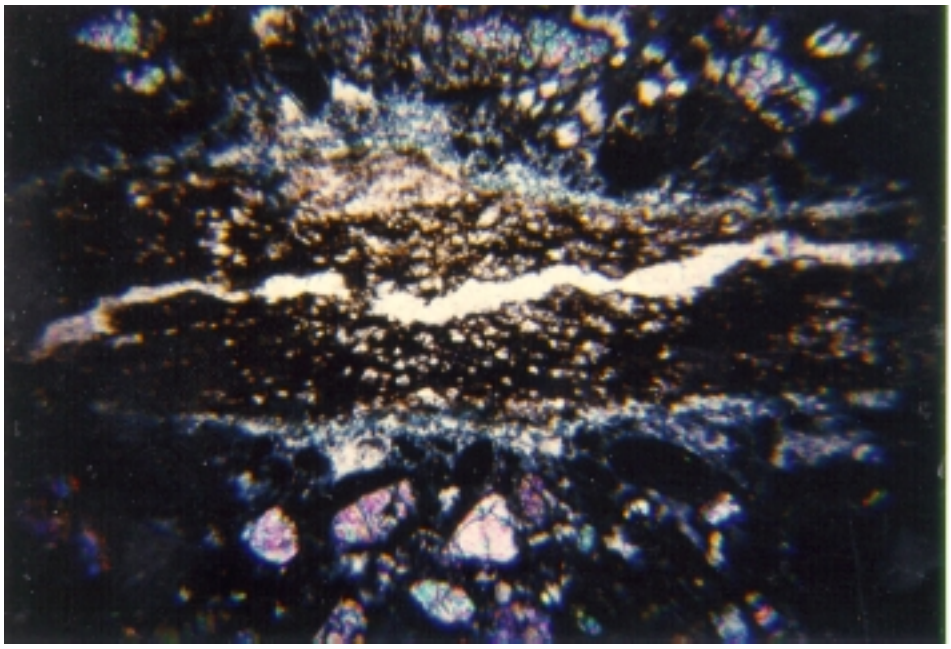

Plate 7. Shale xenolith (brown material). Crossed Nicols, 20X.

Groundmass. Serpentine and calcite dominate the mineralogy of the groundmass. Under crossed Nicols, these two minerals give the groundmass a light-gray to dark-green-gray appearance which is spotted with numerous opaque minerals and small brown grains of perovskite. The opaques are mostly magnetite, ilmenite, opaque perovskite grains, and a trace of chromite. The groundmass also contains trace amounts of apatite and chlorite.

Serpentine. Serpentine averages 30 percent of the composition of the samples studied. It has entered the kimberlites principally as an alteration product of olivine. Complete alteration of olivine phenocrysts has resulted in pseudomorphs of serpentine after olivine (see Plate 8). Under plane light the serpentine has a pale-green or yellow color. The serpentine is mostly antigorite (Kerr, 1959; Harvey, 1980).

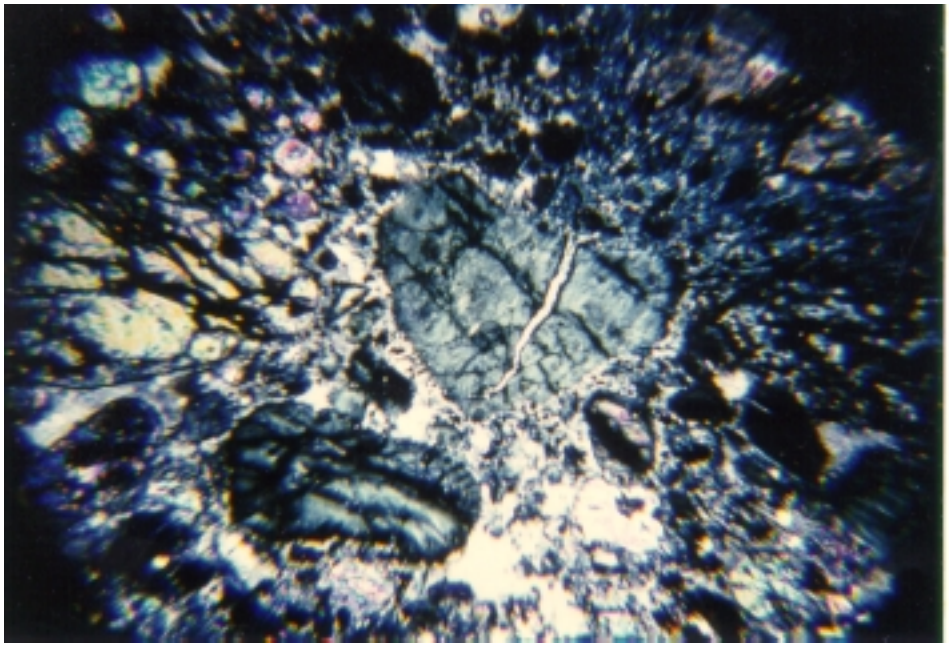

Plate 8. Serpentine pseudomorphs (green material) after olivine. Crossed Nicols, 20X.

Calcite. Calcite is abundant in the groundmass, and this is typical of kimberlites (Dawson, 1967; Bolivar, 1972). It is light to dark gray under crossed Nicols, and mostly occurs as anhedral grains filling interstices between phenocrysts and fractured grains. Hunt and Bolivar (1972) performed carbon-oxygen isotope analysis, and determined most of the calcite was of primary igneous origin. Minor amounts of calcite and dolomite occur in xenoliths, but this is clearly of sedimentary origin. The igneous calcite was interpreted as mantle-derived from primary kimberlitic fluids by Schulze (1981).

Other Minerals in the Groundmass. Magnetite, perovskite, and trace amounts of chromite and chlorite occur scattered throughout the groundmass. These minerals are also present in the alteration rims around phenocrysts. Magnetite is opaque in thin section but could occasionally be identified because of its distinct cubic outline. It was identified in polished section by its small grain size and higher reflectance than ilmenite. Magnetite averaged 6 percent of the total rock mass from polished-section point counts.

Small brown grains of perovskite were observed in thin section under crossed Nicols and plane light. Perovskite is a common accessory mineral in kimberlites (Dawson, 1967) and averaged 1 percent of the total rock mass from thin-section point counts.

Trace amounts of apatite and chlorite are also present in the groundmass. Apatite occurs as very small (less than 0.1 mm across) six-sided crystals. Chlorite was released into the groundmass during secondary alteration of other mineral and xenoliths.

Composite Modal Analysis. Table 4 presents a composite modal analysis of the kimberlites compiled using the slab, thin-section, and polished-section point counts and other visual observations. The percentages presented represent relative maximums. For comparison, the results of previous investigators are also given in Table 4.

The Megacryst Suite. Recent studies (Garrison and Taylor, 1980; Schulze, 1981, 1982, 1984; Agee and others, 1982) have defined a megacryst suite from samples collected at the outcrop and float locations (see Figure 1). This suite consists of phenocrysts of ilmenite, garnet, phlogopite, pyroxene, and the larger olivines. The megacrysts are interpreted to have formed "… from a fractionating, mantle-derived liquid at about 150 km depth within the temperature interval of 1165°–1390°C …" (Agee and others, 1982, p. 28). Schulze (1984) pointed out that many of the garnet and pyroxene nodules correlated better with the mineral assemblages found in peridotites, and probably represent xenocrysts from the mantle.

Table 4. Composite modal analysis of kimberlite components.

	kb	*mk*	*A*	*B*	*C*	*D*	*E*
olivine p,x	38.6	39.7	40.0	47.0	43.0	40.6	45.0
serpentine s	32.5	27.3	30.7	22.0	24.0	30.5e	15.0
ilmenite p,x	9.0	13.0	2.2	10.0b	6.0	20.5b	10.0
garnet p,x	2.8	3.3	8.0	10.0	8.0	1–2	10.0
magnetite p,s	5.0	7.0	2.0	–	6.0	–	2.0
phlogopite p,x	1.0	0.0	–	1.0	1.0	1.0	5.0
biotite p,x	0.0	tr.	1.0	–	–	–	1.0
pyroxene p,x	tr.	tr.	1.0	1.0	1.0	1.0	tr.
calcite p,x	7.5	9.3	14.0a	9.0c	8.0	13.6	20.0
perovskite y	1.2	0.7	–	–	–	–	tr.
chromite y	tr.	tr.	–	–	–	–	1.0
apatite y	tr.	tr.	tr.	tr.	tr.	tr.	tr.
chlorite s	1.0	tr.	–	–	1.0	–	5.0
xenoliths	12.6	2.6	–	d	d	4.8	d

p—primary s—secondary y—accessory x—xenocrystic

–xenolith percentages for this study from slab point counts
–ilmenite and magnetite percentages for this study from polished-section point counts
–percentages shown for this study, A, D, and E represent relative maximums

kb–kimberlite breccia (this study)
mk–massive kimberlite (this study)
A–Diller, 1887, massive kimberlite
B–Koenig, 1956, kimberlite breccia
C–Haupt, 1968, both kimberlites
D–Bolivar, 1972, massive kimberlite
E–Harvey, 1980, kimberlite breccia

a–carbonate reported as dolomite in this study
b–includes perovskite, magnetite, chromite
c–includes dolomite
d–no percentage given for xenoliths
e–includes chlorite

Laboratory Magnetic Measurements

Oriented field samples and other specimens were collected from the two outcrops for laboratory investigations. Measurments were made which defined:

1. the magnetic susceptibility of the samples
2. the strength and direction of the total magnetic intensity vector within the samples.

After these values were obtained, the following magnetic parameters were calculated:

1. induced magnetic intensity
2. remanent magnetic intensity
3. permanent dipole moment
4. Koenigsberger ratios.

Table 5 defines the magnetic quantities and symbols used in this thesis.

A Bison magnetic susceptibility meter (model 3101) was used to measure magnetic susceptibility. Seven samples (four kimberlite breccia, three massive kimberlite) were crushed and cleaned with a No. 5 sieve. The larger fragments trapped by the sieve were used for the magnetic susceptibility measurements.

The strength and direction of total magnetic intensity was determined from the oriented samples. The samples were cut into 2-inch cubes and measured with a single-axis fluxgate magnetometer (Schonstedt digital magnetometer model D-2220/R). Two cubes were prepared from the kimberlite breccia outcrop, and one from the massive kimberlite.

Table 5. Definition of magnetic units.		
symbol	*quantity*	*c.g.s. unit*
k	magnetic susceptibility	gauss/oersted
H	geomagnetic field strength	oersted
Jt	total magnetic intensity	gauss
Ji	induced magnetic intensity	gauss
Jn	remanent magnetic intensity	gauss
Mr	permanent dipole magnetic moment	gauss
NRM	natural remanent magnetization	gauss
Qn, Q'n	Koenigsberger ratios	–
D	declination of Jt vector	azimuth
I	inclination of Jt vector	degrees*

(gauss=emu/cubic cm)
* (+) indicates down, (–) indicates up

A value of magnetic intensity was recorded for all six sides of each cube. Vector analysis was used to obtain the strength and direction of the total magnetic intensity vector. This vector was then rotated back to the field orientation of the cube.

Once the magnetic susceptibility and strength of the local geomagnetic field are known, the induced magnetic intensity can be found by multiplying these two quantities (Ji=kH). Since the total magnetic intensity of a material is the vector sum of its remanent and induced intensities (Irving, 1964, p. 10), the magnetic quantity Jn was obtained through subtraction (Jn=Jt–Ji).

The permanent magnetic dipole moment was calculated using the following equation (modified from Breiner, 1973, p. 35):

$$Mr=(Jt(L/2))/2$$

where L=length of cube side.

Two of Koenigsberger's ratios were calculated. Qn is the ratio of remanent intensity to induced intensity (Qn=Jn/Ji). The ratio of remanent intensity to susceptibility is Q'n (Q'n=Jn/k). When either of these two ratios exceeds 1, it is an indicator that the material being measured possesses a stable NRM (Nagata, 1961, p. 148–149; Irving, 1964, p. 92).

The results of the laboratory magnetic measurements and calculations are presented in Table 6. The magnetic data of Warren (1956) and Harvey (1980) are listed in Table 7 for comparison.

Table 6. Results of laboratory magnetic measurements and calculations.			
magnetic quantity	*units*	*massive kimberlite*	*kimberlite breccia*
k	gauss/oe	0.00192	0.00109
Jt	gauss	0.01760	0.00986
Ji	gauss	0.00107	0.00064
Jn	gauss	0.01650	0.00925
Mr	gauss	0.14400	0.08070
Qn	–	15.4	14.5
Q'n	–	8.6	8.5
D	azimuth	060	339
I	degrees	+14	+21

(+) indicates downward inclination

Table 6 shows that the magnetic properties of the massive kimberlite are approximately 1.8 times as strong as the kimberlite breccia. This supports the suggestion in the Petrography section (this study) that the content of magnetite and ilmenite is higher in the massive kimberlite than in the kimberlite breccia.

The Koenigsberger ratios indicate the magnetic properties of both rock types are largely due to remanent magnetization. Harvey (1980) concluded most of the remanent magnetization was caused by a combination of:

1. the higher percentage of ilmenite over magnetite
2. the more stable magnetic character of ilmenite over magnetite.

A higher percentage of ilmenite over magnetite was suggested in the petrographic analysis of this study (see p.

19). However, this writer believes the abundance of ilmenite contributes to the dominance of remanent magnetization in a different way.

Ilmenite is common in igneous rocks, but by itself cannot increase the natural magnetization of a rock (ilmenite is not magnetic at room temperature, and has a Neel temperature of –216°C; Strangway, 1970). Strangway (1970) noted the importance of ilmenite in igneous rocks is its ability to diminish the grain size of magnetite via exsolution. Strangway (1970, p. 32) stated "… the effect of this is to create great magnetic stability in the magnetite. The role of ilmenite is, therefore, of an accessory nature." Recall from the Petrography section (this study) that magnetite occurred in the groundmass and in alteration rims surrounding other minerals, always very fine grained, but never as phenocrysts.

Table 7. Warren's (1956) and Harvey's (1980) magnetic measurement data for kimberlite breccia samples.

Warren's (1956) sample	*rock type*	*depth*	*magnetic susceptibility (gauss/oe)*	
1	peridotite	surface	0.009	

Harvey's (1980) samples	*rock type*	*depth*	*magnetic susceptibility (gauss/oe)*	*magnetic polarization (gauss) (NRM)*
A	peridotite	surface	0.000441	0.0724
B	peridotite	surface	0.000448	0.0926
4A	peridotite	surface	–	0.0156
4B	peridotite	surface	–	0.0104
4C	peridotite	surface	–	0.0143
4D	peridotite	surface	–	0.0096
4E	peridotite	surface	–	0.0145
4F	peridotite	surface	–	0.0119
6A	peridotite	surface	–	0.0094
6B	peridotite	surface	–	0.0080
7C	peridotite	surface	–	0.0203
7D	peridotite	surface	–	0.0219
7E	peridotite	surface	–	0.0216

(mean moment of samples 4A–7E is 0.0143 gauss)

From the data in Table 6 (p. 26, this study), paleomagnetic pole positions were calculated for both kimberlite types using equations defined by McElhinny (1973, p. 23–26), and compared to pole positions compiled by Strangway (1970, p. 147–154). A Triassic pole position at 57°N, 137°E was determined for the kimberlite breccia. The massive kimberlite yielded a Cambrian pole position at 28°N, 20°E. The latter is not plausible because the kimberlites intrude Pennsylvanian rocks.

Neither remanent vector can be considered statistically valid for two reasons:

1. the directions are based on only three measurements (one from the massive kimberlite, two from the kimberlite breccia)
2. the cubes used for determining the vector directions were not subjected to demagnetization techniques to remove secondary or unstable magnetic components (see Strangway, 1970, p. 77–83).

Ground Magnetic Mapping Procedures

Collection of Data

Magnetic data were gathered using a Barringer GM-122 proton precession magnetometer. This instrument measures the strength of the earth's total magnetic field in gammas. Diurnal magnetic variations were measured using the method described by Dobrin (1960, p. 136–138).

Survey lines were placed perpendicular to the strike of the intrusives where possible (see Figure 13). To avoid magnetic interference from power lines crossing the northeasternmost intrusive, survey lines were placed parallel to the power lines. Tie lines and short radial lines were used to collect additional data. Regional data were taken along local roads to help define any regional magnetic gradients. The spacing between data stations along a particular line was determined using the following rules of thumb (present author):

1. if the magnetic gradient from the last station was less than 10 gammas, 100-foot spacing was used
2. if the gradient from the last station was between 10 to 50 gammas, 50-foot spacing was used

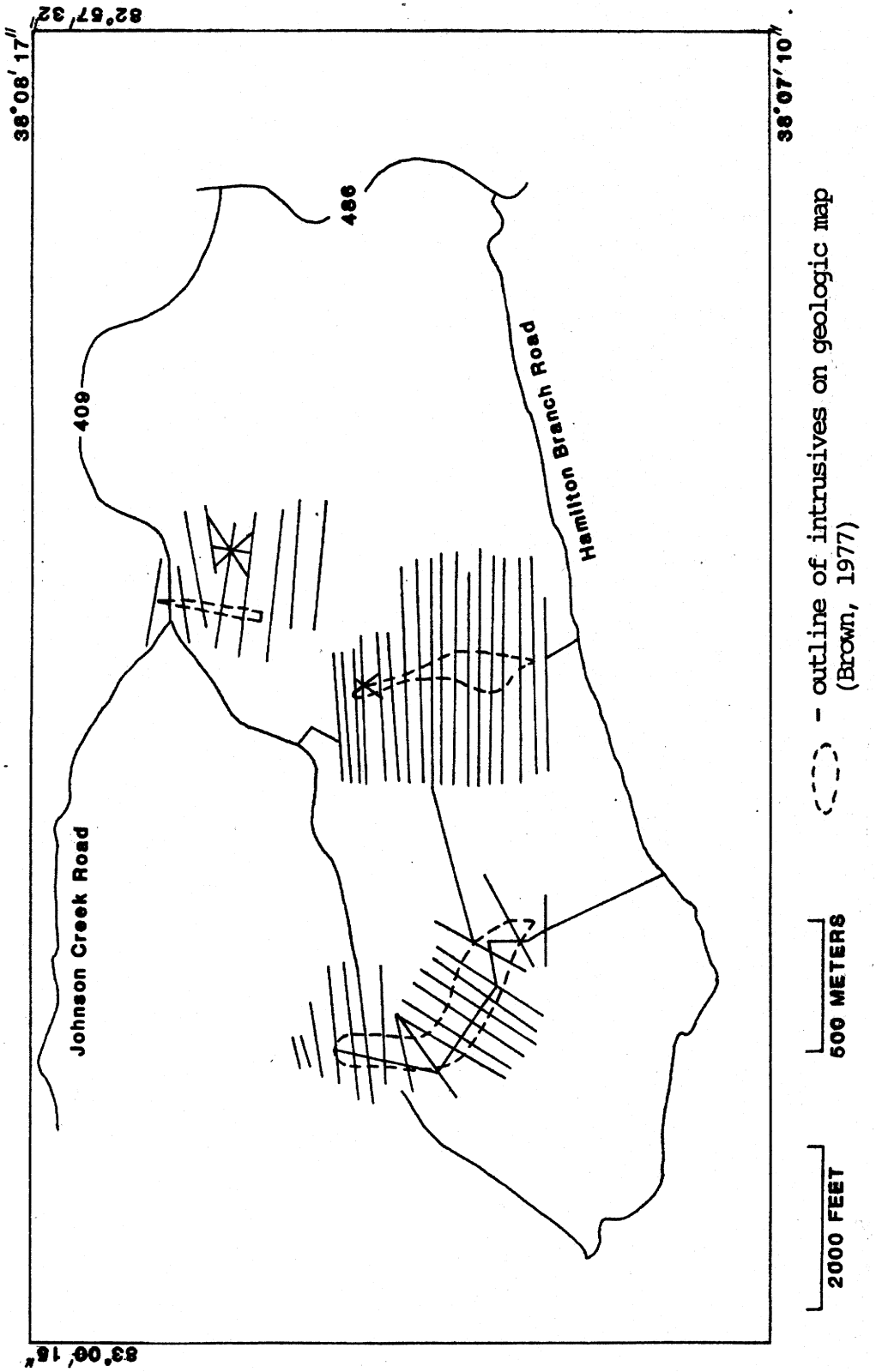

Figure 13. Location of survey lines and roads used to collect regional data.

3. if the gradient from the last station exceeded 50 gammas, 25-foot spacing was used.

To establish map control, notes were kept on the elevation change and topographic features between stations. Occasionally spacings over 100 feet were used to avoid power lines and other objects that would affect magnetic readings. The distances for station and line spacing were measured by pacing, and rescaled if necessary to fit reference points on the topographic base map. These rules also applied when collecting regional data close to the intrusives. In areas more remote from the intrusives, data were taken on spacings up to a half-mile interval.

After the collection of magnetic data was completed, the end points of all survey lines were mapped with Brunton compass and tape measure and plotted on a base map (1:6,000 scale). A total of 1,123 magnetic readings was taken. The position and value of each reading on the base map is listed in Appendix A.

Preparation of the Total Magnetic Intensity Map

Two corrections were made before values were entered on the base map for contouring. There was always some difference between the paced length of a survey line and the mapped length. The following equation (present author) was used to adjust the spacings to the mapped length of a survey line:

mapped length of a survey line=X+2X+4X
where X=adjusted length of 25' spacings
2X=adjusted length of 50' spacings
4X=adjusted length of 100' spacings.

Larger spacings were adjusted in a similar manner.

It was mentioned in the previous section that during the time magnetic data were being collected, the diurnal magnetic variation was measured. A continuous diurnal variation chart was constructed to determine the amount of correction needed each day.

A computer program was written to tabulate the refined data using one survey line at a time. First, the program calculated the value of total magnetic intensity corrected for diurnal variation at the first station. Based on the adjusted spacings, the station's distance from an endpoint of the survey line was computed. After the program completed the calculations for the first station, it looped back to do the second station, and so on.

This program is named the Diurnal Corrections Program. It performed other minor functions and listed additional data. The program is listed in Appendix B with sample input and output files. After all of the survey lines and regional data were reduced, the values were plotted and contoured. The resulting total magnetic intensity map (Map 1) is included in this CD-ROM.

Modeling and Interpretations

Preparation of Residual Total Magnetic Intensity Maps

Nine anomalies were chosen for magnetic modeling from the total magnetic intensity map. A separate residual intensity map was prepared for each anomaly. Magnetic modeling was performed using the residual intensity maps. Before these maps could be made, a correction was needed to compensate for a regional gradient identified from Map 1. This correction was necessary to negate the influence of the larger, deeper, magnetized sources that would interfere with the modeling of small shallow units (less than 30 meters deep). It was also important to set all of the magnetic intensity values relative to a common base for proper comparison.

The interpolated positions of the total magnetic intensity contours that define the regional gradient are shown in Figure 14. Figure 14 also includes an index for the area covered by Map 1.

A residual total intensity aeromagnetic map for Elliott County is presented in Figure 15. The data for this map were collected at an average ground clearance of 1,000 feet (Johnson and others, 1980). The patterns on this map reflect differences in the ferromagnetic content of the underlying basement rock

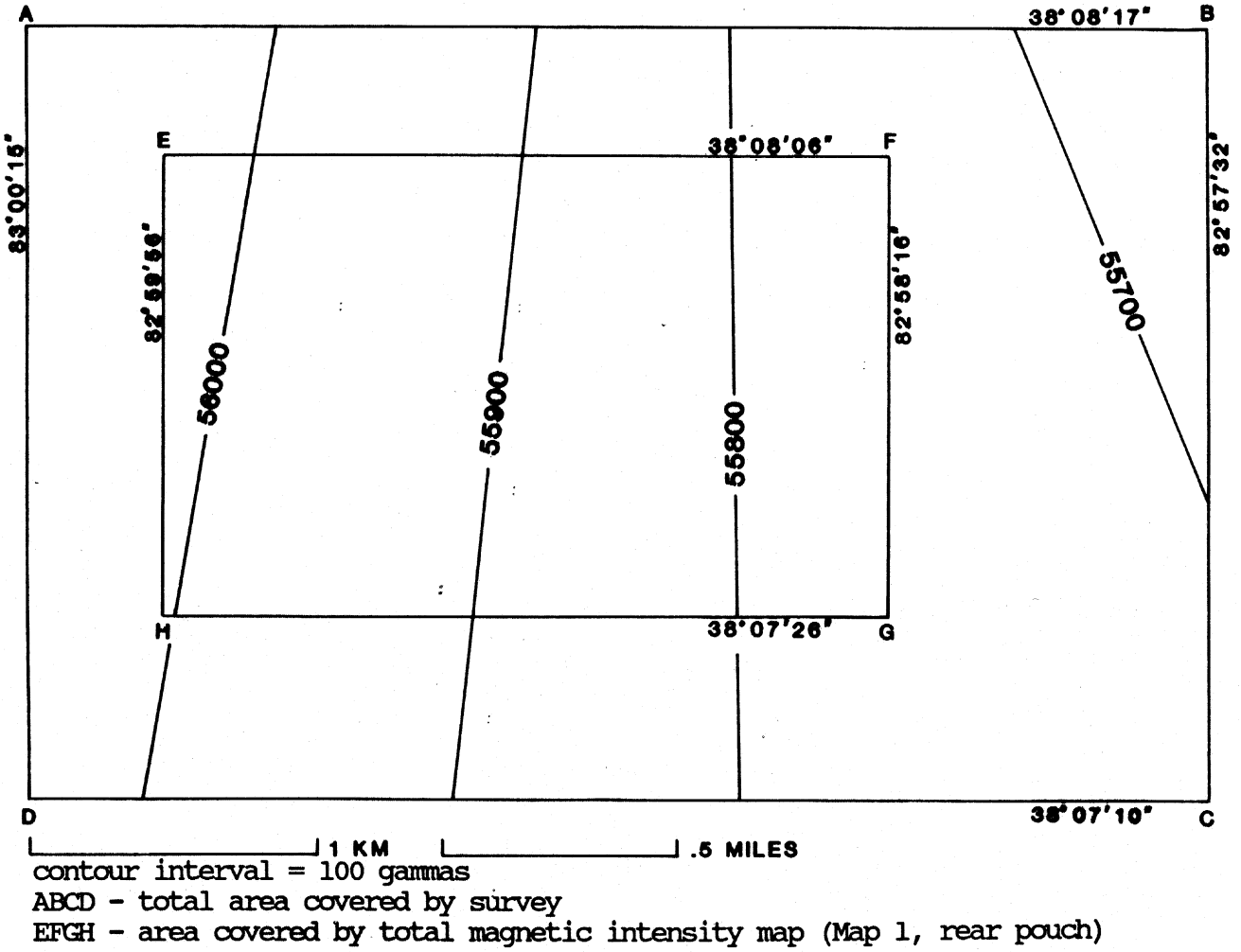

Figure 14. Interpolated position of total magnetic intensity contours used to define regional gradient in study area.

(Vacquier and others, 1963). The magnetic gradient in Figure 14 compares well with the magnetic gradient passing through the study area in Figure 15.

A computer program named the Regional Gradients Reductions Program was written to remove the regional gradient. It also set the magnetic intensity values as either a positive or negative value relative to a common base. The position of each value on the base map was assigned coordinates relative to a positive X-Y grid system. An inspection of the regional gradient indicated it increased approximately 200 gammas per mile in a westward direction. The values were set using 55,700 gammas as a common base. The aforementioned parameters were used to design the Regional Gradients Reductions Program. Figure 16 graphically illustrates how the regional gradient was removed using an east-striking anomaly curve. The program is listed in Appendix B with input and output files.

After the values were processed by the Regional Gradients Reductions Program, they were replotted and contoured. Map 2 is an index map of the nine residual intensity maps. Each map and its respective anomaly will be referred to by the code names shown on Map 2.

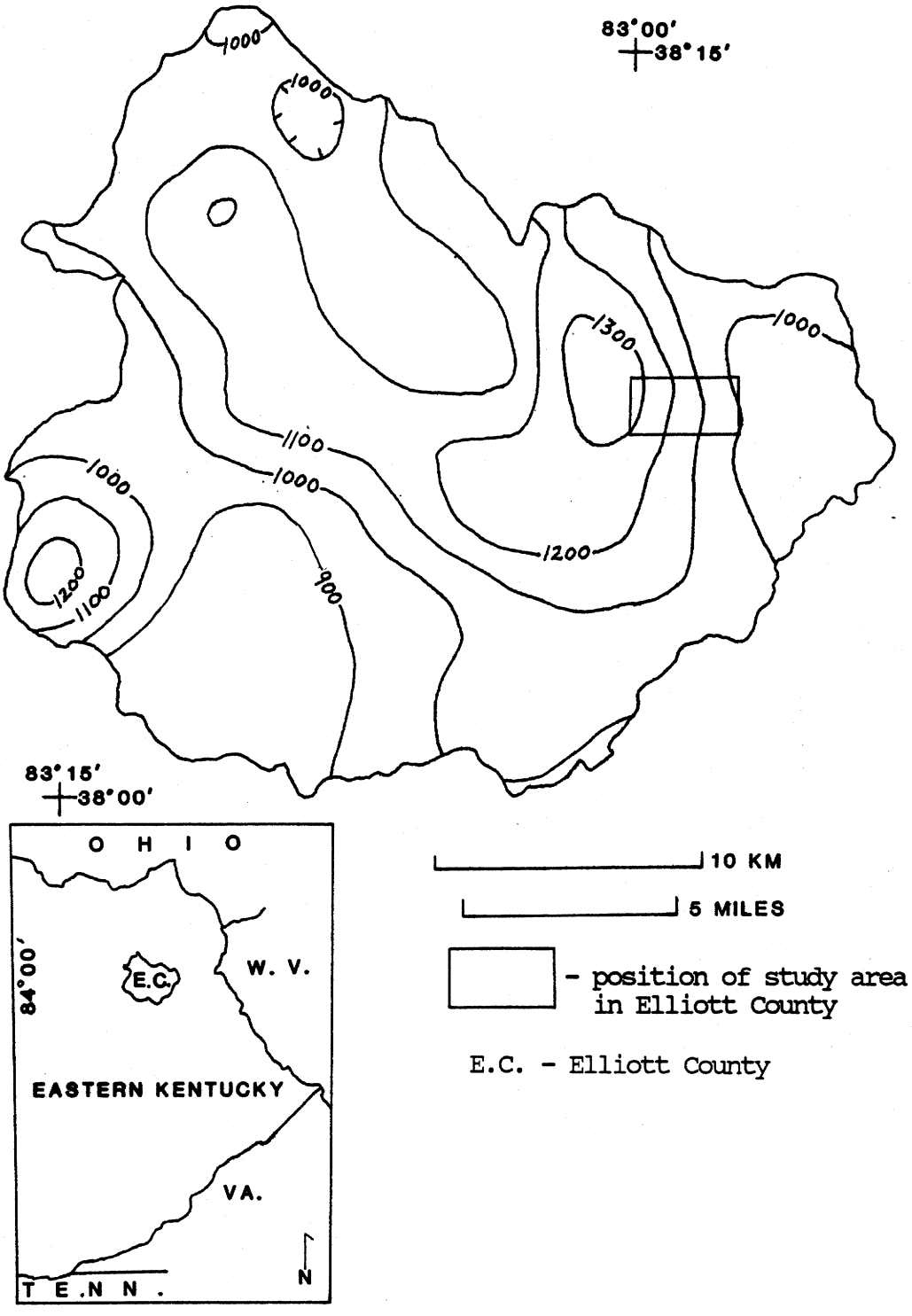

Figure 15. Residual total intensity aeromagnetic map of Elliott County (modified from Johnson, Haygood, and Kunselman, 1980).

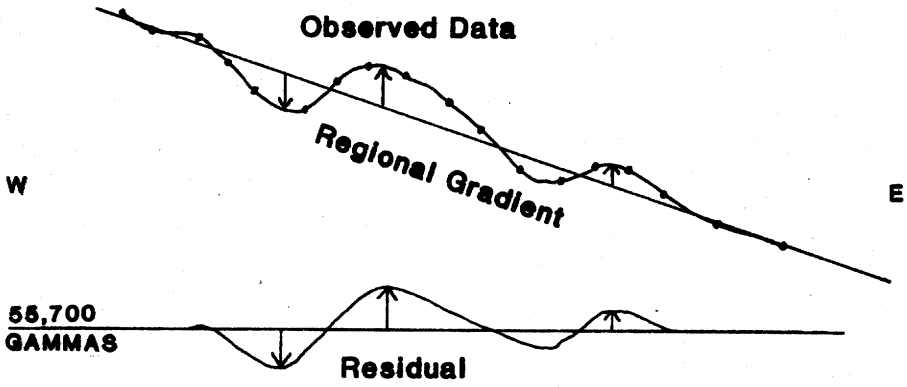

Figure 16. Graphic illustration of removal of regional gradient (modified from Breiner, 1973).

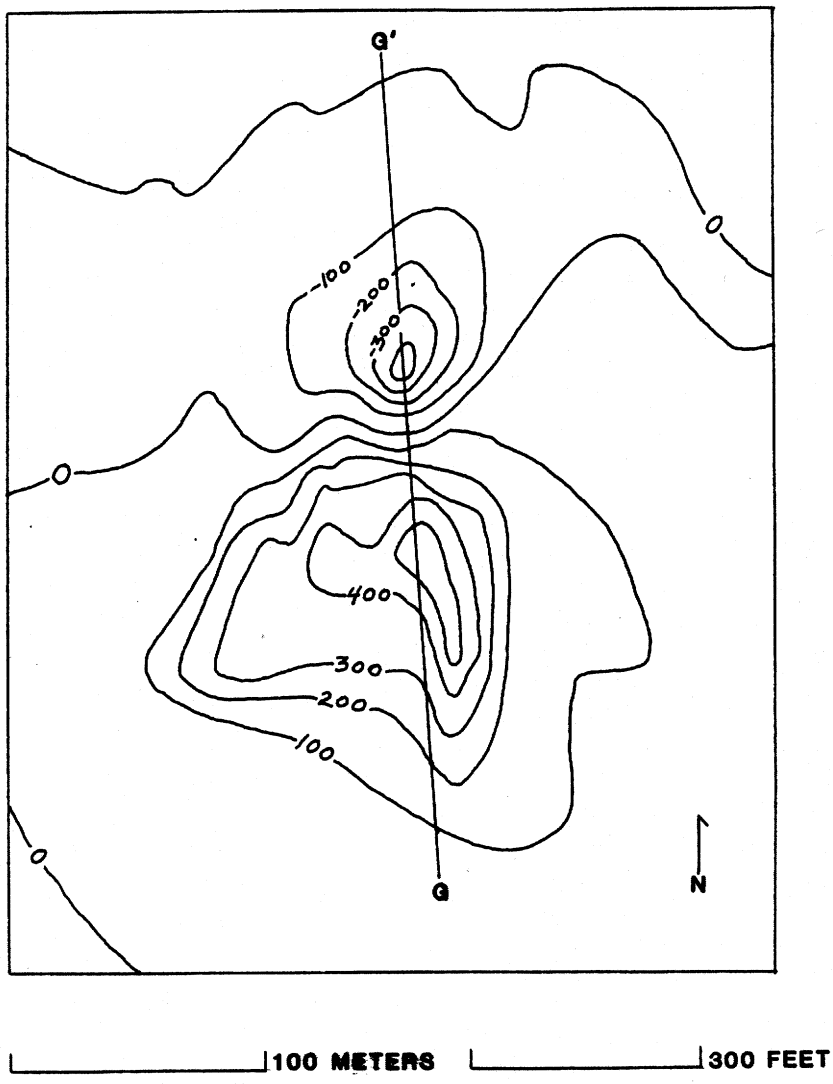

Figure 17. K1 anomaly: observed residual intensity map (in gammas).

The K1 Anomaly: Modeling

The K1 anomaly shall serve as an example for the modeling process. Figure 17 shows the area defined to model this anomaly, the observed residual intensity map, and the profile chosen for two-dimensional analysis (line G–G').

To perform three-dimensional modeling, Magnetics Program 302[1], MAG3D was chosen. MAG3D was selected because of two advantages it affords in modeling. From the data generated by MAG3D, computed magnetic intensity maps can be made and compared directly with observed magnetic intensity maps. Also, MAG3D can produce data for magnetic fields due to any arbitrary three-dimensional shape. These advantages provide more accuracy than only using a two-dimensional method of comparing profiles.

There are other features of MAG3D that make it well suited for this study. MAG3D can examine bodies having any strength or direction of remanent magnetization. This is important because the Koenigsberger ratios (see Laboratory Magnetic Measurements, this study) indicate the dominance of remanence in pro-

[1] A complete description of the algorithm employed in MAG3D is given in Talwani, M., 1965, "Computation with the help of a digital computer of magnetic anomalies caused by bodies of arbitrary shape": Geophysics, v. 30, no. 5, p. 797–817.

ducing the anomalies. The body being modeled can be placed at any magnetic latitude or declination. Output values are equal to the residual intensity at the point of observation. The latter allowed for direct comparison with observed maps without having to make any vector adjustments.

The models were examined via a two-step computer process. In the first step, MAG3D was used to generate magnetic intensity values from a model. The output instructions of MAG3D were modified so desired information was retained in data files. One of the output files contained a list of the observed and computed magnetic intensity values. The position of each value was held in another file. After running MAG3D, the file of values was reviewed to determine if a computed field map produced from the present model might satisfy the observed field map.

The decision to make a computed field map was the second step. A small program was written to join the essential parts of the two files described above. This new file was read into a graphics contour plotting program called GRID (Davis, 1973). The simulated contour plots were made on a Digital Equipment Corporation Decwriter IV. A section of GRID was modified to output the range of values in each contour interval. The model was accepted if the computed profile matched well with the observed profile. If not, slight modifications were made to the model until the desired fit was achieved.

Figure 18 shows the computed residual intensity field map for the K1 anomaly and the position of the model responsible for this field. The profiles along G–G' compare well (see Figure 19). A graphic illustration showing the relationship between the model position, topographic expression, and computed profile was also made (see Figure 20).

An elevation increase is seen in a northward direction across Figure 20. Although slight, it necessitated elevation corrections for the K1 anomaly. Elevation corrections were also needed for five other anomalies.

Figures 21 and 22 exhibit the computed residual intensity field

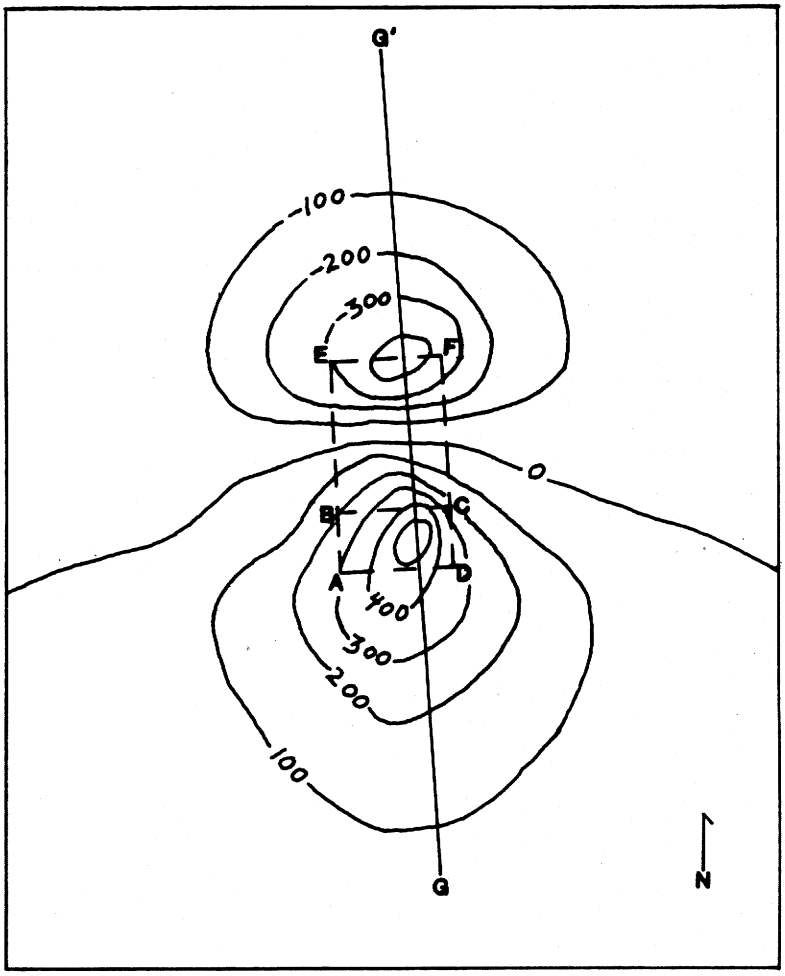

G–G' - profile location
BEFC - upper contour for model
AEFD - lower contour for model
Jn = 0.0092 gauss
D = 357°
I = +4°

Figure 18. K1 anomaly: computed residual intensity map (in gammas) with elevation corrections.

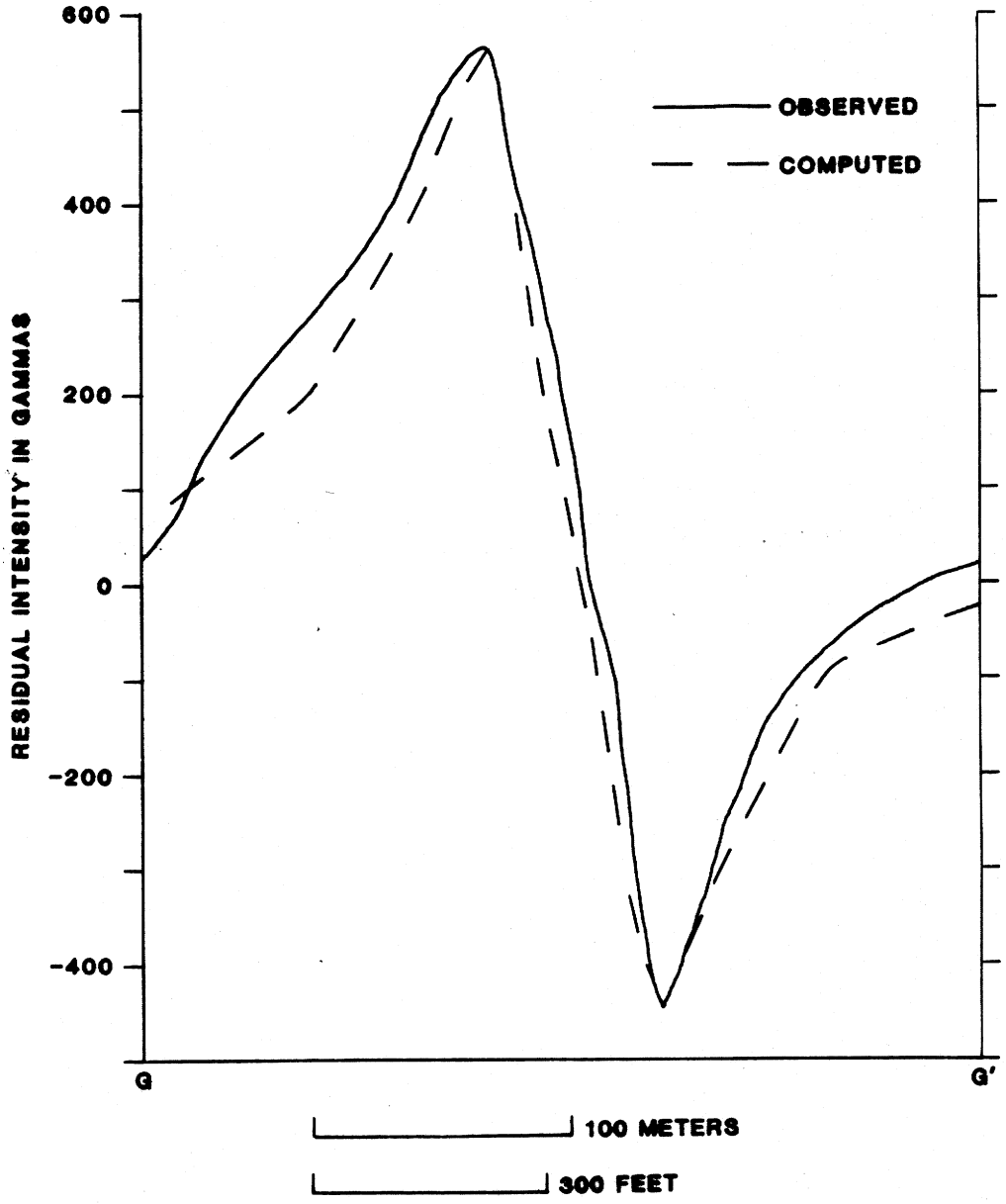

Figure 19. K1 anomaly: observed profile and computed profile with elevation corrections along G–G'.

and profile comparison for the K1 anomaly without elevation corrections. In Figure 18 the top of the model was placed 85 feet below the lowest elevation along G–G' (720'). The surface elevation is held constant at 720 feet across G–G' in Figure 21, with the top of the model 85 feet below the surface.

Elevation changes were entered into the input files and processed by MAG3D. In an aeromagnetic survey, elevation corrections are usually ignored unless topographic relief is extreme (over 1,000 meters). The need for elevation corrections was discovered during modeling, for it was found that even with small elevation changes, if the top of the magnetized unit was close to the surface (as is the case throughout this study), the value of magnetic intensity could vary greatly. In one case, a change of 50 feet caused a variation of over 900 gammas.

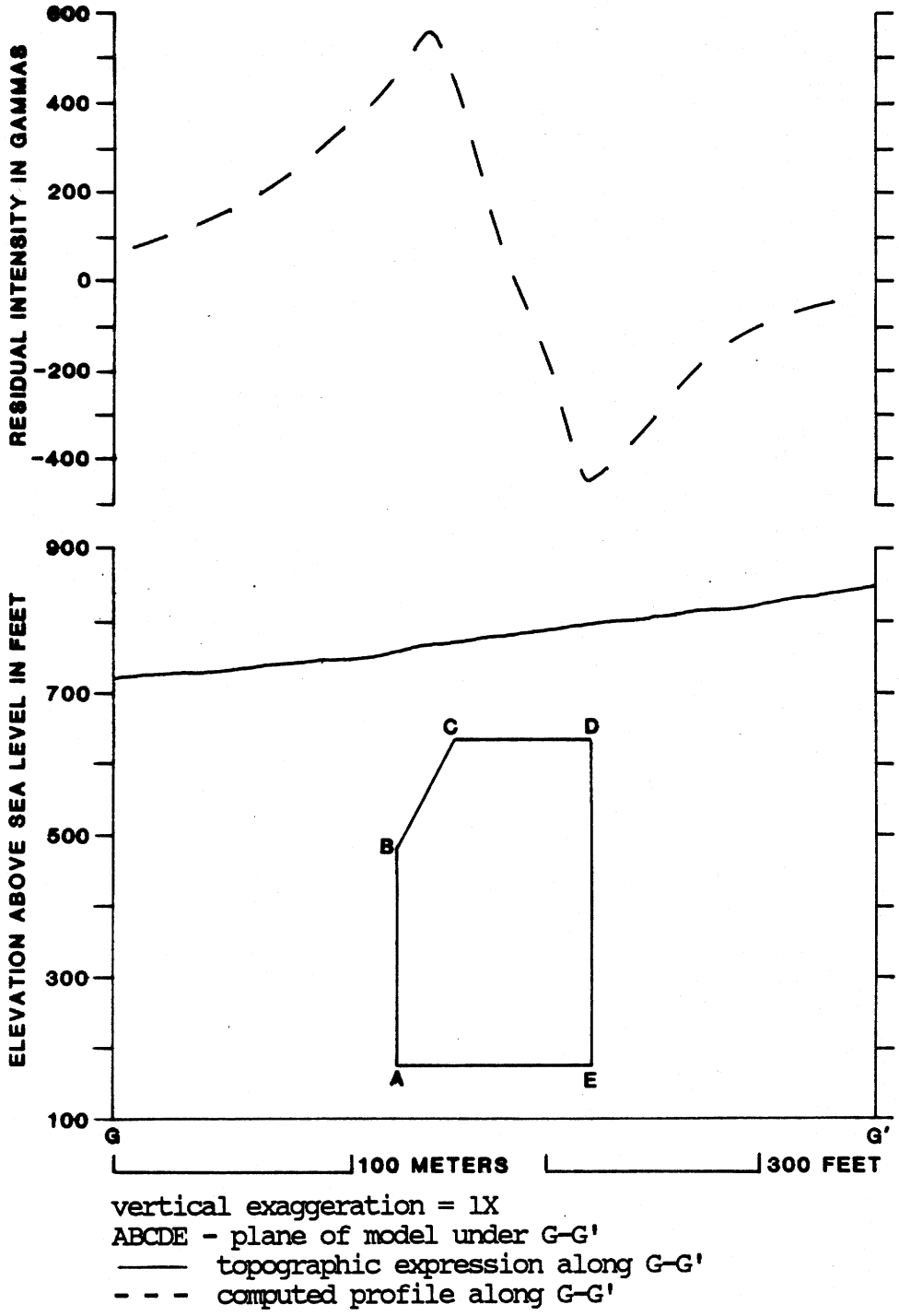

Figure 20. K1 anomaly: model position, topographic expression, and computed profile with elevation corrections along G–G'.

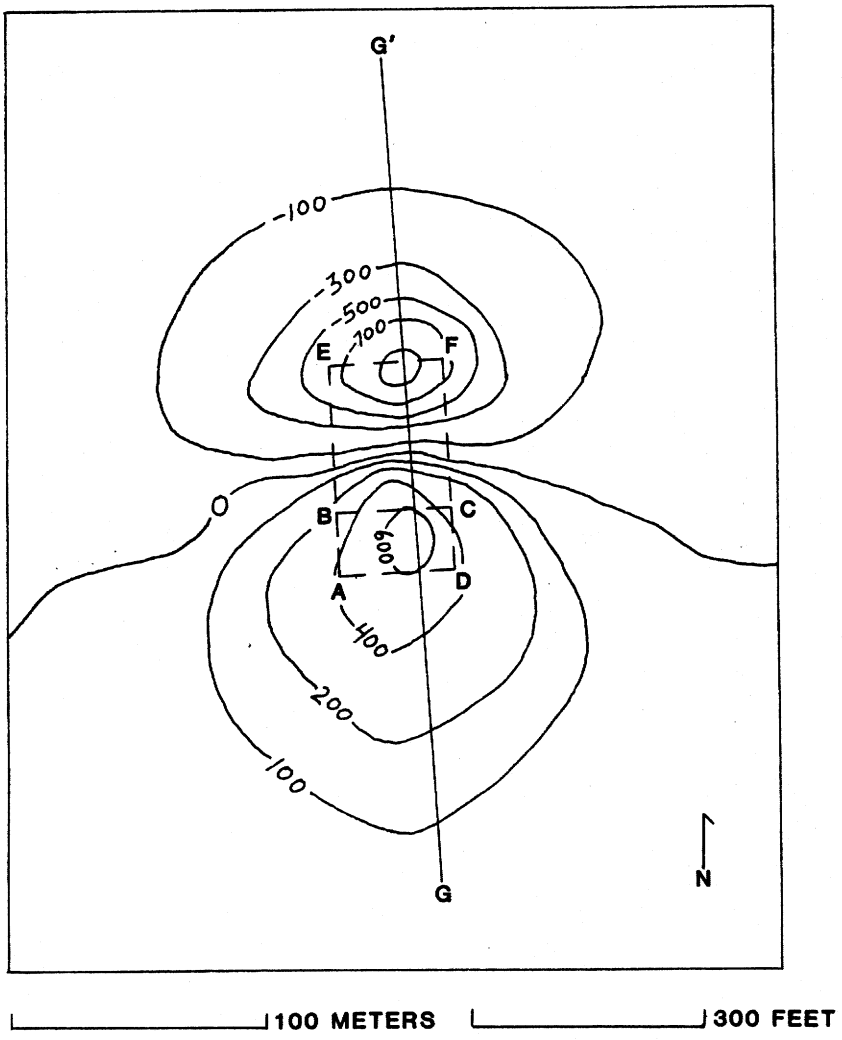

G-G' - profile location
BEFC - upper contour for model
AEFD - lower contour for model
Jn = 0.0092 gauss
D = 357°
I = +4°

Figure 21. K1 anomaly: computed residual intensity map (in gammas) without elevation corrections.

The K1 Anomaly: Interpretations

The rectangular prism model shown in the preceding series of figures for the K1 anomaly is interpreted as an elliptical pipe. It occupies the same volume as the prism, and the long axis trends north–south. For a better profile match, the southern edge was beveled off.

The differences between magnetic fields generated by a square prism and cylinder of equal volume were examined and found to be minimal. The fields were generated using the same magnetic parameters. The prism used for modeling the K1 anomaly is defined by the following parameters:

top contour: length=59 meters, width=44 meters

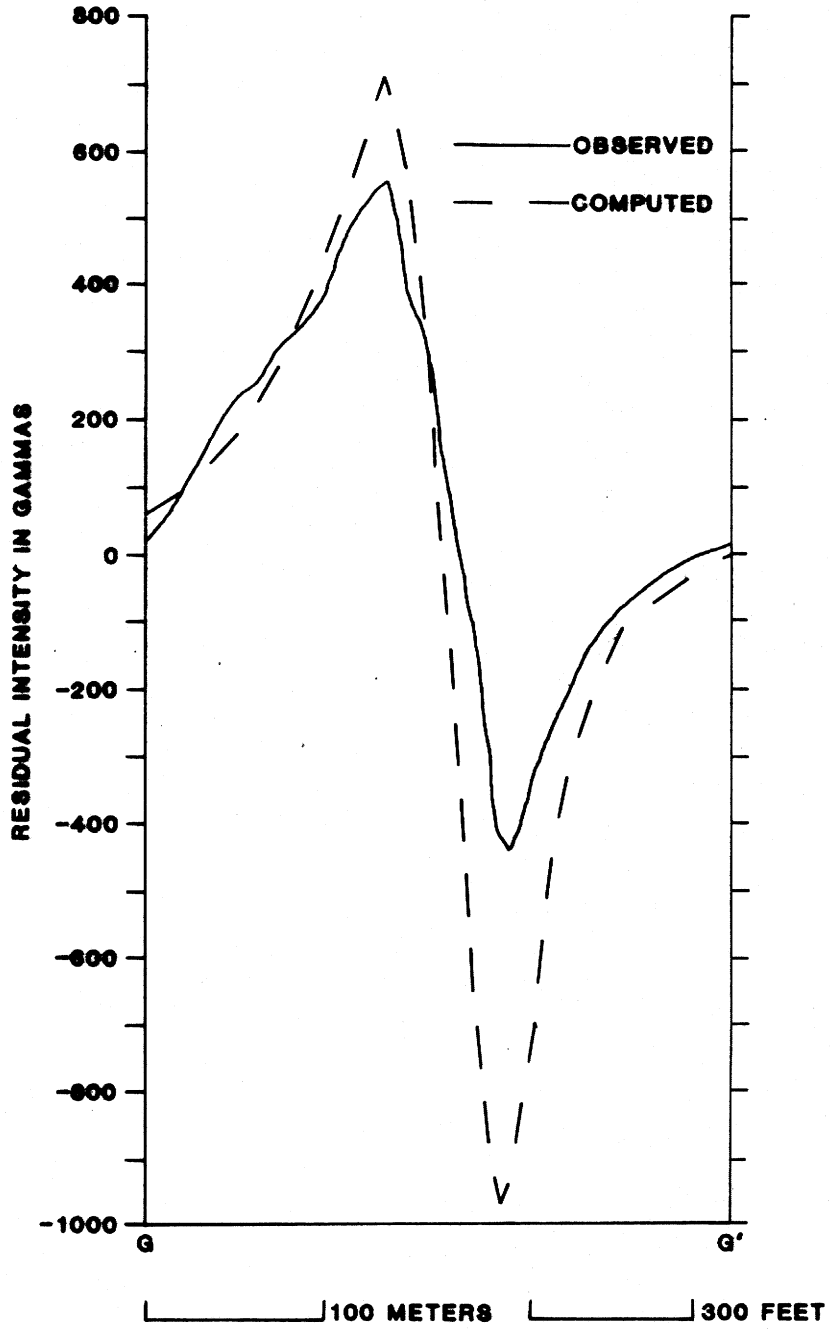

Figure 22. K1 anomaly: observed profile and computed profile without elevation corrections along G–G'.

intermediate and bottom contours: length=83 meters, width=44 meters

total thickness=136 meters

Jn=0.0092 gauss, D=357°, I=+04°

The values used in modeling for the earth's magnetic latitude and declination were 68° and 4°W, respectively. These values were held constant throughout the modeling.

The Jn value used above is very close to the Jn value obtained from the kimberlite breccia outcrop. The D and I values differ slightly, but agree well with Harvey's (1980, p. 44) interpretation of the kimberlite having a remanent magnetization direction that is "… nearly horizontal or very low angle in a northerly direction."

The K2 Anomaly

Most intricate of all the anomalies is the K2 anomaly. The observed residual intensity map is shown in Figure 23. Profile J–J' does not pass through the most extreme values, because the latter were obtained directly over outcrop. The position chosen for J–J' was considered most representative of the entire anomaly.

The two magnetic lows near A and B were not included in modeling. Both lows occur in a streambed flanking the kimberlite breccia outcrop to the west. The lows were interpreted to be the result of draped effects.[2] An alternate explanation would be that they were caused by different levels at the top portion of the intrusive (John LaBrecque, personal communication, 1984). Attempts were not made to reproduce these lows in modeling, with the exception of elevation corrections.

[2] For an explanation of draped effects, see Grauch, V.J.S., and Campbell, D.L., "Does draping aeromagnetic data reduce terrain-induced effects?": Geophysics, v. 49, no. 1 (Jan. 1984), 4 figs.

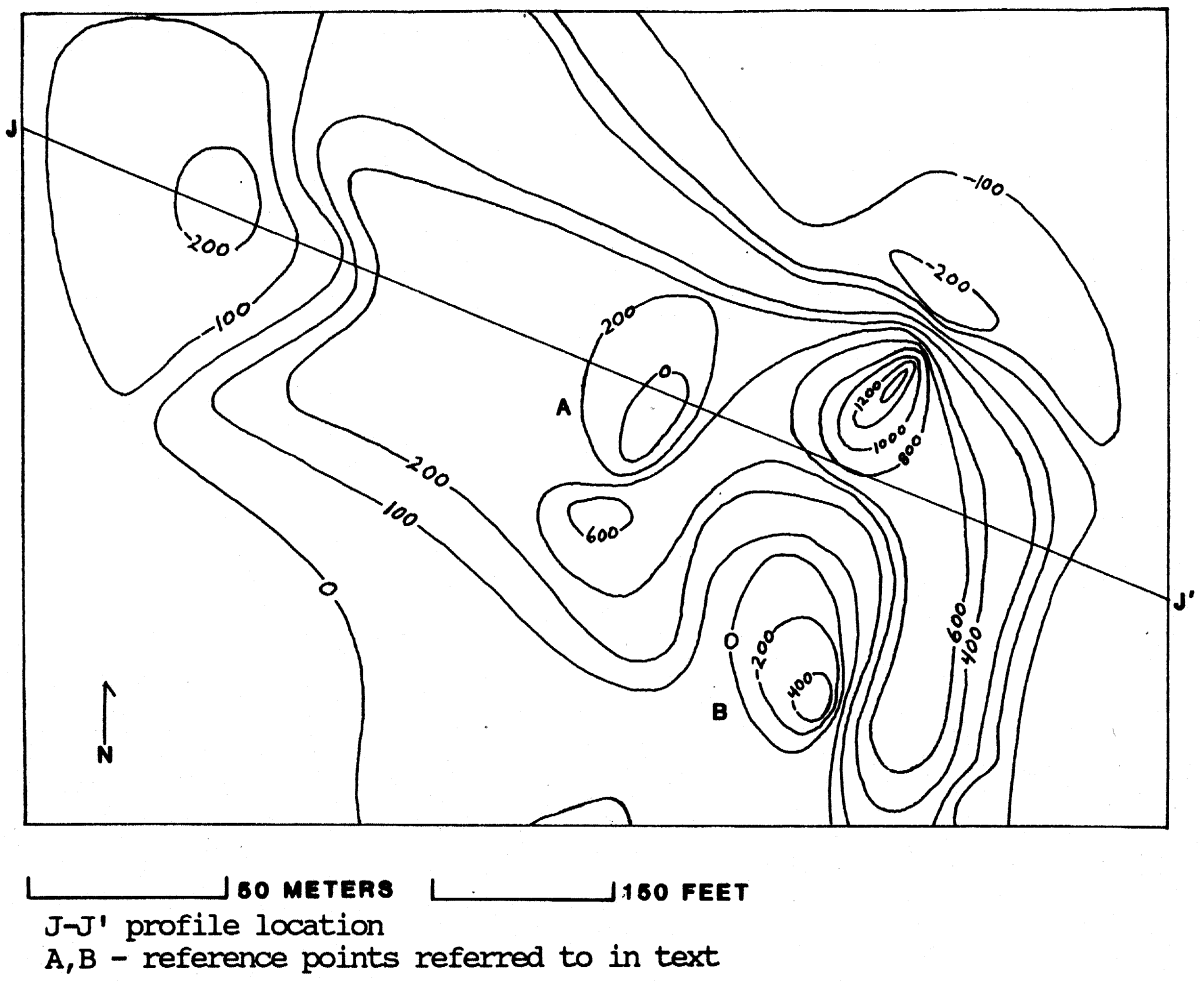

Figure 23. K2 anomaly: observed residual intensity map (in gammas).

The interpretation of the model illustrated in Figures 24 through 26 is that of a north-trending elliptical pipe with a sill protruding from its upper portion in a northwest direction. The sill pinches out away from the pipe. The following proportions define this model:

pipe part of model:

avg length=117 meters, avg width=32 meters

total thickness=182 meters

sill part of model:

length along J–J' (from line EF to line AD, Fig. 24)=146 meters

total thickness (along line DB, Fig. 26)=30 meters

Jn=0.0075 gauss, D=295°, I=+47°

The Jn used to model this anomaly was less than the Jn obtained from the kimberlite breccia outcrop sample. Considering the variability in the xenolith content of the kimberlite breccia, the difference is negligible. To model the anomaly, a D=295° and I=+47° were used. These values also differ from the D and I values obtained from the outcrop samples. Without further subsurface data, it cannot be determined which set of values best reflects the entire intrusive.

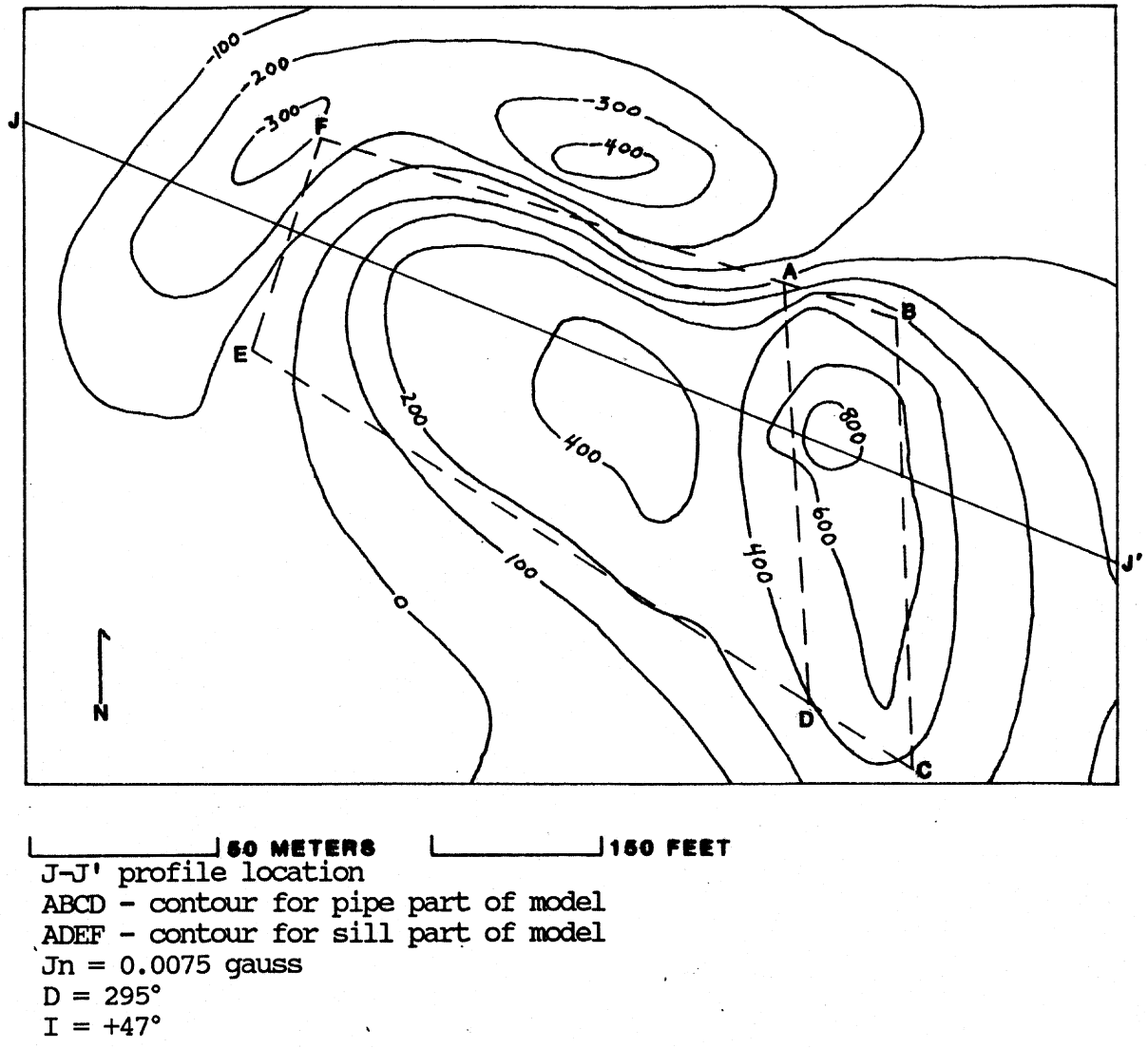

Figure 24. K2 anomaly: computed residual intensity map (in gammas).

The K3 Anomaly

Figures 27 and 28 show the observed and computed fields for the K3 anomaly. On the observed map, there is an increase in magnetic intensity in the northwest corner. This is an overlap from the magnetic field of the K2 anomaly. Also on the observed map, there are two northwest extensions along the 200-gamma contour. These could be due to digitations off of the main rock mass. No attempt was made to reproduce these features in modeling.

The model for the K3 anomaly is interpreted as an elliptical pipe similar to the model for the K1 anomaly (see Figures 18 through 20). There are some minor differences. On the K3 pipe, the northern edge was beveled off for a better profile match. The K3 pipe is thicker, but not as long as the K1 pipe. Given below are the specifications for the rectangular prism used to model this anomaly:

top contour: length=38 meters, width=45 meters

intermediate and bottom contours: length=64 meters, width=45 meters

total thickness=180 meters

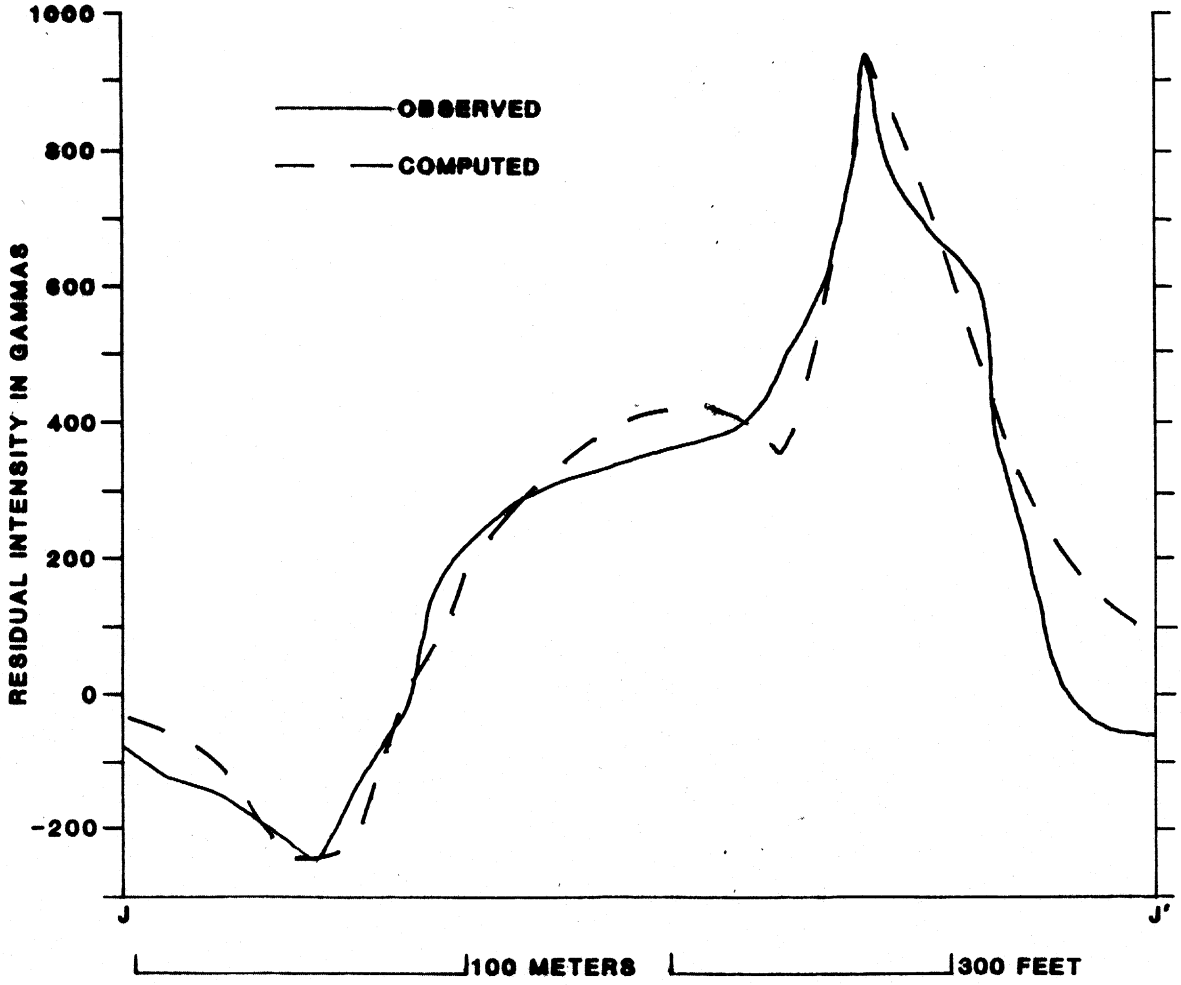

Figure 25. K2 anomaly: observed and computed profiles along J–J'.

Jn=0.01 gauss, D=337°, I=+06°

The Jn and D values used to model the K3 anomaly agreed well with the values obtained from the kimberlite breccia outcrop. The inclination was steeper; however, a shallower inclination may have been used for modeling if lower magnetic intensity values existed on the observed map. The absence of lower values is most likely due to overlap from the K2 field. On the computed map a –100-gamma depression is present over the northwest corner of the model, but as mentioned before, the K2 overlap was not assessed in modeling.

The K4 Anomaly

Smallest and simplest of all the anomalies modeled was the K4 anomaly. A thin circular pipe is the interpretation of the model presented in Figures 31 through 34. The dimensions of this model are given below:

top and bottom contour: side=10 meters
total thickness=181 meters
Jn=0.0145 gauss, D=339°, I=+21°

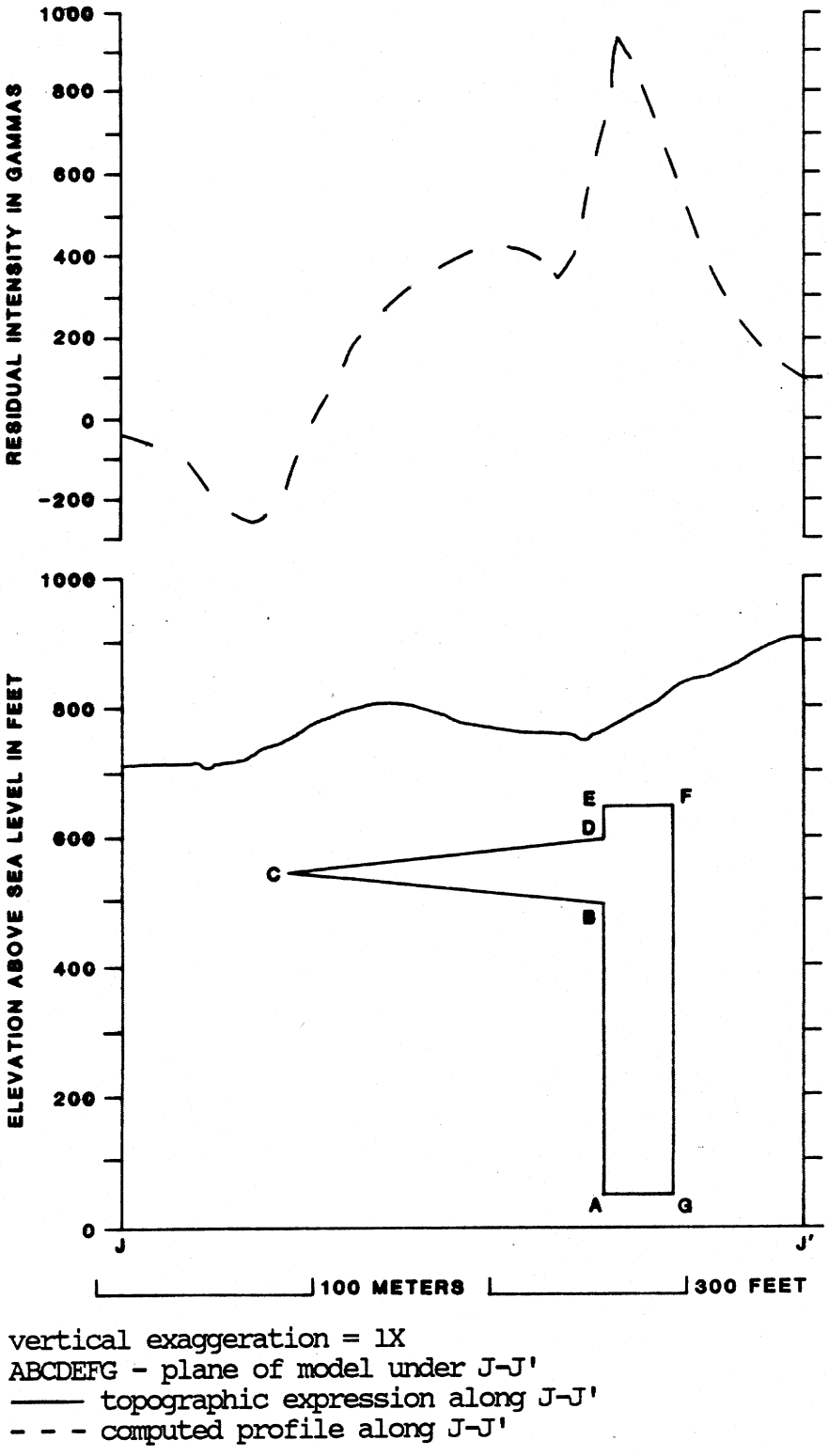

Figure 26. K2 anomaly: model position, topographic expression, and computed profile along J–J'.

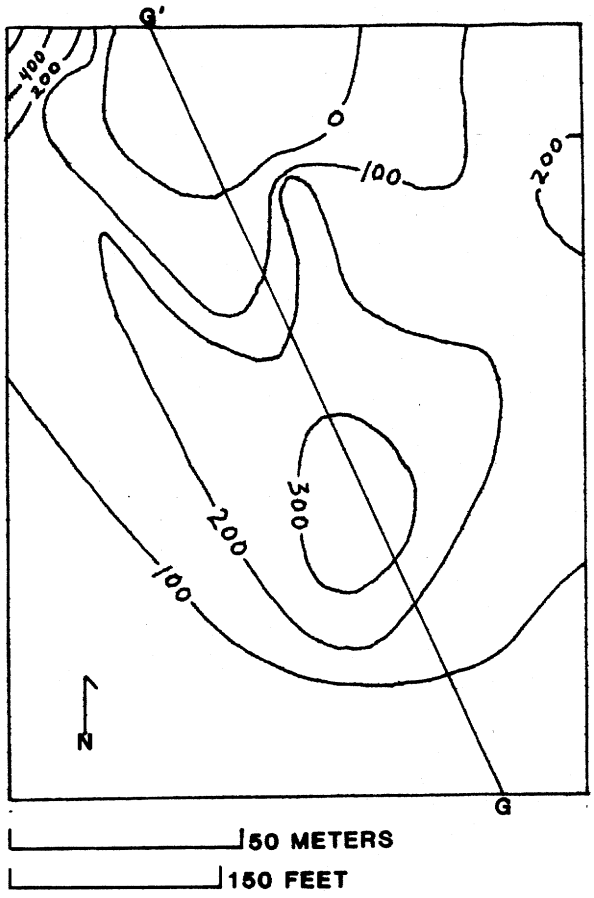

G-G' - profile location

Figure 27. K3 anomaly: observed residual intensity map (in gammas).

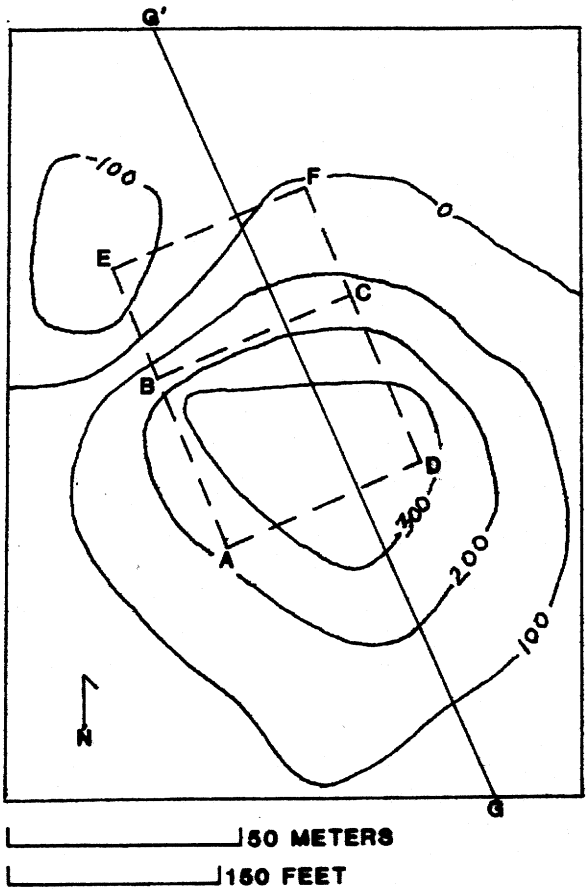

G-G' - profile location
ABCD - upper contour for model
AEFD - lower contour for model
Jn = 0.01 gauss
D = 337°
I = +60°

Figure 28. K3 anomaly: computed residual intensity map (in gammas).

The 100, 200, 300 gamma contours are seen to extend off of the observed intensity map in an east-southeast direction. There could an extremely thin dike associated with this pattern, but this was not considered in modeling.

The D and I values chosen for modeling agree very well with those from the kimberlite breccia sample. The Jn value is about 50 percent stronger, but this value was necessary to reproduce the residual high of 700 gammas.

Summary of the K Area

Previous interpretations of the kimberlite in the K area show it to be one continuous curving intrusive (concave to the northeast) approximately 600 meters in length (see Diller, 1887; Haupt, 1967; Brown, 1977). This interpretation is primarily based on the extent of relict pyrope and ilmenite left over in the soil from weathered kimberlite.

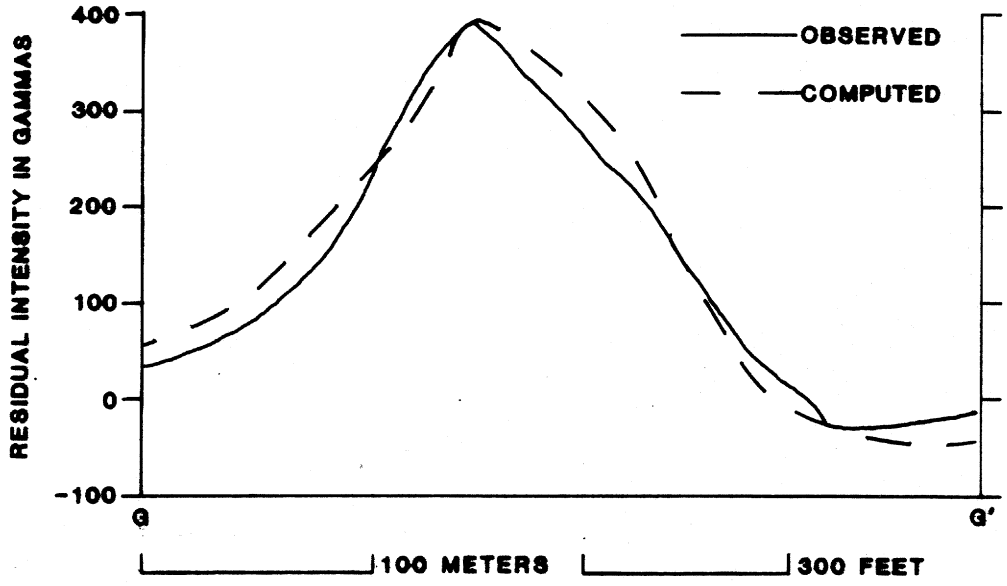

Figure 29. K3 anomaly: observed and computed profiles along G–G'.

This study does not support the latter view. An arcuate belt of four small kimberlite pipes is presented here as the cause of the anomaly patterns in the K area. Modeling indicates that the walls of the pipes are vertical.

Harvey (1980, p. 89) concludes the kimberlite "… could be described as a slab of strongly magnetized ultramafic rock 665 feet thick intruding into essentially nonmagnetic country rock." Harvey's conclusion was based on an aeromagnetic survey centered close to the kimberlite breccia outcrop.

This study does not support the view of the kimberlite as a slab either, but Harvey's thickness of 665 feet does compare well with the depths determined in the modeling of this study. These depths should be regarded with caution. The resolving power of the modeling method for the bottom edge of an intrusive diminishes proportionally to the square of the distance to that bottom edge. Although the values determined for the total thicknesses of the pipes satisfied the modeling requirements, it is possible the intrusives extend down to their source area in the mantle. The roots may be rather narrow and undetectable in the field measurements.

The following values represent the averages of the remanent components used in modeling the four pipes:

Jn=0.0103 gauss, D=332°, I=+33°

The bulk properties of this pipe belt can be described as having a remanent magnetic intensity of approximately 0.01 gauss. The direction of the remanent vector is north–northwest at a low angle.

The G1 Anomaly

The observed field map for the G1 anomaly is shown in Figure 35. A residual high, over 800 gammas, is present in the southeast sector. This high is probably due to a satellite body near the main rock mass causing the G2 anomaly, and not considered in modeling.

A dike with vertical sides is the interpretation for the model presented in Figures 36 through 38. The strike of the dike is N45°E. The top of the dike is level at 610 feet (185 meters) above sea level along the northern half. Along the southern half, the top slopes down to an elevation of 460 feet (140 meters) at the southern edge. The following measurements were used to create this model:

top contour: length=113 meters, width=29 meters

intermediate and bottom contours: length=224 meters, width=29 meters

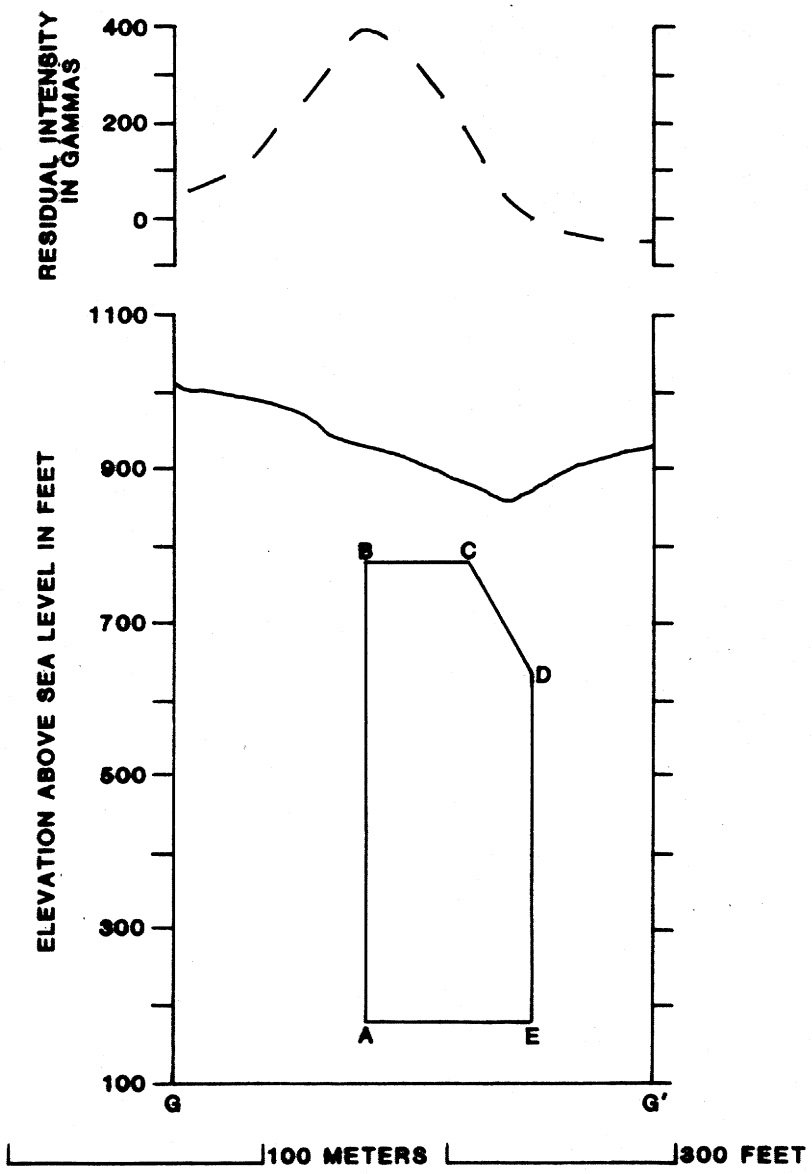

vertical exaggeration = 1X
ABCDE - plane of model under G-G'
——— topographic expression along G-G'
- - - computed profile along G-G'

Figure 30. K3 anomaly: model position, topographic expression, and computed profile along G–G'.

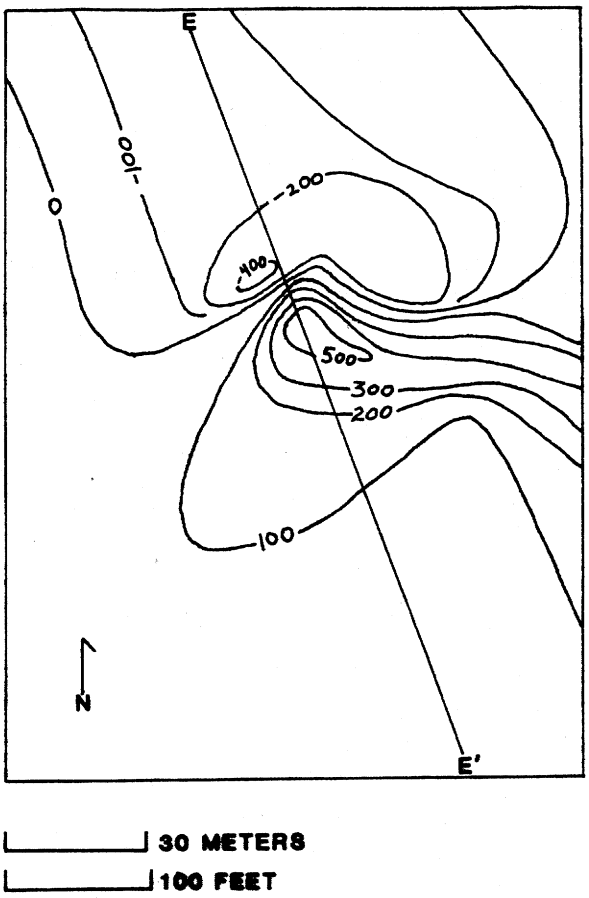

Figure 31. K4 anomaly: observed residual intensity map (in gammas).

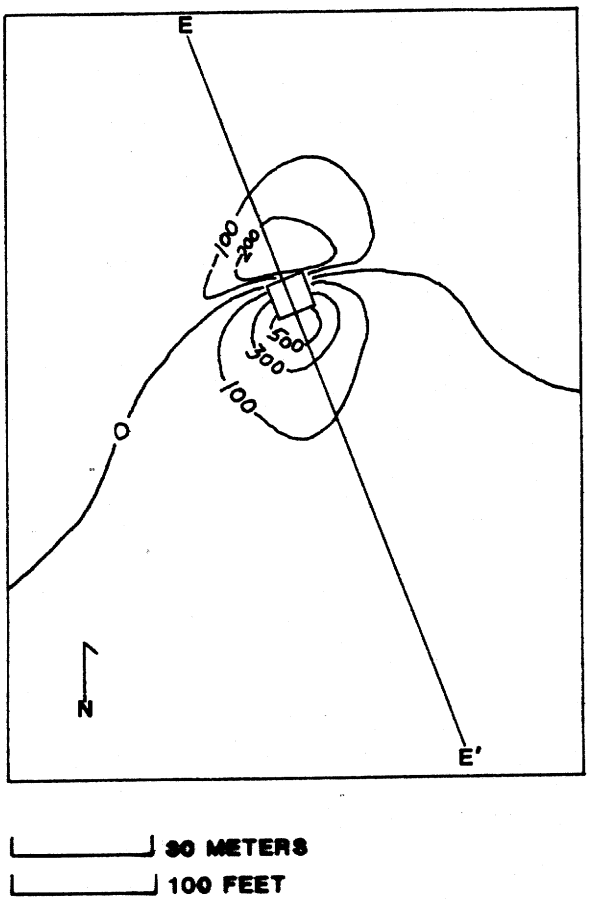

Figure 32. K4 anomaly: computed residual intensity map (in gammas).

total thickness=181 meters

Jn=0.0165 gauss, D=052°, I=+10°

The Jn used in modeling was the same Jn found for the massive kimberlite outcrop sample. The D and I values are in close agreement with the outcrop sample.

A small magnetic high exists west of the magnetic high located on profile G–G'. The smaller high was not involved in modeling. It could be the result of a digitation or satellite body adjacent to the dike.

Another model for the G1 anomaly is presented to illustrate the advantage of comparing computed field maps (see Figures 39 and 40). The model would be interpreted as a slightly elliptical pipe with vertical sides defined by these parameters:

top and bottom contours: length=105 meters, width=90 meters

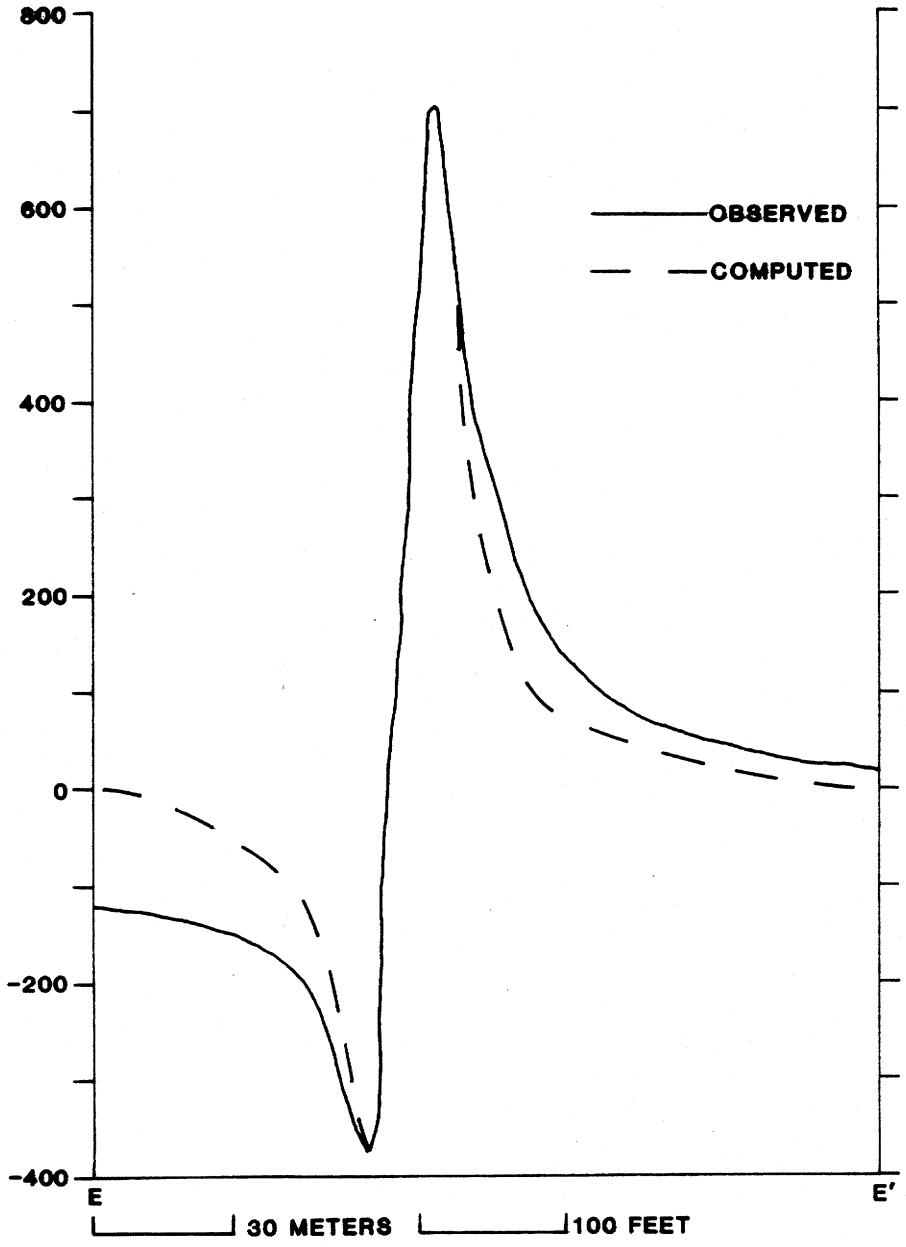

Figure 33. K4 anomaly: observed and computed profiles along E–E'.

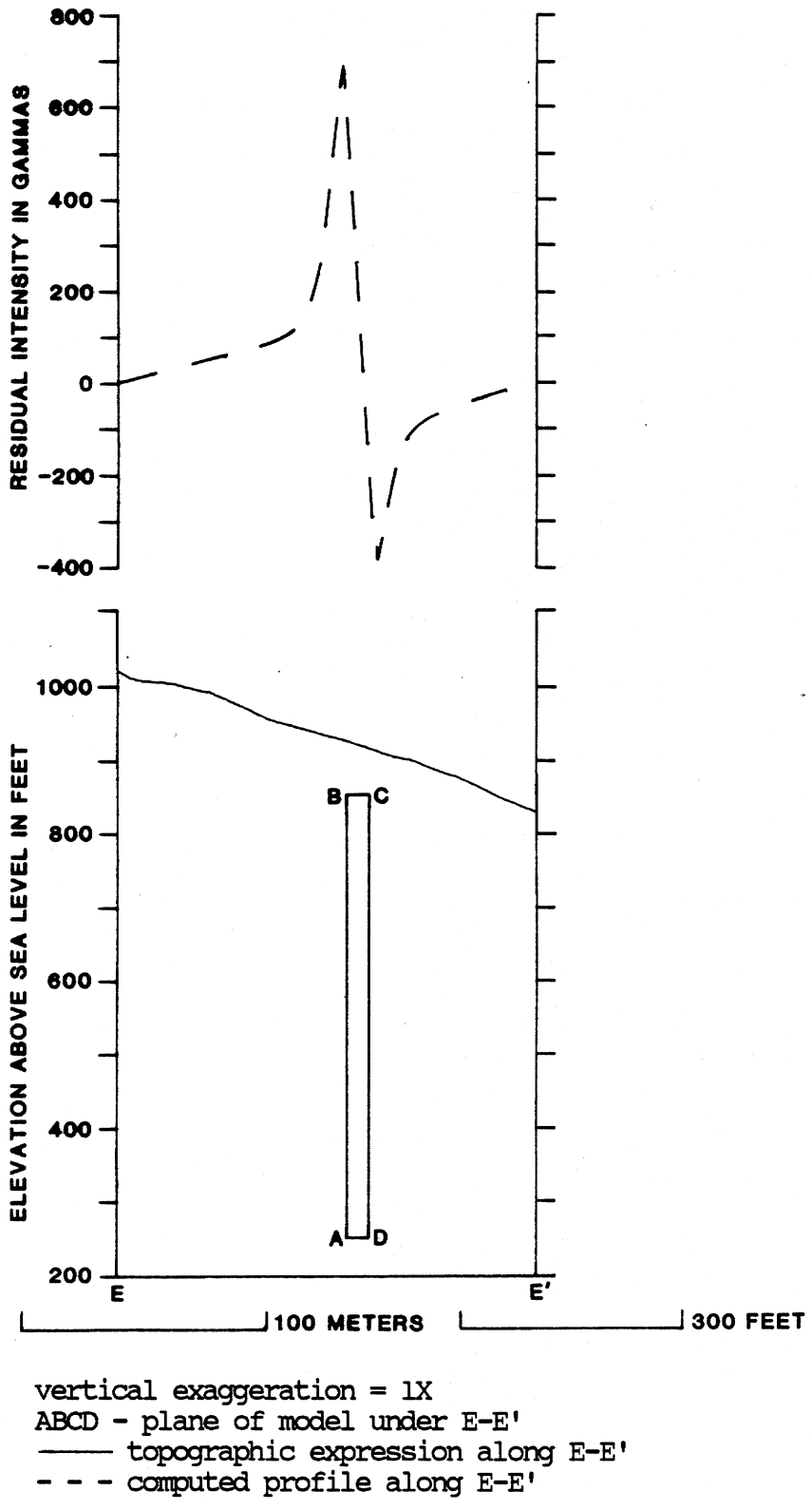

Figure 34. K4 anomaly: model position, topographic expression, and computed profile along E–E'.

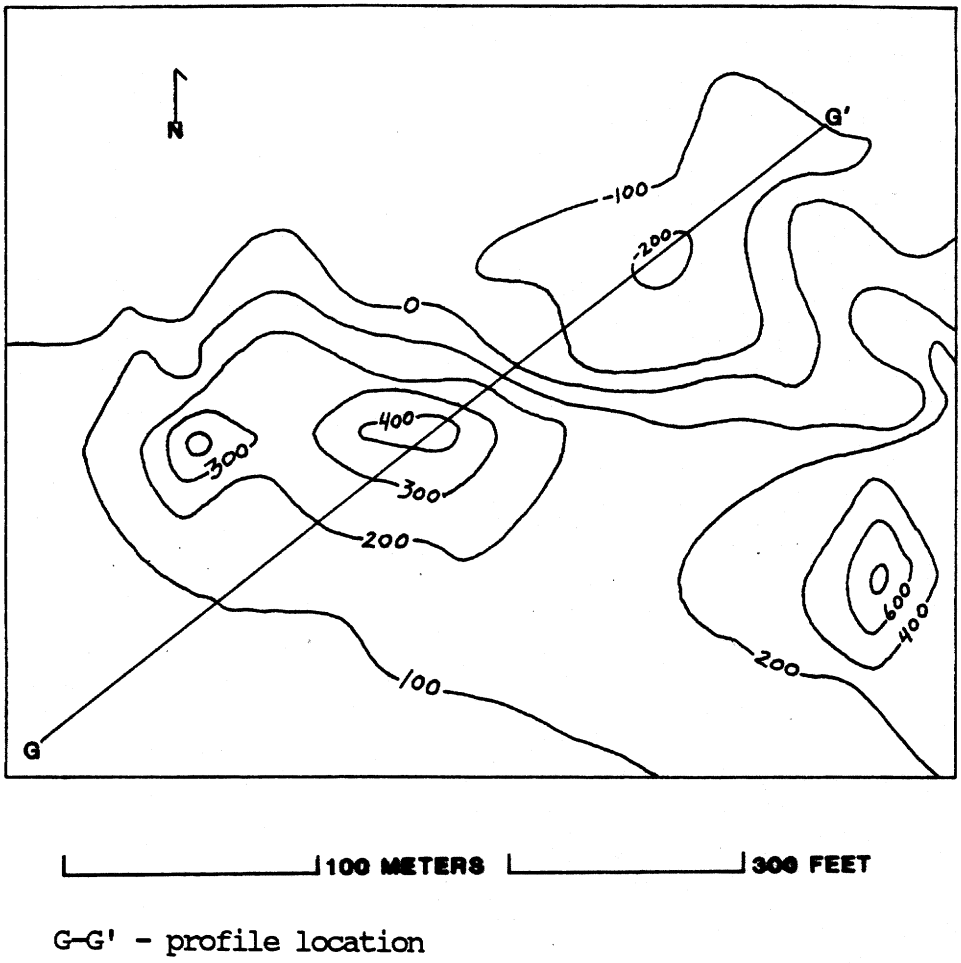

Figure 35. G1 anomaly: observed residual intensity map (in gammas).

total thickness=182 meters
Jn=0.0168 gauss, D=052°, I=+10°

Using a two-dimensional profile comparison (Figure 40), the model would appear acceptable; however, the contour pattern on the computed residual intensity map (Figure 39) was considered too wide, so the model was refined.

The G2 Anomaly

A very thin dike with vertical sides is proposed to be the cause of the G2 anomaly. The dike strikes N8°W. Figures 41 and 42 show the observed and computed field maps. The top of this dike is irregular. The highest part is directly under the slope between the high and low peaks of the anomaly curve (see Figure 44).

The dike was modeled using the following parameters:
top contour: length=31 meters, width=9 meters
intermediate and bottom contours: length=226 meters, width=9 meters
total thickness=180 meters
Jn=0.017 gauss, D=060°, I=+68°

The only value used in modeling that does not fit well with the massive kimberlite outcrop sample is the inclination. An I=+68° was necessary to reproduce the residual high peaking over 800 gammas. As

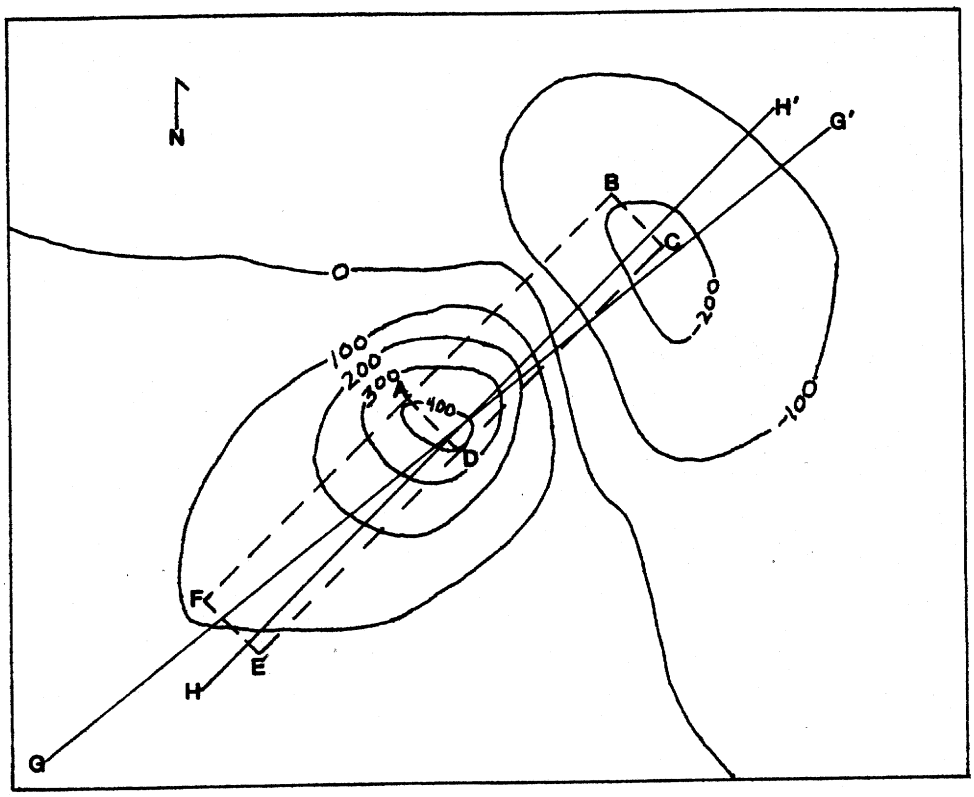

G-G' - profile location for figure 37
H-H' - profile location for figure 38
ABCD - upper contour for dike model
FBCE - lower contour for dike model
Jn = 0.0165 gauss
D = 52°
I = +10°

Figure 36. G1 anomaly: computed residual intensity map for dike model (in gammas).

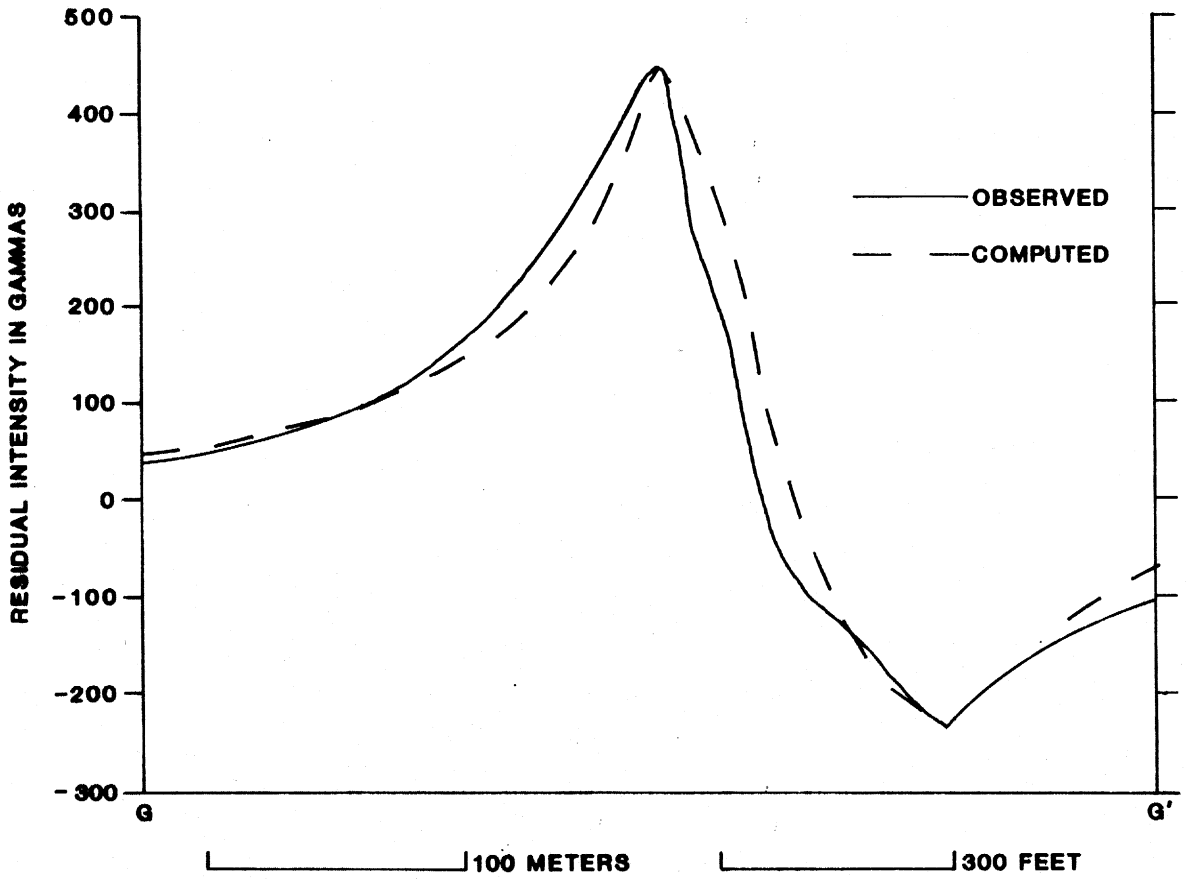

Figure 37. G1 anomaly: observed and computed profile for dike model along G–G'.

with the K2 anomaly, a larger suite of outcrop samples and possibly oriented drill-core samples need to be examined in the lab to reconcile the differences.

The G3 Anomaly

The model generated for the G3 anomaly is the largest of all the models. The observed field map is shown in Figure 45. Two profiles were chosen for comparisons because of the extreme width of this anomaly.

Although the computed field map displays a much more symmetrical contour pattern than the observed map, reasonably good fits were achieved for both sets of profiles (see Figures 46 through 48). Graphic comparisons between the model position, topographic expression, and computed profile were prepared for each profile location (see Figures 49 and 50).

A large elliptical pipe with vertical walls and an irregular top is the interpretation of this model. The bulk of the model consists of a pentagonal-shaped prism. A rectangular prism (long axis is east–west) forms the top level. This configuration was used to satisfy the irregular contour pattern on the observed intensity map. The model was constructed as follows:

top contour: length=116 meters, width=91 meters
intermediate and bottom contour (refer to Figure 52):
 sides KJ, JN, MN=191 meters
 side KL=119 meters
 side LM=128 meters
total thickness=182 meters

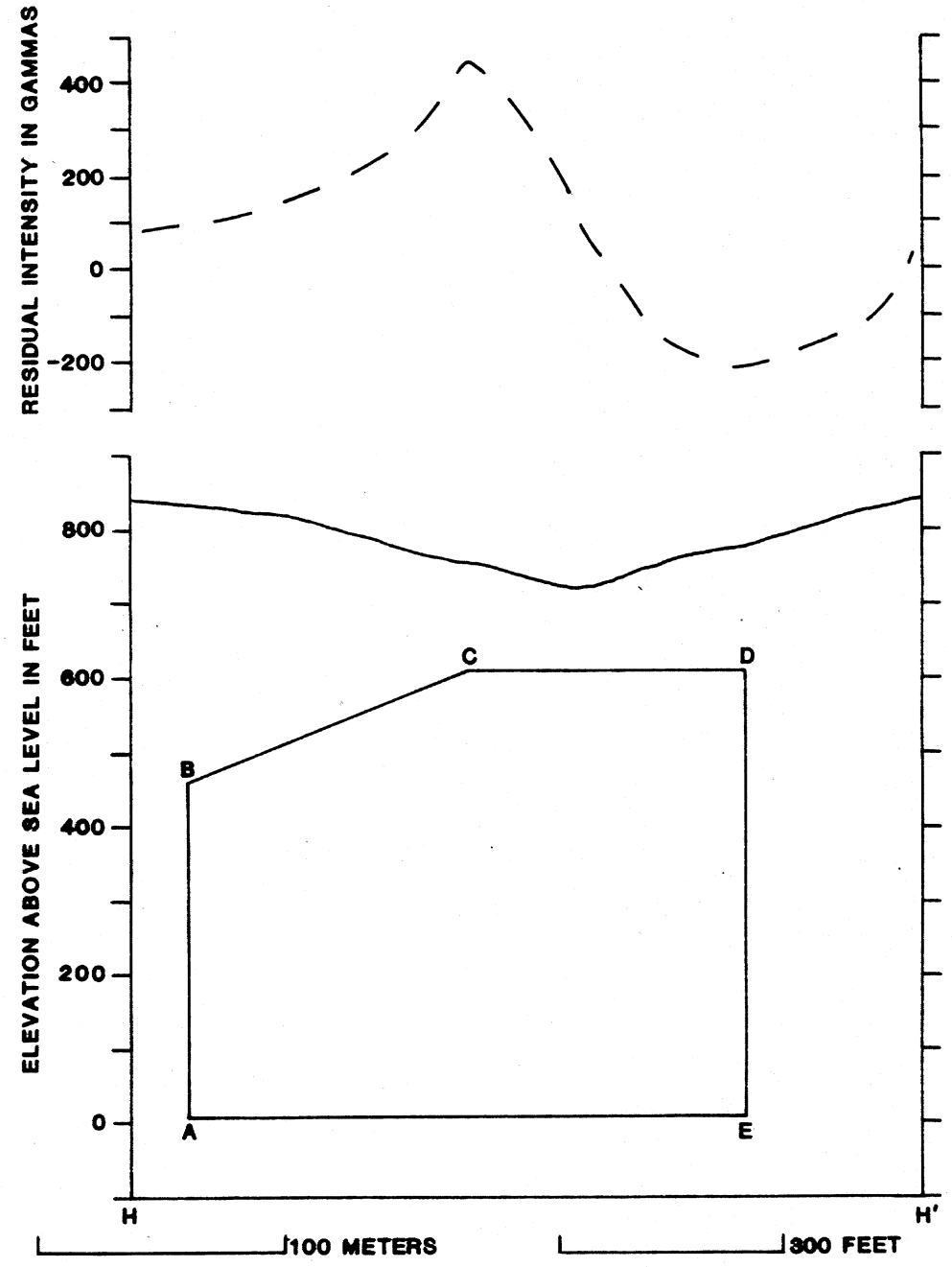

Figure 38. G1 anomaly: model position, topographic expression, and computed profile for dike model along H–H'.

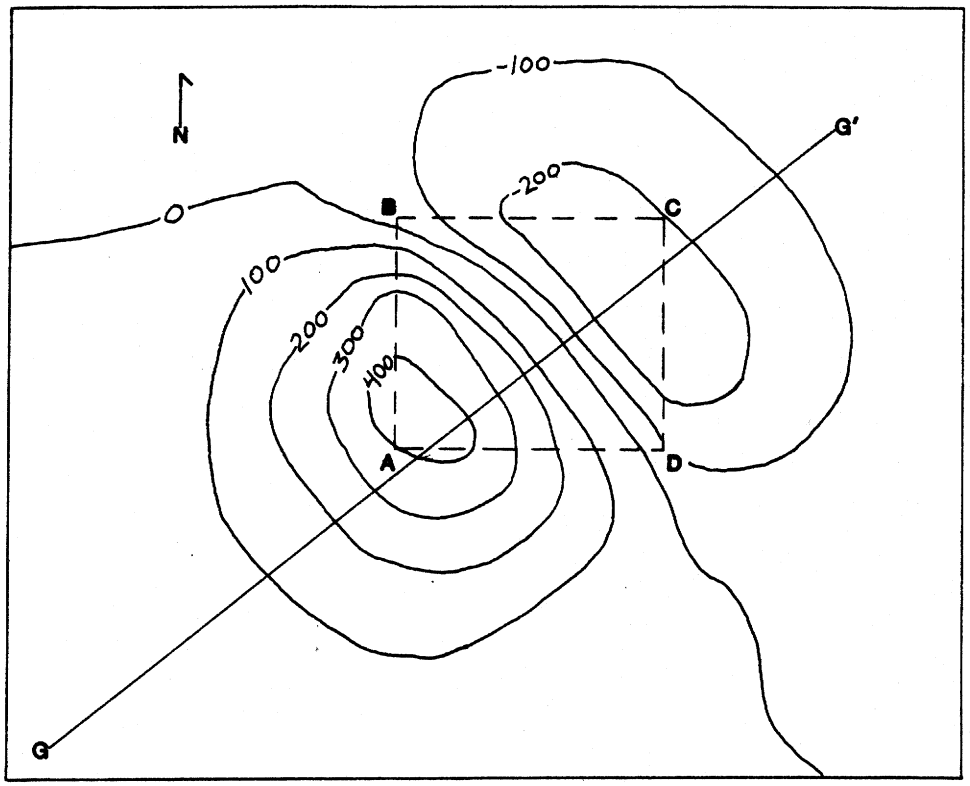

Figure 39. G1 anomaly: computed residual intensity map for pipe model (in gammas).

Jn=0.0057 gauss, D=014°, I=+68°

The remanent magnetic components used to model this anomaly do not compare well with the values obtained from the massive kimberlite outcrop sample. A more appropriate comparison would be with an oriented sample from the G3 pipe, but no fresh outcrop was found in this vicinity.

Twice in its history, the G3 pipe was mined for diamonds. Shortly before 1910, the pipe was open-pit mined, and shafts were sunk to intercept other portions (Crandall, 1910, p. 86–89). More trenching was done from 1965 to 1970. The trenched material was washed through a sluice box (Brown, 1977). Undoubtedly, the kimberlite in the upper portion of the pipe became disoriented due to brecciation and movement of material as a result of mining activities. It is proposed that this disturbed upper portion accounts for the irregular magnetic anomaly pattern on the observed map.

The P1 Anomaly

The P1 anomaly was fairly simple to model. The observed field map is shown in Figure 51. A dike with vertical sides striking N33°E is the interpretation for the model displayed in Figures 52 through 54.

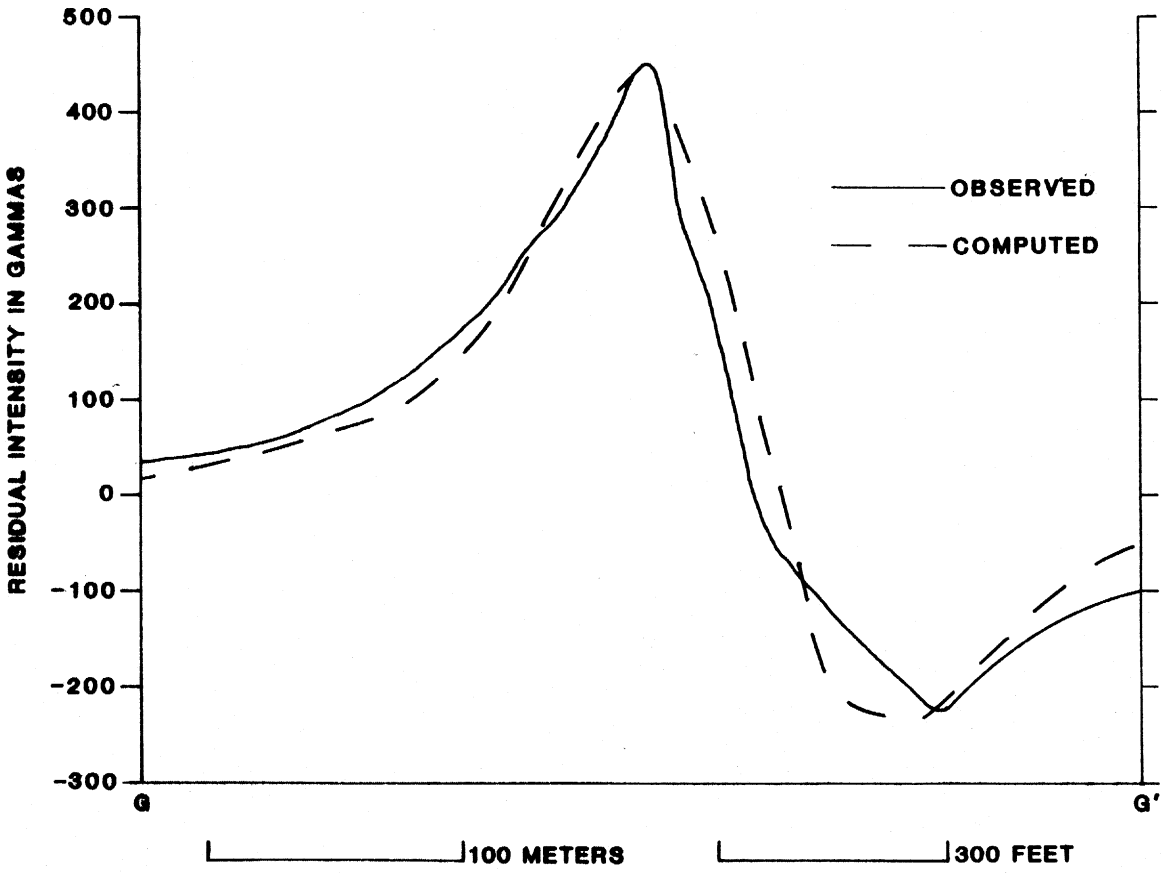

Figure 40. G1 anomaly: observed and computed profile for pipe model along G–G'.

This dike bears some similarity to the G1 dike. The top of the northern half is level at 600 feet (182 meters) above sea level. The southern half slopes down to 380 feet (115 meters). The parameters used to produce this model are given below:

top contour: length=104 meters, width=20 meters
intermediate and bottom contour: length=240 meters, width=20 meters
total thickness=182 meters
Jn=0.0151 gauss, D=044°, I=+41°

The P2 Anomaly

The observed and computed intensity maps for the P2 anomaly are shown in Figures 55 and 56. A small residual high peaking over 300 gammas borders the northern edge of the observed map. This small high was not included in modeling. A small, thin, north-trending dike may be the cause of this anomaly.

The model for the P2 anomaly is presented in Figures 56 through 58. It is interpreted as a north-striking dike with vertical sides. The top is level at 600 feet (182 meters) above sea level and positioned directly under the high of the anomaly curve. The north and south edges slope down to 450 feet (137 meters). This model was made using the following dimensions:

top contour: length=60 meters, width=13 meters
intermediate and bottom contours: length=195 meters, width=13 meters
total thickness=182 meters
Jn=0.0165 gauss, D=048°, I=+68°

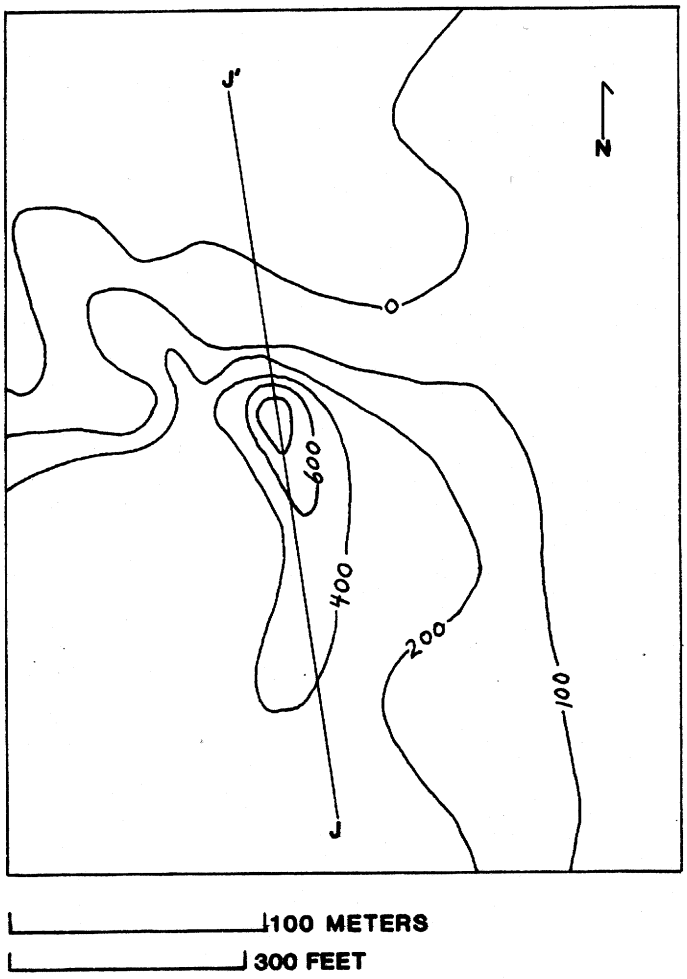

Figure 41. G2 anomaly: observed residual intensity map (in gammas).

On the observed map it can be seen that the residual high used in modeling is surrounded by residual lows on the west, north, and northeast. A declination of 048° was chosen because it passes through the residual low containing the lowest magnetic intensity values.

There were no outcrops in the P area. This limited comparisons between the remanent components used in modeling the P anomalies and remanent components derived from oriented samples. However, the remanence used to model the P anomalies compare well with each other, and fairly well with the G models. Of the two available outcrop samples, the P area models compare best with the massive kimberlite sample.

Summary of the G and P Areas

No previous investigation, known to the author, has ever indicated the presence of kimberlite in the G1 area. Magnetic modeling suggests that a dike exists in this vicinity. Only subsurface drilling can substantiate the existence of this proposed body.

Earlier studies of the G2 and G3 areas differ. Haupt (1967) interpreted the kimberlite in this area as one continuous dike trending north–south for 2,100 feet (638 meters). Bolivar (1972) concluded that the kimberlite at these localities represents separate pipes.

This investigation supports the interpretations discussed in Crandall's 1910 report. Crandall was present when the G3 area was excavated for diamonds shortly before 1910. Crandall reported (1910, p. 87) "Excavations recently made show that the hard refractory portions of the dike are narrow wall-like intrusions in a large crater-shaped mass of peridotite or kimberlite…." Crandall (1910, p. 88) also noted "… an arm-like extension…" trending north from this exposed crater.

If the G2 dike is projected past the southern boundary of the computed field map (see Figure 42), it will intersect the northern portion of the G3 pipe. An anomaly south of the G2 anomaly and just north of the G3 which was not modeled lends support to this idea (see Map 1). This situation closely resembles Crandall's (1910) interpretation of a crater-shaped mass with a northward extension.

Anomalies in the P area point to the presence of at least two thin dikes. A dike in the P1 area was indicated on the Willard geologic quadrangle (Brown, 1977), and by Crandall (1910). It is possible the P1 dike extends past the southern boundary of the P1 computed map.

No evidence of an intrusive in the P2 area was shown on the Willard geologic quadrangle. Haupt (1968) reinvestigated this area because Diller (1887) suggested there was a northeast offshoot from the G3 intrusive based on pyrope and ilmenite in the soil. After covering the area thoroughly, Haupt claimed to have found no trace of kimberlite east of the G3 area.

A dike comparable in size to the P1 dike was modeled in the P2 area. The anomaly pattern on Map 1 (rear pouch) suggests a pair of en echelon dikes striking in a northerly direction exists in this region. The P2 dike may separate into two branches beyond the southern boundary of its computed field map (see Figure 56).

The G and P areas were discussed together because of similarities in the remanence used for modeling in these regions. The average remanent strength and direction for the five models in the G and P areas is:

Jn=0.0142 gauss, D=044°, I=+51°

The intrusives have an average remanent magnetic intensity just over 0.014 gauss. The direction of the remanent vector is northeast at a moderate inclination. The total thicknesses used for models in the G and P areas are between 180 to 182 meters. These depths should be regarded with caution for the same reasons cited for the intrusives in the K area (see p. 43, this study).

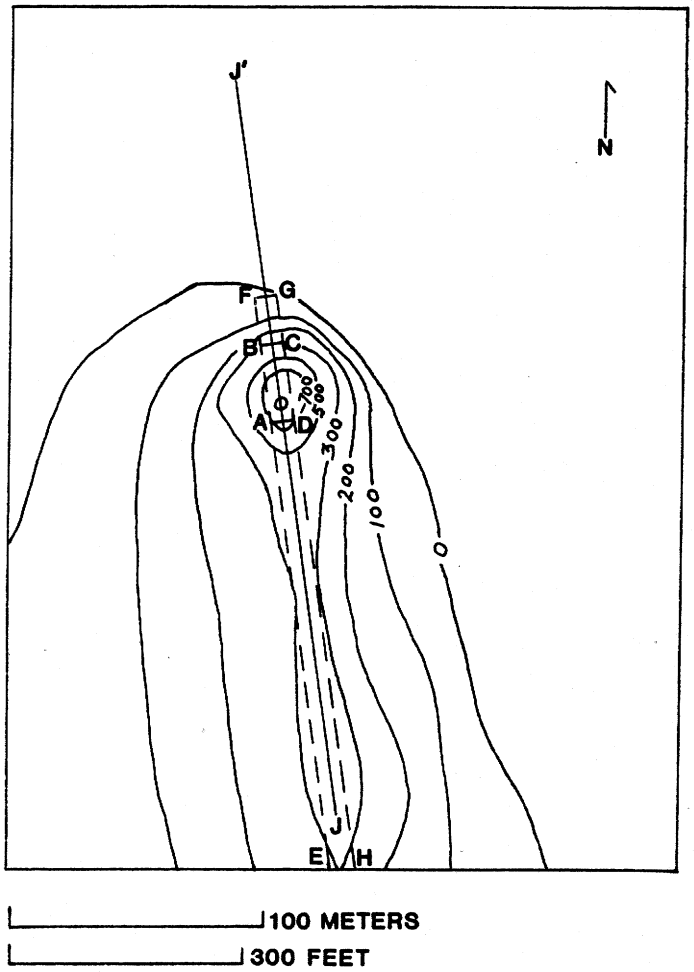

Figure 42. G2 anomaly: computed residual intensity map (in gammas).

Relation of Intrusives to Regional Structure and Theory of Emplacement

The intersections of major transverse structural features have played an important role in the emplacement of kimberlites and other intrusives. This seems likely for intrusions located within the Appalachian Plateau and intracratonic region. Parrish and Lavin (1982) showed that the two known kimberlite intrusions in Pennsylvania are located at cross-structural lineament intersections. The structural features involved with the Pennsylvanian kimberlites are the Rome Trough and structure-parallel faulting transverse to the latter. Parrish and Lavin (1982, p. 344) claimed that "… this model of kimberlite intrusion can also be used to explain the location of known New York kimberlites."

The relationship between major fault zones and ore deposits located along a structure called the 38th Parallel Lineament was studied by Heyl (1972). He noted several major mining districts and many noncommercial mineralized zones were located at or adjacent to the intersections of this lineament and major transverse structural features. Examples include the Illinois-Kentucky Fluorspar District, which occurs at the intersection of the lineament with the New Madrid Fault Zone and the Hicks Dome. This area contains over 50 peridotite dikes, oval-shaped kimberlite intrusions, and explosion breccias. The Central Kentucky Mining District is located near the junction of the Cincinnati Arch and the portion of

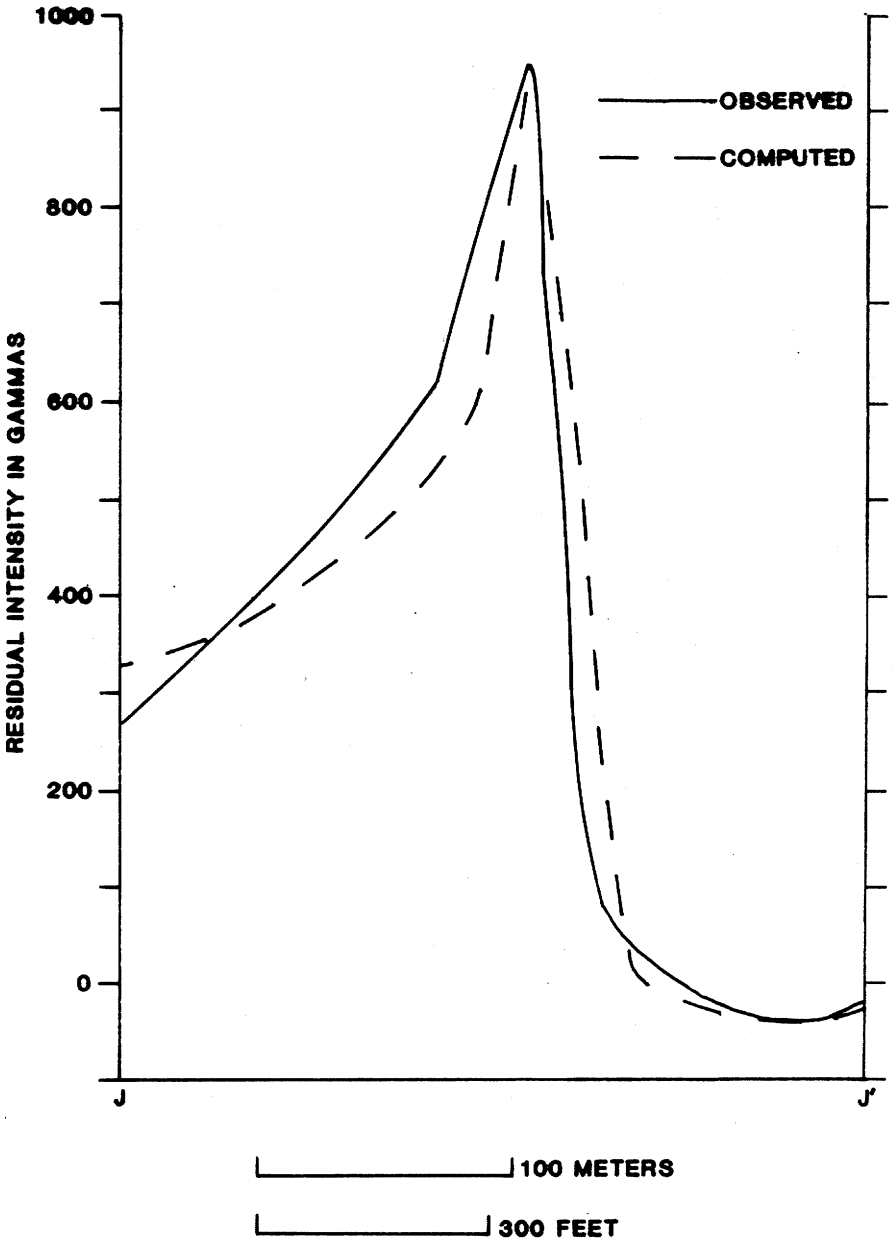

Figure 43. G2 anomaly: observed and computed profiles along J–J'.

the lineament passing through central Kentucky. Veins have been mined here for fluorite, barite, galena, and sphalerite (Heyl, 1972).

Approximately 20 kilometers southwest of the Elliott County intrusives, the axis of the Waverly Arch (Woodward, 1961) crosses the Kentucky River Fault System. The Kentucky River Fault System has been recognized as a surface expression of faults bordering the northern side of the Rome Trough (Ammerman and Keller, 1979; Dever, 1980; Ettensohn, 1980). Considering the aforementioned theories, it is reasonable to suspect the intersection of the Waverly Arch with the Rome Trough had a profound influence on the emplacement of the intrusives.

The Kentucky River Fault System, the Waverly Arch, and the surface fracture pattern have separately received attention as factors that controlled the intrusion. Based on random field measurements,

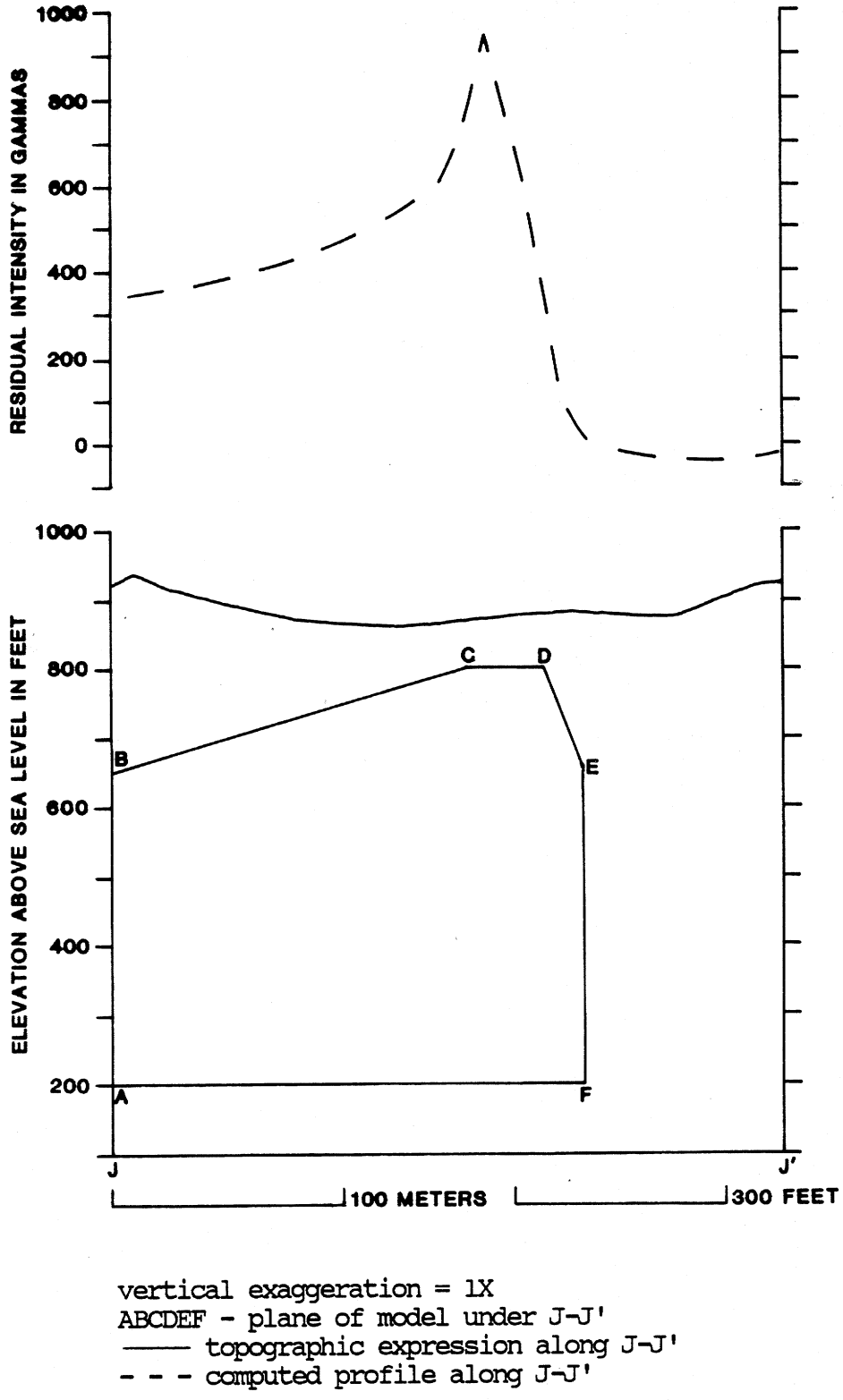

Figure 44. G2 anomaly: model position, topographic expression, and computed profile along J–J'.

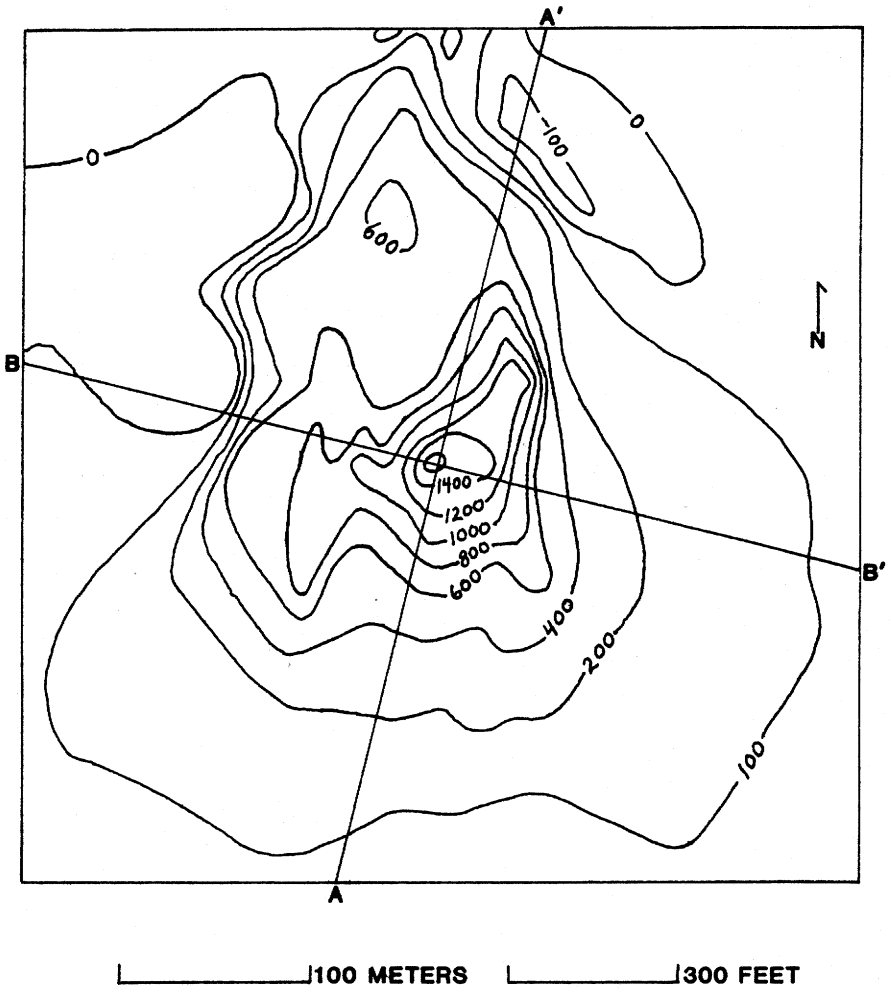

Figure 45. G3 anomaly: observed residual intensity map (in gammas).

Haupt (1968) believed that the magma intruded through tension fractures related to a dominant vertical joint system with orientations of N27–34°E and N56–63°W. Sanderson and Duba (1975) correlated the apparent strike of the intrusives, a north–south joint set, and the orientation of the Waverly Arch as indicators of a regional weakness in the basement. They (Sanderson and Duba, 1975, p. 111) proposed "… that the magma found its way into the Pennsylvanian host rocks via north–south fractures in the basement." This writer believes that all three structural features played a role in guiding the kimberlitic magma through the crust.

This study has shown that the Elliott County kimberlites contain about 3 percent pyrope garnet. The presence of this high-pressure mineral in an ultramafic composition indicates the magma originated at a depth of at least 80 kilometers (Dawson, 1967). For the kimberlite to be exposed at the surface in Pennsylvanian rocks requires an avenue of movement to have penetrated the uppermost mantle. The question is which structural element is most likely to have produced a route for the intrusives.

From a depth of 80 km and a distance of 20 km off the Kentucky River Fault System–Waverly Arch Axis intersection, magma would have had to migrate to the surface at an average angle of 14° from a

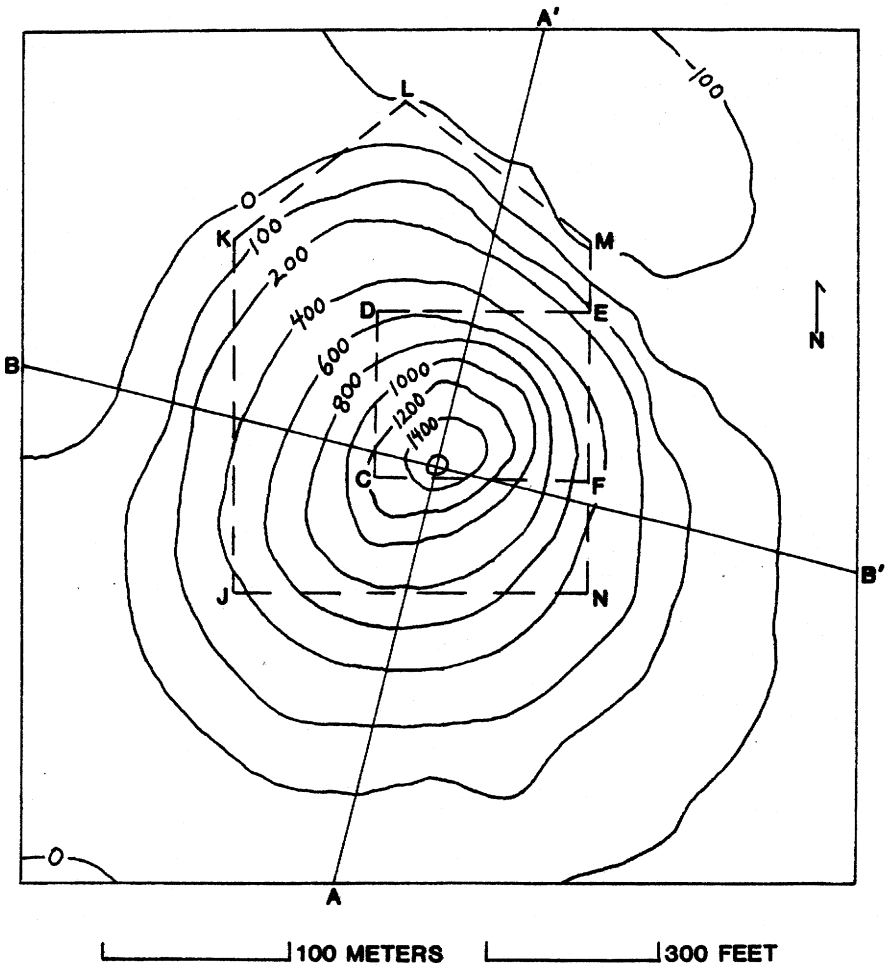

Figure 46. G3 anomaly: computed residual intensity map (in gammas).

vertical line. This does not seem an unreasonable ascent trajectory for the magma. If the magma were generated deeper, the ascent would be steeper (closer to vertical) than the 14° angle.

As discussed earlier, the major subsurface features in the vicinity of the intrusives are the north–south-trending Waverly Arch and the east–west fault zone belonging to the Rome Trough. Although a northeast–northwest joint system was identified in this study, it is unlikely that deep tension fractures related to this system provided a pathway for the intrusives. Structural factors imparted by the formation of the Waverly Arch probably aided the magma's advance into the stratigraphic column, but there is insufficient support that the magma rose through the basement rocks via north–south fractures.

The journey of the intrusives probably began through the east–west faults bordering the northern side of the Rome Trough. Ammerman and Keller (1979, p. 350) said "… the trough is asymmetric in that

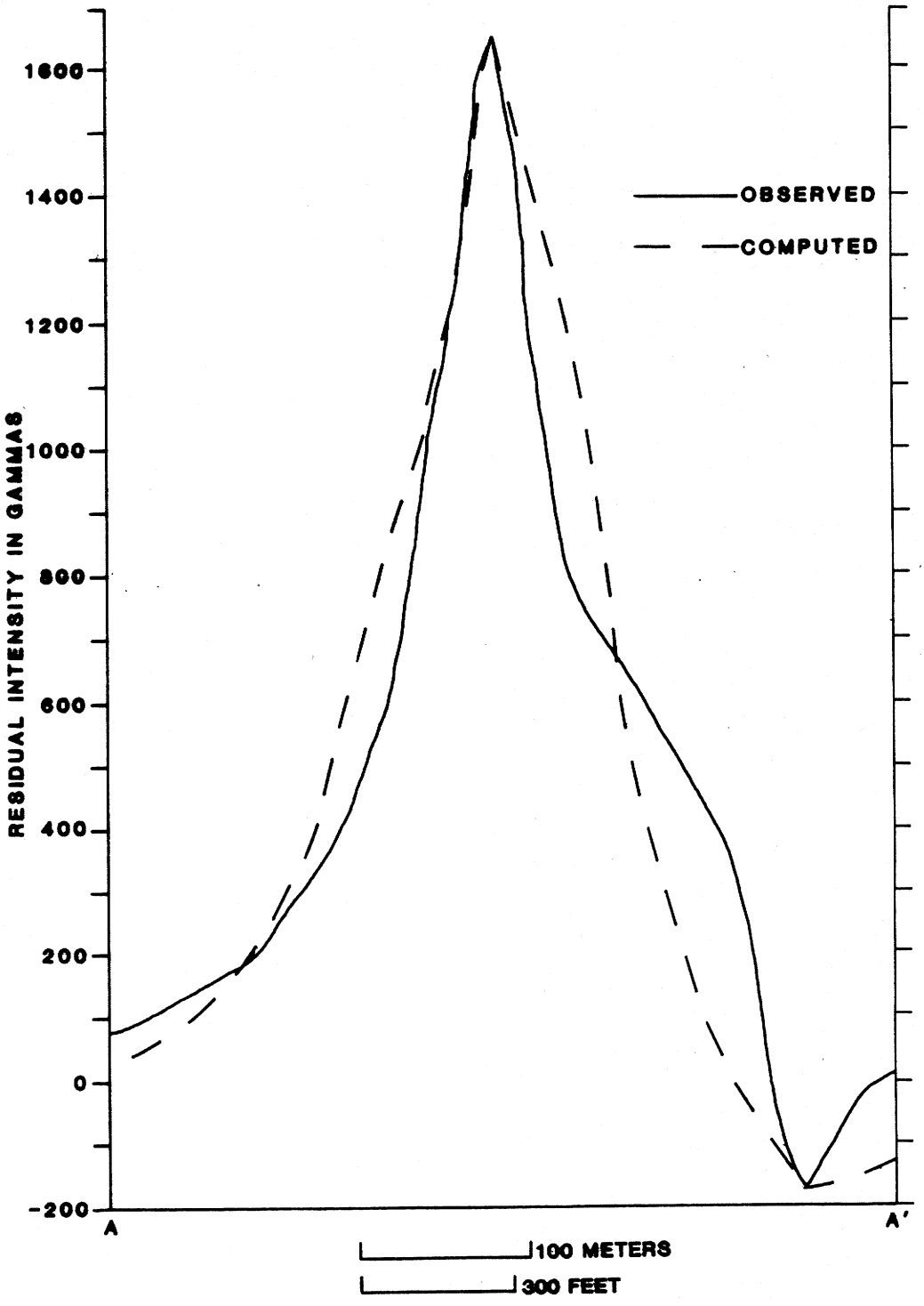

Figure 47. G3 anomaly: observed and computed profiles along A–A'.

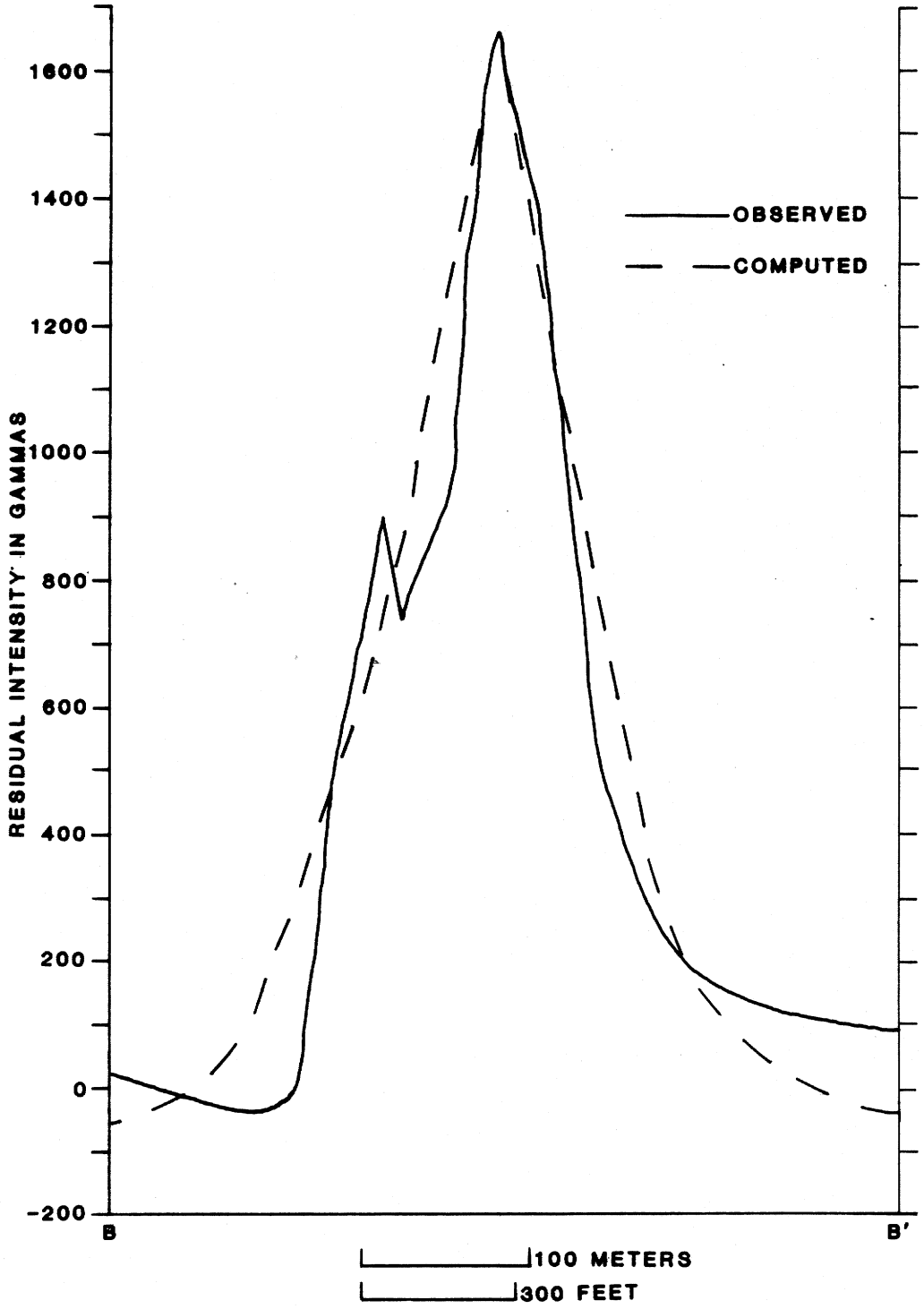

Figure 48. G3 anomaly: observed and computed profiles along B–B'.

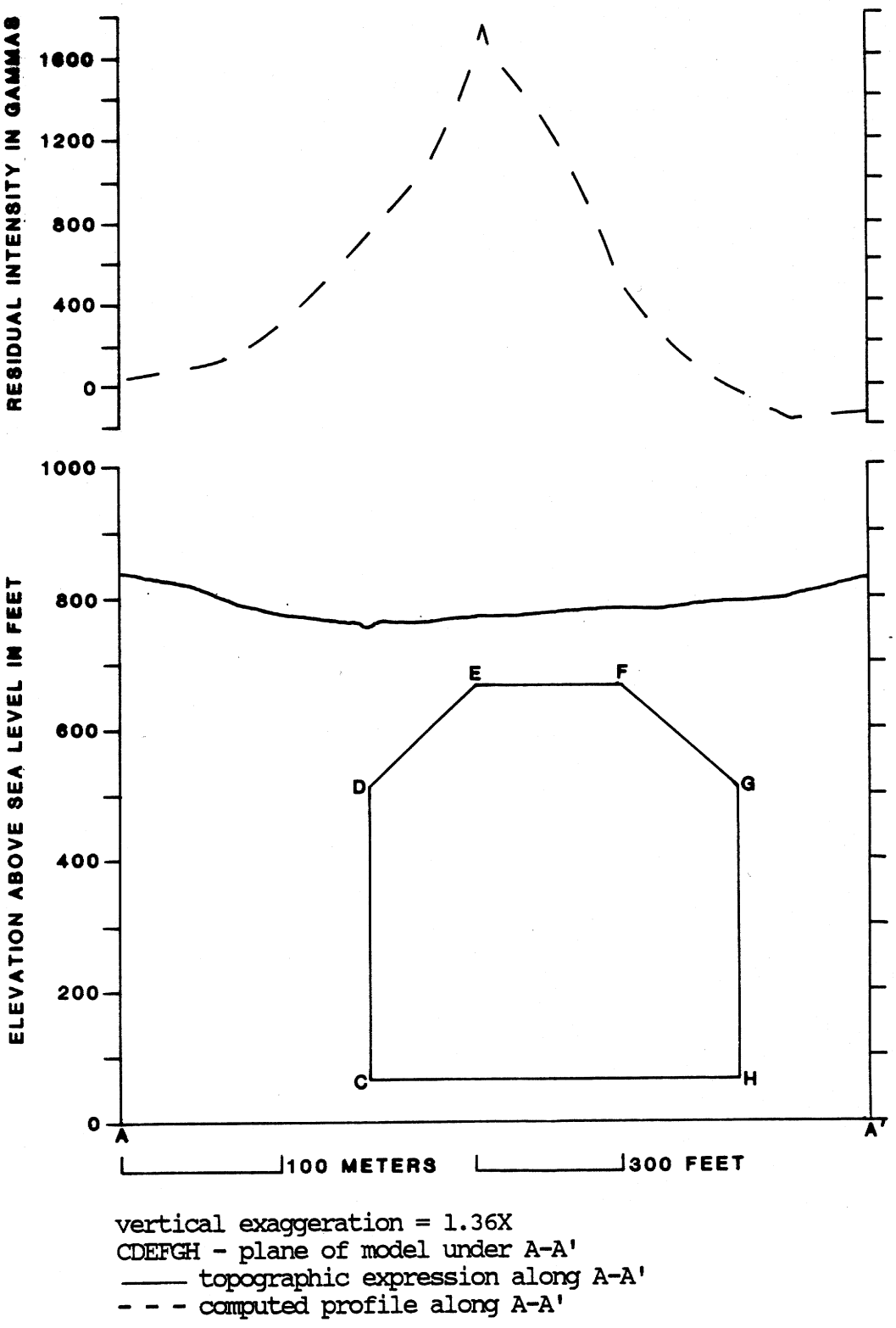

Figure 49. G3 anomaly: model position, topographic expression, and computed profile along A–A'.

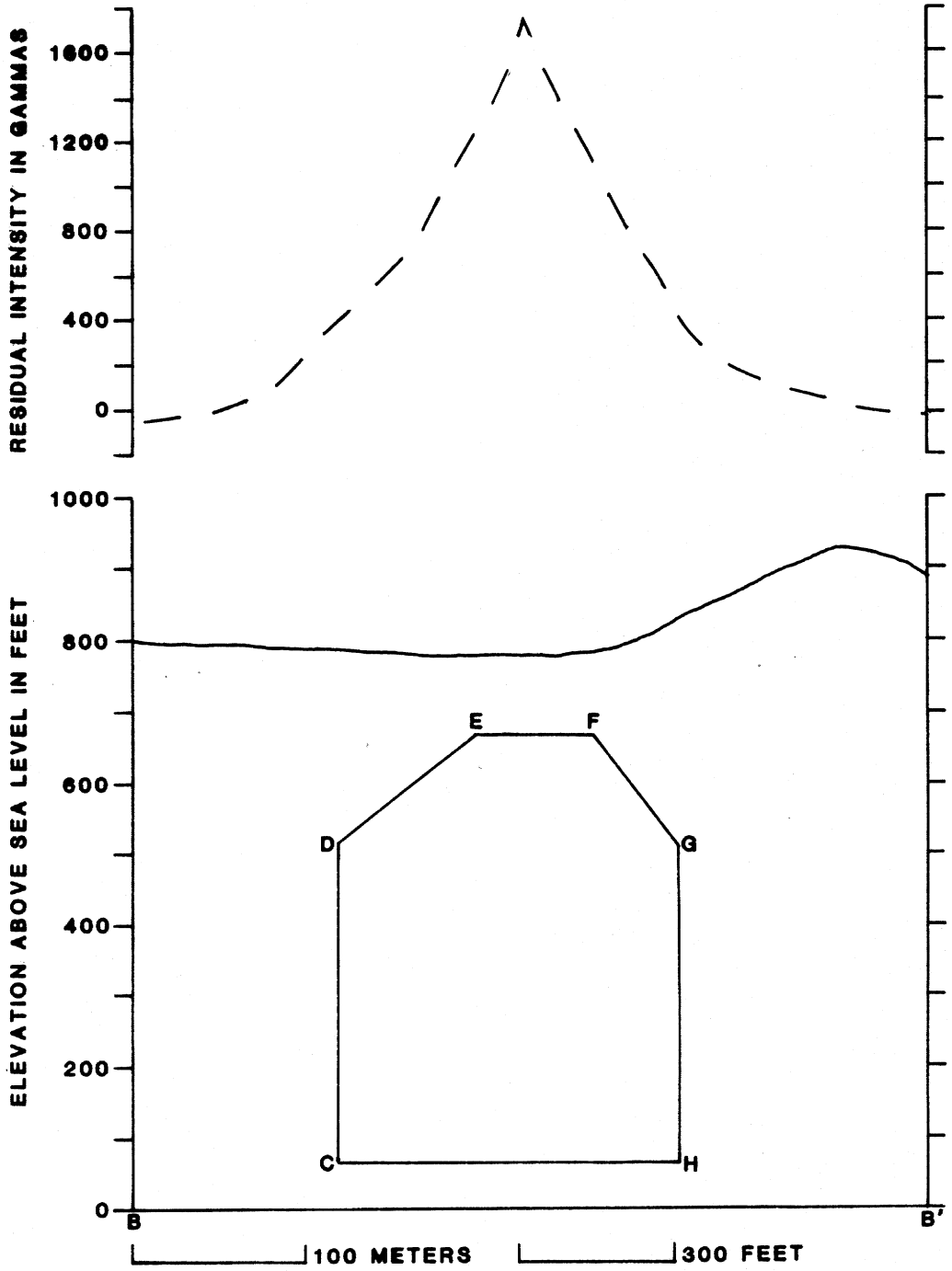

Figure 50. G3 anomaly: model position, topographic expression, and computed profile along B–B'.

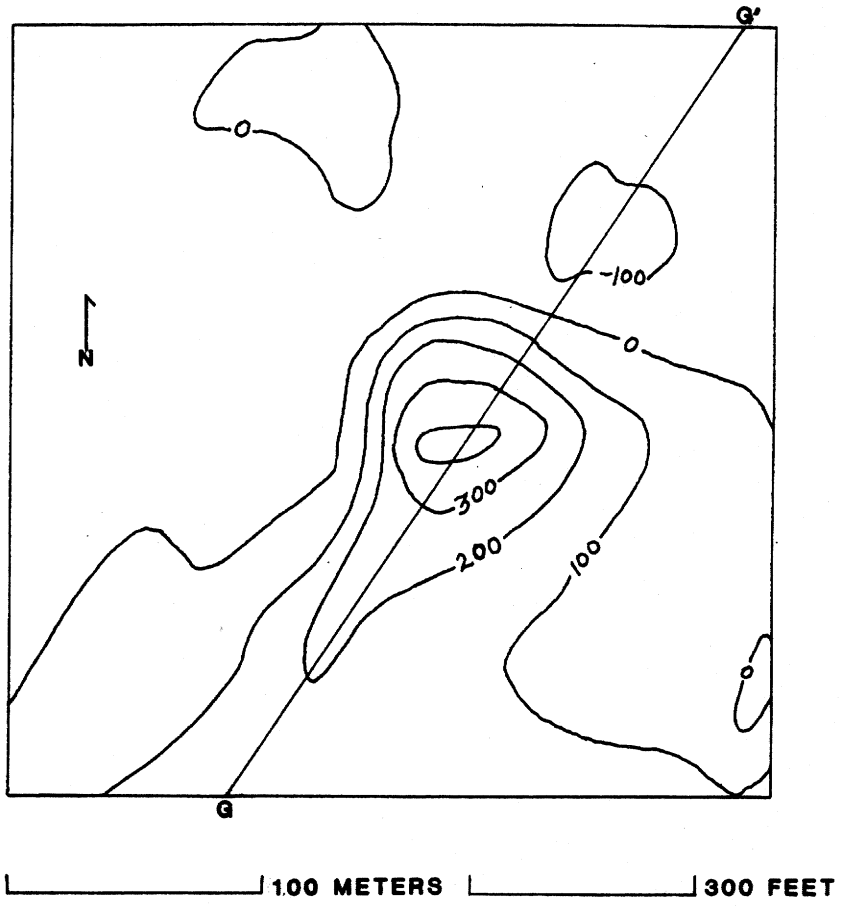

Figure 51. P1 anomaly: observed residual intensity map (in gammas).

the throw along faults forming the northern boundary is, in general, much greater than along faults forming the southern boundary." They noted the displacement along one of these faults northeast of the intrusives was over 1,200 meters. These fractures are suspected by this writer to have given the magma a route through the basement rocks by penetrating the uppermost mantle.

Bolivar (1972) presented strong petrographic evidence that the magma intruded through a series of pulses. It came to rest in intermediate chambers until volatile gases built up enough pressure for the next advance. Bolivar (1972, p. 49) mentioned that "… the magma reached an intermediate chamber(s) which was ultimately contained under impermeable cap of sedimentary rock." This author believes that after the magma reached the intermediate chamber under sedimentary rock, it burst through the junction of the Waverly Arch and Kentucky River Fault System. This junction should have crated a weak point in the sedimentary cap. Close to the surface, the magma had a variety of paths to intrude. These paths were formed by the two orthogonal joint sets described in the Lineament Survey section (this study). Of the four dikes modeled in this study, two trend north–south, and two northeast. This is an indication that the magma followed the north–south and northeast fracture sets at shallow depths. Many cross-cutting fractures were available to provide loci for pipe formation.

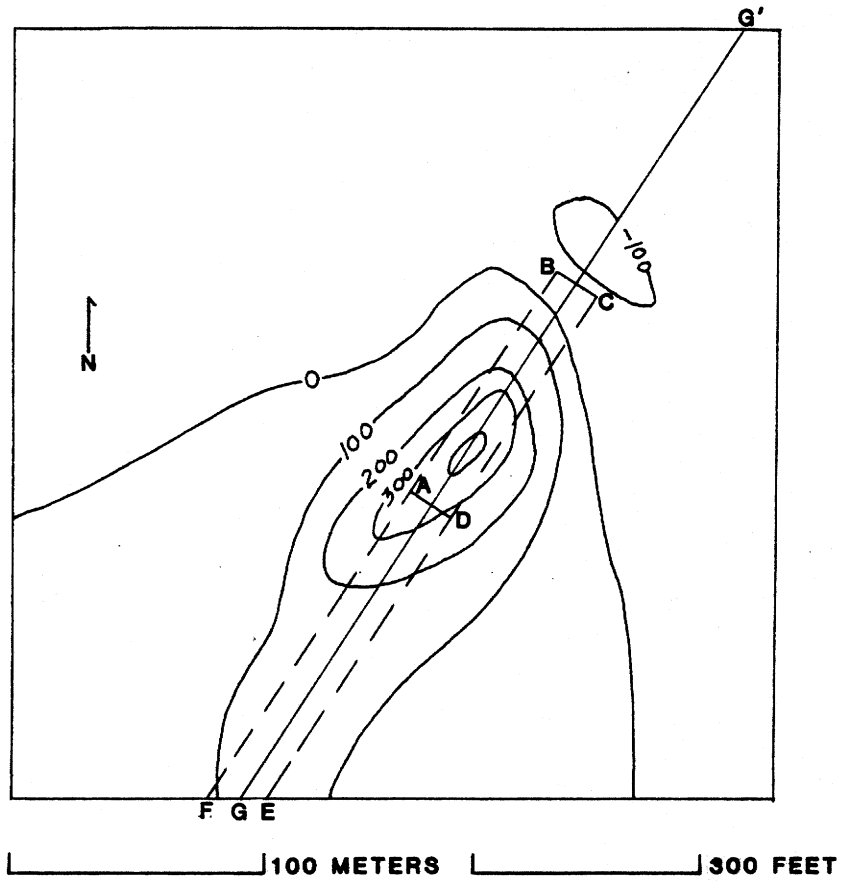

Figure 52. P2 anomaly: computed residual intensity map (in gammas).

Age of Intrusives and Tectonic Framework During Time of Emplacement

The most widely accepted radiometric age for the Elliott County intrusives is an Early Permian date of 269 million years (Zartman and others, 1967). Xenocrystic biotite from the kimberlite breccia outcrop was measured using K-Ar and Rb-Sr methods. The authors note the date obtained could be higher than the actual date of emplacement due to the xenocrystic nature of the biotite.

A suite of kimberlite breccia outcrop samples was examined by Harvey (1980). These samples were cut into small cores, subjected to stepwise thermal demagnetization up to 500 oersteds, and measured with a Schonstedt SSM-1A spinner magnetometer. Based on the paleomagnetic data derived from these samples, Harvey concluded an Late Permian–Early Triassic date was the best estimation for the age of the intrusives.

There are no radiometric age data available for the massive kimberlite. The only paleomagnetic measurements made on the massive kimberlite were performed in this study. While the age determinations cited above may be pertinent for the intrusives in the K area, they can only be used as suggestions

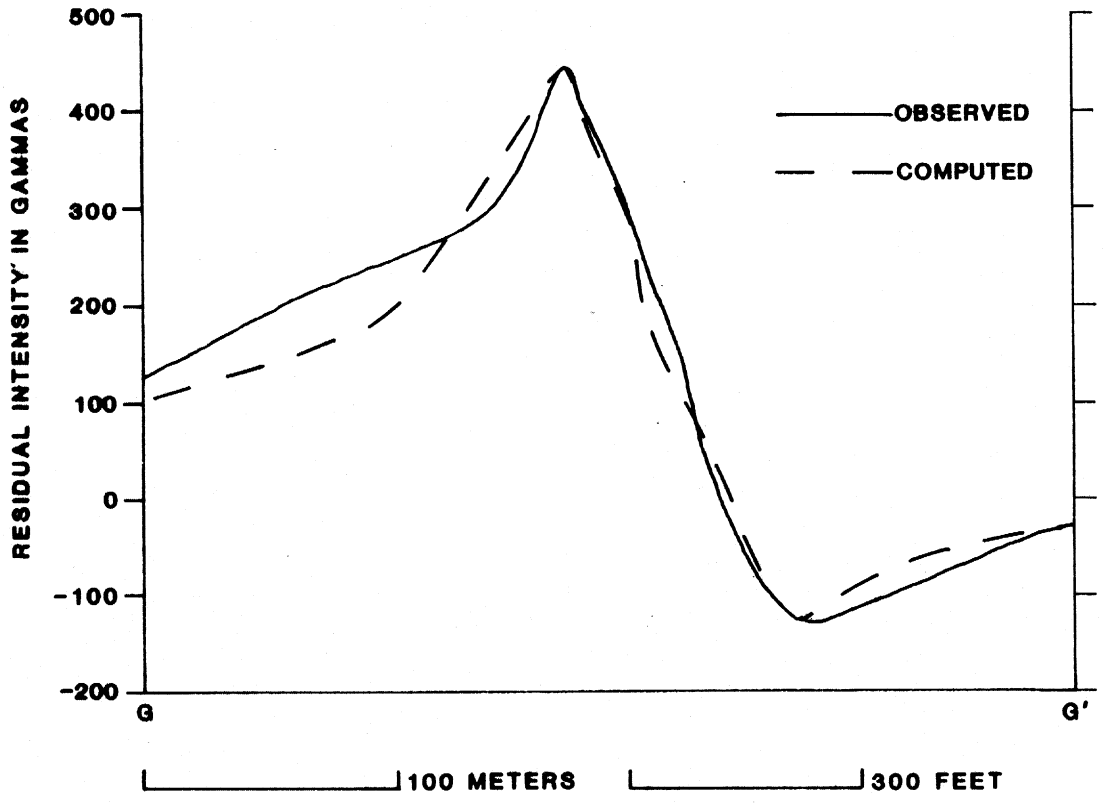

Figure 53. P1 anomaly: observed and computed profiles along G–G'.

for the kimberlite in the G and P areas. Considering the available data, Harvey's (1980) Late Permian–Early Triassic estimate is geologically plausible. This period will be used to evaluate the tectonic framework during the time of emplacement. The kimberlites cannot be older than Pennsylvanian in age because they intrude rocks of that period. Even if the radiometric age is inherently high, its discordance with Harvey's paleomagnetic age estimate is not severe.

The tectonic activity of Permian–Triassic time was characterized by vertical block faulting and basaltic eruptions on all continents. This activity signified the breakup of the continents and the initial opening of the Atlantic Ocean (Dott and Batten, 1976).

Sykes (1978, p. 621) believed most of the South African kimberlites were "… emplaced along preexisting zones of weakness that were reactivated during the early opening of the South Atlantic." The Elliott County kimberlites could have been intruded in a similar manner.

During the initial opening of the North Atlantic, the faults bordering the Rome Trough were probably reactivated. Much evidence has been presented that there was post-Pennsylvanian movement along the Kentucky River Fault System (Dever, 1980; Ettensohn, 1980; Sergeant and Haney, 1980). This author suggests that the Elliott County intrusives were emplaced when the tectonic framework was in a tensional phase. Hatcher (1972, p. 2753) indicated that "… from the Permian to the Triassic, the stress field orientation in the lithosphere changed so that earlier compression was replaced by tension."

May (1971) reconstructed the network of principal stress trajectories throughout the continents bordering the North Atlantic by using the pattern of Triassic–Jurassic diabase dikes. He (May, 1971, p. 1289) noted that "… the dikes are everywhere parallel to the lines of tensile stress…."

In summary, a Permian–Triassic date of intrusion fits well with the tectonic framework of that time. This author believes the kimberlites intruded when the faults bordering the Rome Trough were reacti-

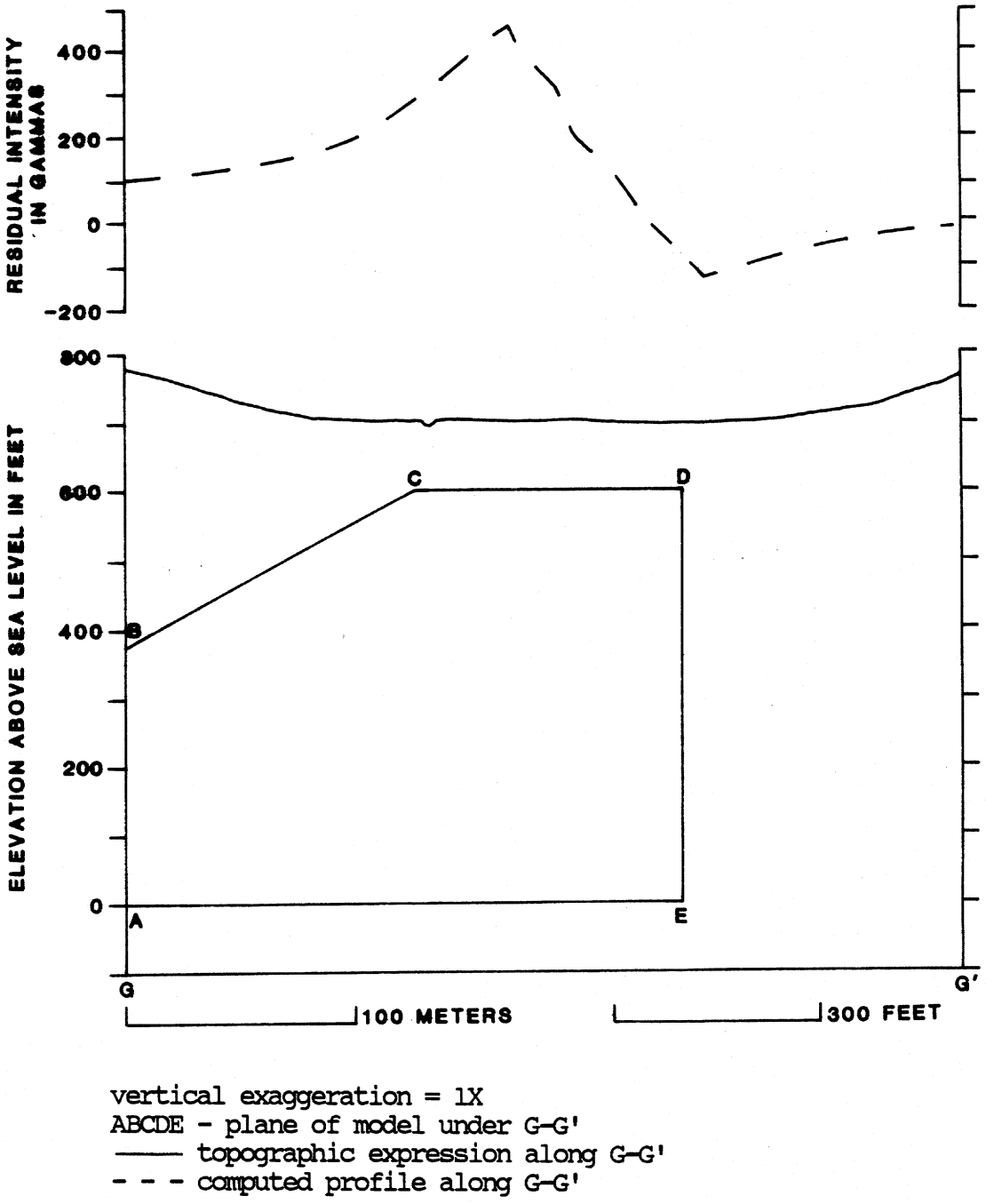

Figure 54. P1 anomaly: model position, topographic expression, and computed profile along G–G'.

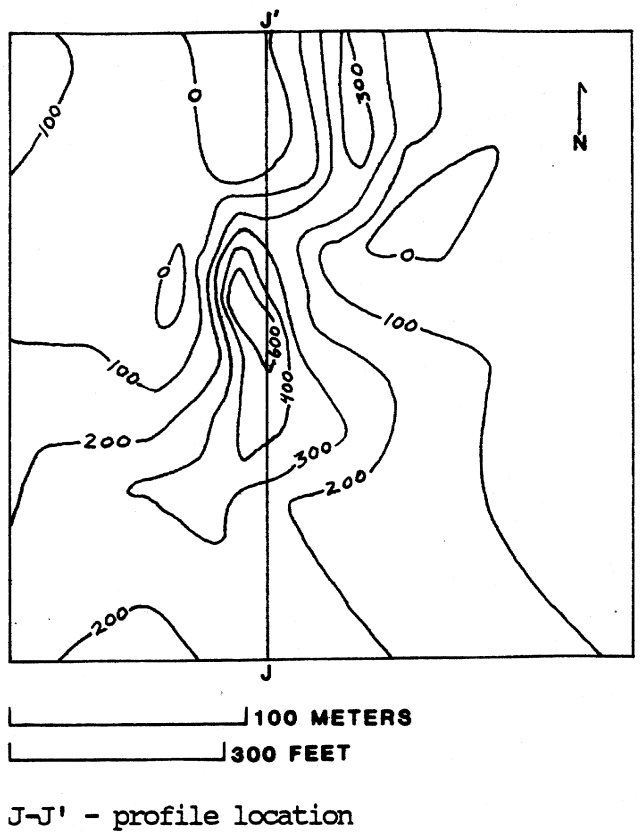

Figure 55. P2 anomaly: observed residual intensity map (in gammas).

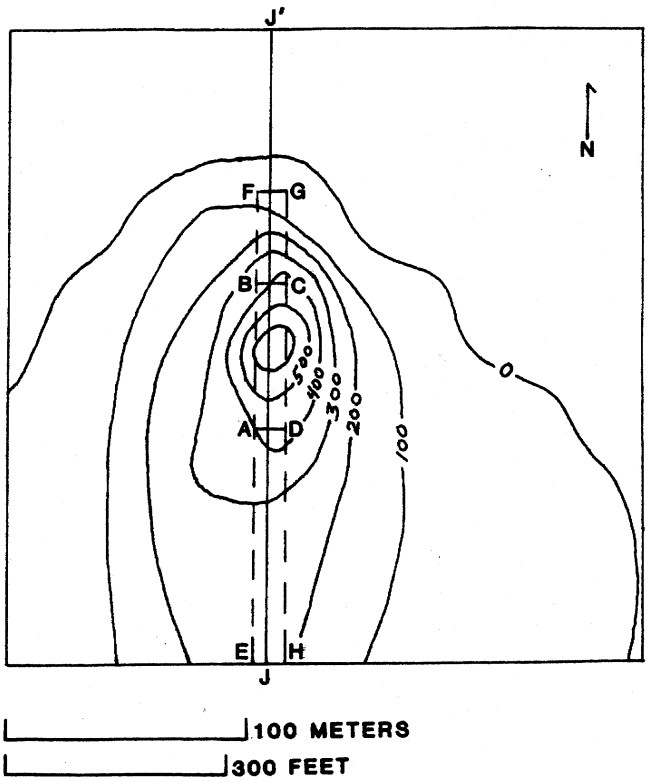

Figure 56. P2 anomaly: computed residual intensity map (in gammas).

vated by tensional stresses. These stresses were transmitted through the crust during the initial opening of the North Atlantic.

Conclusions

This thesis has furnished a good illustration of the utility of a ground magnetic survey as an exploration tool. An aeromagnetic survey (Harvey, 1980) was useful in determining the overall magnetic anomaly signature associated with the Elliott County intrusives. The resolution provided by this surface study made possible detailed mapping and modeling of nine separate kimberlite units.

The modeling produced a variety of pipe-like and dike-like forms. At least one other body that was not modeled exists in the area covered by detailed mapping. It is possible more intrusives exist in the surrounding region, but these units are expected to be small.

An ancillary paleomagnetic study yielded a Triassic paleomagnetic pole position for a kimberlite breccia sample and an unacceptable Cambrian pole position for a massive kimberlite sample. Radiometric data exist only for the kimberlite breccia, which was dated at 269 million years (Zartman and others, 1967).

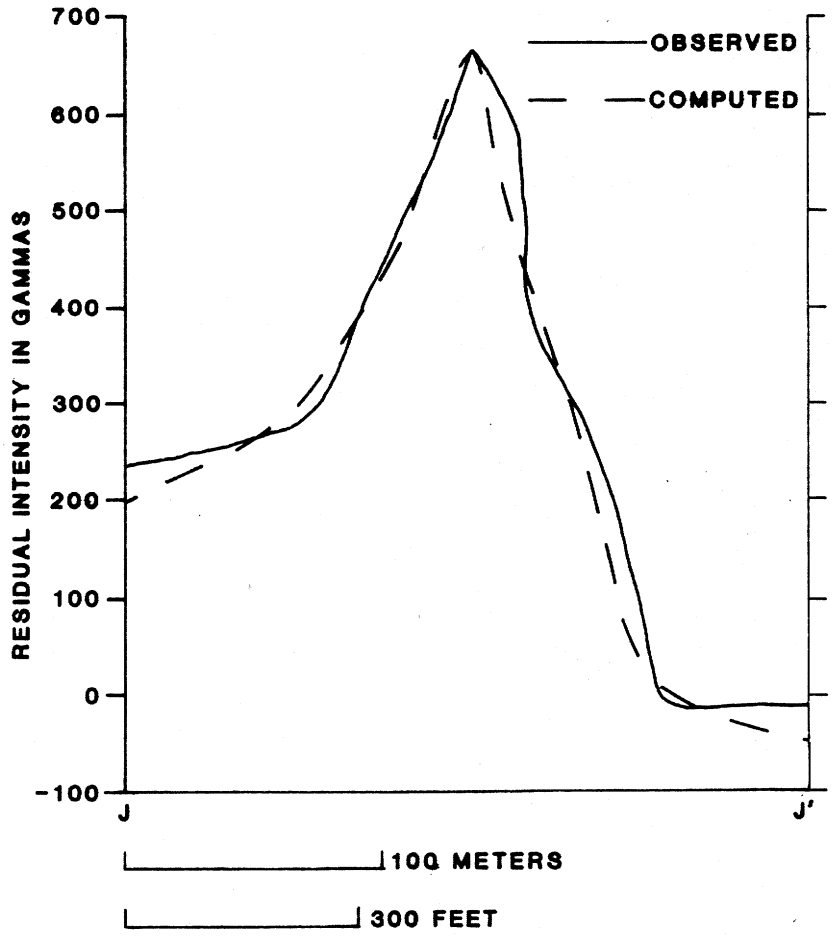

Figure 57. P2 anomaly: observed and computed profiles along J–J'.

This author suggests that more paleomagnetic and radiometric work be done on the massive kimberlite for a more conclusive description of its history. A suite of oriented samples could be collected and examined to determine a statistically valid paleomagnetic pole position for this outcrop. Also, some of the biotite noticed in hand samples could be separated and radiometrically dated.

The Elliott County intrusives are interpreted as a small ultramafic (kimberlitic) pipe and dike field. Cross-structural lineaments provided a zone of weakness for the emplacement of this field. These lineaments are represented in the subsurface by the north–south-trending axis of the Waverly Arch, and the east–west system of faults bordering the northern side of the Rome Trough. The initial opening of the North Atlantic during Permian–Triassic time reactivated the zone of weakness and allowed this intrusion to occur.

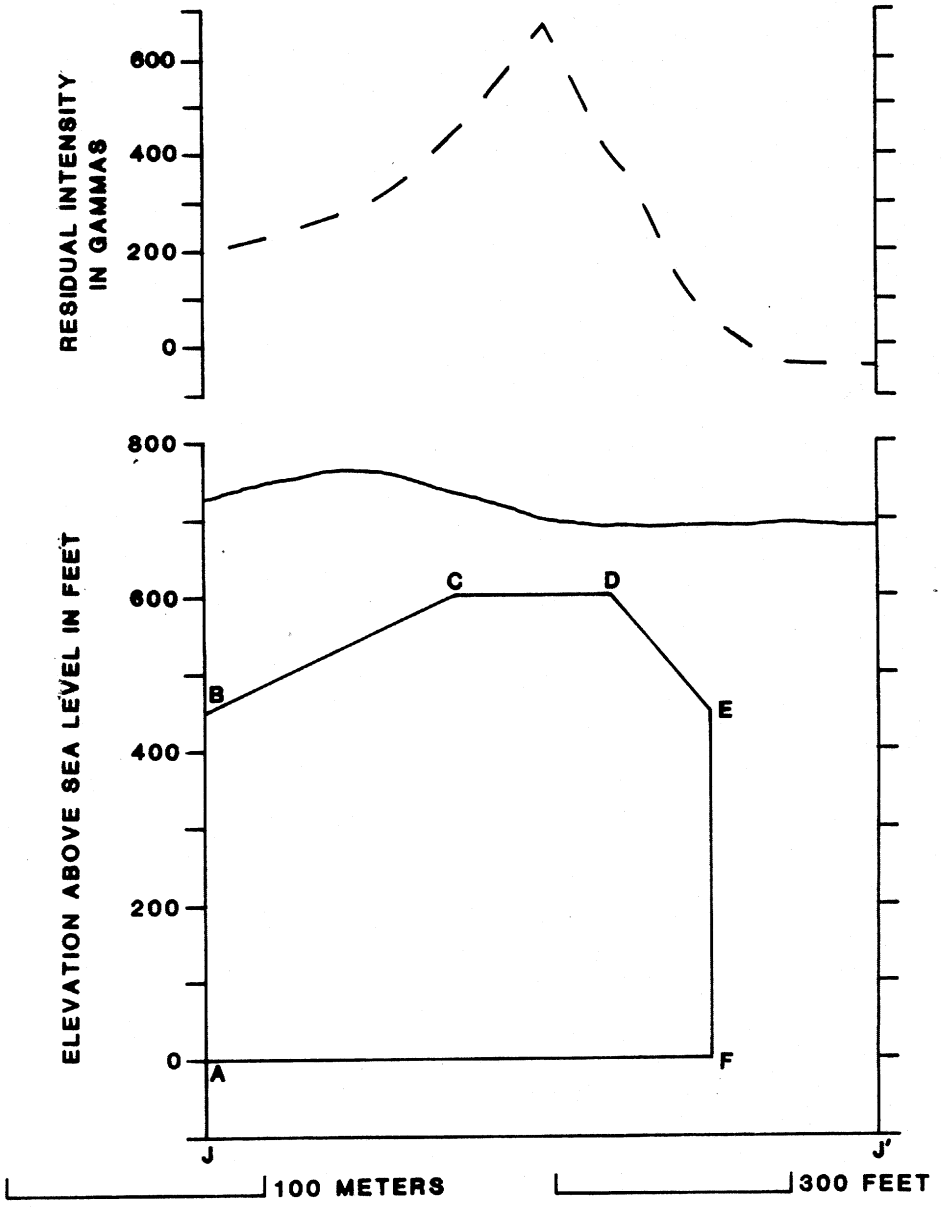

vertical exaggeration = 1X
ABCDEF - plane of model under J-J'
——— topographic expression along J-J'
- - - computed profile along J-J'

Figure 58. P2 anomaly: model position, topographic expression, and computed profile along J–J'.

References Cited

Agee, J.J., Garrison, J.R., and Taylor, L.A., 1982, Petrogenesis of oxide minerals in kimberlite, Elliott County, Kentucky: Am. Mineral., v. 67, p. 28–42.

Ammerman, M.L., and Keller, G.R., 1979, Delineation of Rome Trough in eastern Kentucky by gravity and deep drilling data: Amer. Assoc. Petrol. Geol. Bull., v. 63, p. 341–353.

Bass, M.N., 1960, Grenville boundary in Ohio: Jour. of Geol., v. 68, p. 673–677.

Bolivar, S.L., 1972, Kimberlite of Elliott County, Kentucky: M.S. thesis, Eastern Kentucky University, Richmond, Ky., 61 p.

Bolivar, S.L., 1977, Geochemistry of the Prairie Creek, Arkansas and Elliott County, Kentucky intrusions: Ph.D. dissertation, The Univ. of New Mexico, Albuquerque, N.M., 268 p., maps.

Bonnett, R.B., 1975, Analysis of Pleistocene and Holocene drainage changes northwest of the Nitro, West Virginia, region: Proceedings of the West Virginia Academy of Science, v. 47, nos. 3–4, p. 205–211.

Breiner, S., 1973, Applications manual for portable magnetometers: Sunnyvale, California, Geometrics, 58 p.

Brown, W.R., 1977 Geologic map of the Willard quadrangle, eastern Kentucky: U.S. Geol. Quad Map, GQ-1387.

Crandall, A.R., 1885, The occurrence of trap rock in eastern Kentucky: Science, v. 6, p. 222.

Crandall, A.R., 1910, Coals of the Licking Valley Region and of some contiguous territory, including an account of Elliott County and its dikes: Kentucky Geol. Survey Bull. 10, 90 p., maps.

Creason, Joe, 1950, Here lie diamonds—maybe: Courier-Journal Magazine, Oct. 1, p. 41–44.

Davis, J.C., 1973, Statistics and data analysis in geology: New York, John Wiley and Sons, Inc., 550 p.

Dawson, J.B., 1967, *in* P.J. Wyllie, ed., Ultramafic and related rocks: New York, John Wiley and Sons, Inc., 1967, p. 240–321.

Dever, G.R., Jr., 1977, The lower Newman Limestone: Stratigraphic evidence for Late Mississippian tectonic activity, *in* Dever, G.R., Jr., and others, Stratigraphic evidence for Late Paleozoic tectonism in northeastern Kentucky: Field trip guidebook, Eastern Section, Amer. Assoc. Petrol. Geol.: Lexington, Ky., Kentucky Geol. Survey, ser. 10, p. 8–18.

Dever, G.R., Jr., 1980, The Newman Limestone: An indicator of Mississippian tectonic activity in northeastern Kentucky: Proceedings of the Technical Sessions, Kentucky Oil and Gas Association 36th and 37th Annual Meetings, 1972 and 1973, M.K. Luther, ed., p. 42–54.

Dever, G.R., Jr., Ettensohn, F.R., and Haney, D.C., 1984, Relationship between the Kentucky River Fault System and Paleozoic sedimentation in eastern Kentucky: Geol. Soc. Of Am. Abstracts with Programs, v. 16, no. 3, p. 133.

Diller, J.S., 1886, Notes on the peridotite of Elliott County, Kentucky: Am. Jour. Sci., 3rd ser., v. 32, p. 21–25.

Diller, J.S., 1887, Peridotite of Elliott County, Kentucky: U.S. Geol. Survey Bull. 38, 31 p.

Dobrin, M.B., 1960, Introduction to geophysical prospecting [2d ed.]: New York, McGraw-Hill, Inc., p. 263–320.

Dott, R.H., and Batten, R.L., 1976, Evolution of the earth: New York, McGraw-Hill, Inc., 504 p.

Ettensohn, F.R., 1980, An alternative to the barrier-shoreline model for deposition of Mississippian and Pennsylvanian rocks in northeastern Kentucky: Geol. Soc. Of Am. Bull., pt. II, v. 91, p. 934–1056.

Ettensohn, F.R., and Peppers, R.A., 1979, Palynology and biostratigraphy of Pennington shales and coals (Chesterian) at selected sites in northeastern Kentucky: Jour. of Paleontology, v. 53, p. 453–474.

Freeman, L.B., 1951, Regional aspects of Silurian and Devonian subsurface stratigraphy in Kentucky: Am. Assoc. Petrol. Geol. Bull., v. 35, no. 1, p. 1–33.

Freeman, L.B., 1953, Regional subsurface stratigraphy of the Cambrian and Ordovician in Kentucky and vicinity: Kentucky Geol. Survey, ser. 9, Bull. 12, 352 p.

Garrison, J.R., and Taylor, L.A., 1980, Megacrysts and xenoliths in kimberlite, Elliott County, Kentucky: A mantle sample from beneath the Permian Appalachian Plateau: Contrib. Mineral. Petrol., v. 75, p. 27–42.

Grauch, V.J.S., and Campbell, D.L., 1984, Does draping aeromagnetic data reduce terrain-induced effects?: Geophysics, v. 49, no. 1, p. 75–80.

Haney, D.C., Hester, N.C., and Hoge, H.P., 1975, Evidence for fault-controlled deposition of Pennsylvanian sediments in central and eastern Kentucky: Geol. Soc. of Am. Abstracts with Programs, v. 7, p. 495–496.

Haney, D.C., Hester, N.C., and Hoge, H.P., 1976, Structural control on Paleozoic sedimentation in eastern Kentucky [abs.]: Am. Assoc. Petrol. Geol. Bull., v. 60, p. 1620.

Harris, L.D., 1975, The eastern aulacogen and its relation to Devonian shale-gas production: Eastern Gas Shales Symposium, 2nd, v. 2, p. 55–70.

Harvey, C.M., 1980, A low altitude aeromagnetic survey of a peridotite intrusion in Elliott County, Kentucky: M.S. thesis, the Ohio State Univ., Columbus, Ohio, 103 p.

Hatcher, R.D., Jr., 1972, Developmental model for the southern Appalachians: Geol. Soc. Of Am. Bull., v. 83, p. 2735–2760.

Haupt, J.R., 1967, Field and laboratory investigations of the Elliott County, Kentucky, peridotite dikes: M.S. thesis, Miami Univ., Oxford, Ohio, 62 p.

Heyl, A.V., 1972, The 38th Parallel Lineament and its relationship to ore deposits: Economic Geology, v. 67, p. 879–894.

Horne, J.C., Baganz, B.P., Ferm, J.C., and Cantrell, C.L., 1976, Carboniferous sedimentary response to contemporaneous tectonism in eastern Kentucky [abs.]: Am. Assoc. Petrol. Geol. Bull., v. 60, p. 1620–1621.

Hunt, G.H., and Bolivar, S.L., 1972, Oxygen and carbon isotope ratios of carbonate from kimberlites in Elliott County, Kentucky: Geol. Soc. Am. Abstracts with Programs, v. 4, no. 2, p. 81–82.

Irving, E., 1964, Paleomagnetism and its applications to geological and geophysical problems: New York, John Wiley and Sons, Inc., 399 p.

Johnson, R.W., Jr., 1960, Basement magnetic and gravity anomalies in southeastern Kentucky: Geol. Soc. of Am. Bull., v. 71, no. 12, pt. 2, p. 2017–2018.

Johnson, R.W., Jr., Haygood, C., and Kunselman, P., 1980, Residual total intensity aeromagnetic map of Kentucky: Eastern sheet: Kentucky Geol. Survey, ser. XI.

Keller, G.R., Soderberg, R.K., and Ammerman, M.L., 1975, Possible Precambrian rifting in the southeast United States [abs.]: Am. Geophys. Union Trans., v. 56, p. 602.

Kerr, P.F., 1959, Optical mineralogy: New York, McGraw-Hill Book Co., 442 p.

King, E.R., and Zietz, I., 1960, Thickness of sedimentary section in Appalachian Basin: Am. Assoc. Petrol. Geol. Bull., v. 44, no. 7., p. 1251–1252.

Koenig, J.B., 1956, The petrography of certain igneous dikes of Kentucky: Kentucky Geol. Survey Bull., 21, 57 p.

Lewis, H.C., 1886, Genesis of diamond: Science, v. 8, p. 345–347.

Lewis, H.C., 1887, On diamontiferous peridotite and the genesis of diamond: Geol. Mag. (Great Britain), v. 4, p. 22–24.

Lidiak, E.G., and Zietz, I., 1976, Interpretation of aeromagnetic anomalies between latitudes 37° and 38° in the eastern and central United States: Geol. Soc. of Am. Spec. Paper 167, 37 p.

May, P.R., 1971, Pattern of Triassic–Jurassic diabase dikes around the North Atlantic in the context of predrift position of the continents: Geol. Soc. of am. Bull., v. 82, p. 1285–1292.

McElhinny, M.W., 1973, Paleomagnetism and plate tectonics: London, Cambridge University Press, 358 p.

McFarlan, A., 1943, Geology of Kentucky: Baltimore, Maryland, Waverly Press, Inc., 531 p.

McGuire, W.H., and Howell, P., 1963, Oil and gas possibilities of the Cambrian and Lower Ordovician in Kentucky: Lexington, Kentucky, Spindletop Research Center (for Kentucky Dept. Commerce), 216 p.

McLaughlin, D.B., 1954, Suggested extension of the Grenville orogenic belt and the Grenville Front: Science, v. 120, p. 287–289.

Meyer, H.O.A., 1976, Kimberlites of the continental United States: A review: Jour. of Geol., v. 84, p. 377–403.

Nagata, Takesi, 1961, Rock magnetism: Tokyo, Maruzen Company, Ltd., 350 p.

Parish, J.B., and Lavin, P.M., 1982, Tectonic model for kimberlite emplacement in the Appalachian Plateau of Pennsylvania: Geology, v. 10, p. 344–347.

Robinson, L.C., Hudnall, J.S., and Richardson, H.T., 1950 (reprinted from 1928), Reconnaissance map of Elliott County, Kentucky: Kentucky Geol. Survey, ser. VI.

Rudman, A.J., Summerson, C.H., and Hinze, W.J., 1964, Geology of basement in midwestern United States: Am. Assoc. Petrol. Geol. Bull., v. 49, no. 7, p. 894–904.

Sanderson, D.D., and Duba, R.W., 1975, The joint pattern of the Tri-State Area, West Virginia, Ohio, and Kentucky: Proceedings of the West Virginia Academy of Science, v. 47, no. 2, p. 106–113.

Schulze, D.J., 1981, Mantle-derived calcite and phlogopite in discrete nodules from a Kentucky kimberlite: Evidence for primary kimberlitic liquids: EOS, v. 63, p. 414.

Schulze, D.J., 1982, The petrology of ultramafic xenoliths from the Hamilton Branch kimberlite pipe, Elliott County, Kentucky [abs.]: Dissertation Abstracts International, v. 43, no. 7, Jan. 1983.

Schulze, D.J., 1984, Cr-poor megacrysts from the Hamilton Branch kimberlite, Elliott County, Kentucky: Kimberlites II: The mantle and crust-mantle relationships, by J. Kornprobst (ed.), p. 97–108.

Sergeant, R.E., and Haney, D.C., 1980, Stratigraphic evidence for Late Paleozoic reactivation of subsurface tectonic elements in northeastern Kentucky: Geol. Soc. of Am. Abstracts with Programs, v. 12, p. 208.

Silberman, J.D., 1972, Cambro-Ordovician structural and stratigraphic relationships of a portion of the Rome Trough: Kentucky Geol. Survey Spec. Pub., ser. 10, no. 21, p. 35–45.

Sosman, R.B., 1938, Evidence of the intrusion temperature of peridotites: Am. Jour. Sci., v. 35, p. 353–359.

Stangway, D.W., 1970, History of the earth's magnetic field: New York, McGraw-Hill Book Co., 168 p.

Sykes, L.R., 1978, Intraplate seismicity, reactivation of pre-existing zones of weakness, alkaline magmatism, and other tectonism postdating continental fragmentation: Reviews of Geophysics and Space Physics, v. 16, p. 621–688.

Talwani, M., 1965, Computation with the help of a digital computer of magnetic anomalies caused by bodies of arbitrary shape: Geophysics, v. 30, no. 5, p. 797–817.

Vacquier, V., Steenland, N.C., Henderson, R.G.; and Zietz, I., 1963, Interpretation of aeromagnetic maps: G.S.A. Memoir 47. New York: The Geological Society of America, 151 p.

Warren, J.R., 1956, A study of magnetic anomalies associated with ultrabasic dikes in the Western Kentucky Fluorspar District: Kentucky Geol. Survey Bull. 19, 38 p.

Webb, J.R., 1969, Geologic history of the Cambrian System in the Appalachian Basin: Kentucky Geol. Survey Spec. Pub., ser. 10, no. 18, p. 7–15.

Werner, E.J., 1981, Tectonic fracture patterns in northeast Kentucky: Proceedings of the West Virginia Academy of Science, v. 53, nos. 2–4, p. 85–92.

Woodward, H.P., 1961, Preliminary subsurface study of southeastern Appalachian Interior Plateau: Am. Assoc. Petrol. Geol. Bull., v. 45, p. 1634–1655.

Zartman, R.E., Brock, M.R., Heyl, A.V., and Thomas, H.H., 1967, K-Ar and Rb-Sr ages of some alkalic intrusive rocks from central and eastern United States: Am. Jour. Sci., v. 265, p. 848–870.

Appendix A: Positions of Total Magnetic Intensity Values

The following values were used to construct the total magnetic intensity map. The position of each value is given as an X, Y coordinate on a positive right-handed square grid system. The origin of the grid is at 24,000 meters east and 20,500 meters north on the Universal Trans Mercator system.

The Z value is the raw field value of total magnetic intensity, uncorrected for diurnal variation or regional magnetic gradients. The magnetic data can be reproduced using any scale. Index maps for the line locations within the K, G, and P survey areas follow the data.

LINE K100

X	Y	Z
334	574	56047
346	579	56018
369	589	56033

LINE K200

X	Y	Z
335	559	56039
351	565	56017
374	574	56017

LINE K300

X	Y	Z
322	547	56011
327	548	56009
332	549	56004
337	550	56012
343	550	55990
348	551	55969
351	551	55975
353	552	55964
360	553	55978
367	554	55977
374	555	55991
380	556	55995
387	557	55974
394	558	55987
400	559	55993
407	560	55996
414	561	55995

LINE K400

X	Y	Z
315	524	56000
327	524	55968
332	525	56001
338	526	56011
341	526	56000
345	526	55975
348	526	55942
351	527	55901
353	527	55847
356	528	55822
360	528	56095
364	528	55549
368	529	55711
376	529	56006
384	530	56011
392	531	56001
409	532	55984
425	523	55980
441	535	55967
458	537	55953

LINE K500

X	Y	Z
298	500	56033
314	501	56042
330	503	56052
334	503	56061
338	504	56078
342	505	56310
346	505	56336
350	505	56311
354	506	56520
358	507	56389
362	507	56412
366	507	56560
370	508	56401
374	509	56278
378	509	56150
382	510	56118
390	511	56085
398	512	56020
406	513	56016
414	514	56007
422	515	56009
430	516	56057
446	518	56009
462	520	56006

LINE K600

X	Y	Z
301	484	56025
318	486	56032
326	487	56051
353	490	56307
362	491	56334
366	491	56341
370	492	56573
373	492	56426
378	493	56128
386	493	56107
394	494	56096
402	495	56068
418	497	56045
434	498	55972
450	500	55980
457	501	55996

LINE K700

X	Y	Z
313	461	55999
329	463	56058
360	465	56032
393	467	56031
424	469	55978
440	470	55981
456	472	55966

LINE K800

X	Y	Z
307	435	55995
326	439	56003
335	440	55991

344	443	55973
352	445	55946
362	447	55947
381	452	55972
400	456	55993

LINE K850

X	Y	Z
299	380	55969
314	393	55952
329	404	55927
336	409	56008
340	412	56327
344	415	56001
348	418	56108
352	421	56067
355	424	56049
359	427	55804
364	430	55944
369	434	55920
379	441	55936

LINE K900

X	Y	Z
322	326	55990
331	342	56002
342	358	56013
347	367	56020
349	371	56049
352	376	56065
354	380	56174
356	384	56252
359	389	56798
362	392	56001
365	397	55952
367	401	56081
369	405	56273
371	408	56051
373	411	55873
375	414	55933
379	421	55970
383	429	55965
391	442	55962

LINE K1000

X	Y	Z
333	316	56000
342	331	56006
350	345	56007
359	359	56004
368	372	56010
372	379	55994
377	388	56171
380	392	56943
382	396	57322
385	400	57575
388	404	55769
390	409	55818
393	413	55875
395	417	55937
398	421	55952
403	429	55961
408	438	55972
414	446	55997

LINE K1100

X	Y	Z
348	300	55997
357	313	56000
366	328	56003
371	335	56007
376	342	56014
378	346	56040
381	349	56081
383	353	56132
385	357	56128
387	360	56182
390	363	56026
392	367	56188
397	375	55985
399	378	56003
404	385	55920
409	392	55928
413	399	55933
418	406	55934
430	424	55954
436	435	55963

LINE K1200

X	Y	Z
363	294	55995
373	309	56026
378	316	56007
383	324	56018
388	331	56043
393	339	56107
396	342	56184
398	346	56242
401	350	56026
404	353	56079
406	357	56314
409	361	55980
414	368	56001
419	376	56052
424	383	56159
426	387	55963
432	395	55892
437	402	55918
442	410	55936
452	425	55954

LINE K1300

X	Y	Z
378	285	55991
390	302	56002
395	310	56013
401	318	56040
404	322	56070
407	327	56193
410	331	56348
412	335	56374
415	339	56247
418	343	56217
421	347	56180
424	350	56107
427	355	56222
429	360	56213
432	364	56008
435	367	55994
437	371	55987
440	375	55954
445	382	55889
450	390	55903
455	397	55924
466	412	55958

LINE K1400

X	Y	Z
397	277	55985
405	291	55994
415	306	55997
420	313	56016
424	320	56031
428	327	56062
433	335	56092
436	339	56096
438	342	56094
441	345	56085
443	349	56088
445	353	56076
448	356	56078
450	360	56014
452	364	55878
455	368	55881
457	370	55842
462	378	55882
473	395	55909
479	404	55942

LINE K1500

X	Y	Z
453	296	56066
456	302	56069
463	315	56073
466	321	56063
470	328	56074
471	331	56091
473	334	56144
475	337	56338
476	340	56663
478	343	56094
480	347	55758
483	354	55921
487	362	55959
496	377	55988
506	397	55983
512	408	55984

LINE K1600

X	Y	Z
457	285	56022
470	293	56022
482	300	56022
495	308	56037
508	316	56170
511	318	56277
515	320	56192
518	322	56022
521	324	55985
527	528	55979
540	336	55995
553	344	55964
565	351	55963

LINE K1700

X	Y	Z
457	274	56028
470	274	56036
482	274	56035
494	274	56019

506	274	56028
518	274	56006
530	274	56001
543	274	55997

LINE KT

X	Y	Z
352	552	55980
350	536	55905
347	521	55920
346	513	55846
344	505	56456
343	497	56388
342	490	56394
340	482	56109
339	474	56103
336	348	56055
334	443	56008
331	427	55961
330	422	55888
329	415	55798
328	412	55767
327	406	56139
327	403	56054
326	401	56037
333	398	56246
339	394	56224
350	387	56221
356	384	56430
362	380	56401
368	377	56031
374	374	55655
378	372	55514
382	369	56722
386	367	56596
390	365	56105
394	362	55994
402	358	55965
405	357	55979
412	351	56143
418	346	55988
424	341	56156
430	336	56310
433	334	56089
444	336	56050
455	338	56064
467	340	55891
473	342	55521
479	343	55659
485	344	55710
485	341	55760
485	339	56108
485	336	56308
485	333	56133
485	331	56042
485	329	56001
485	318	55979
485	313	55978
485	302	55982
493	288	55962
502	274	55955

LINE G100

X	Y	Z
681	522	55884
696	523	55858
711	525	55820
719	525	55794
726	526	55789
734	527	55798
737	527	55797
741	527	55799
745	528	55783
748	528	55779
752	528	55779
760	528	55765
767	529	55743
775	530	55718
782	530	55716
790	531	55761
798	532	55782
805	532	55802
813	533	55818
821	534	55830
828	534	55837
836	535	55843

LINE G200

X	Y	Z
680	512	55875
689	513	55850
698	513	55817
702	513	55885
706	514	55911
711	514	56109
716	515	55892
720	515	55793
729	515	55793
733	516	55780
738	516	55763
742	516	55745
747	517	55744
752	517	55730
761	518	55630
770	519	55737
779	519	55879
787	520	55876
796	521	55813
805	521	55822
815	522	55809
823	523	55816
832	524	55821
840	525	55857

LINE G300

X	Y	Z
679	502	55898
686	502	55907
693	503	56020
699	503	55965
705	503	56127
716	504	56124
728	504	56054
740	505	55867
751	505	55714
758	505	55700
764	505	55725
770	506	56107
777	506	55769
783	506	55861
790	506	56021
797	506	56047
803	506	55943
809	507	55889
816	507	55862
823	507	55841
829	507	55841
836	507	55842
842	507	55842

LINE G400

X	Y	Z
676	493	55913
682	493	55932
688	494	56020
694	494	56090
700	494	56315
711	494	56132
722	495	56281
732	495	56324
742	495	56122
753	496	56003
764	496	55953
774	497	55935
784	497	55926
793	497	55899
802	498	56208
810	498	56805
819	498	56060
827	499	55997
836	499	55940
844	500	55909
854	500	55873
861	501	55859

LINE G500

X	Y	Z
682	467	55931
687	468	55933
693	469	55934
705	469	55952
717	470	55969
729	471	55991
735	472	56006
741	472	56062
753	473	55979
765	474	56069
777	475	56215
783	475	56325
789	476	56690
795	476	56266
806	477	56119
814	478	56306
822	479	56210
826	479	56196
830	479	56178
834	480	56072
839	480	55994
847	480	55894
854	481	55871
862	482	55860

LINE G600

X	Y	Z
681	453	55926
689	454	55948
705	455	55933
721	456	55949
737	457	55958
751	459	55974

767	460	55994
783	462	56041
791	462	56069
799	463	56130
807	463	56244
811	464	56125
815	464	56256
819	464	56125
823	465	56105
826	465	56029
834	465	55956
842	466	55956
850	466	55899
858	467	55887
861	468	55874

LINE G700

X	Y	Z
680	439	55927
700	440	55918
720	441	55924
740	442	55929
750	443	55935
760	443	55940
770	444	55955
780	444	55972
790	445	56007
800	445	56039
810	446	56074
820	446	56125
830	447	56049
840	447	55974
850	447	55924
860	448	55907
870	448	55883
890	449	55867
910	450	55969
930	450	55864
940	451	55863

LINE G800

X	Y	Z
680	421	55926
693	421	55919
705	421	55922
717	422	55926
730	422	55919
742	423	55922
755	423	55932
767	423	55930
779	434	55939
791	424	55941
797	425	55972
803	425	55989
809	425	56066
813	425	56243
816	425	56126
820	426	56148
825	426	56367
830	426	56494
835	426	56332
840	426	55989
844	427	55976
849	427	55868
873	427	55974
892	428	55854
911	429	55898
930	429	55870
949	430	55858

LINE G900

X	Y	Z
670	411	55920
685	412	55932
700	412	55912
715	412	55906
729	412	55905
744	412	55891
759	412	55899
773	413	55902
788	413	55914
802	413	55908
810	413	55909
817	413	56026
821	413	56039
824	413	56119
828	413	56225
832	413	56243
837	413	56139
841	413	55962
845	413	55916
853	413	55878
862	413	55874
872	413	55858
881	413	55892
890	413	55890
907	413	55849
925	413	55859
942	413	55874
949	413	55850

LINE G1000

X	Y	Z
679	398	55815
697	398	55909
709	398	55923
721	398	55913
733	399	55896
745	399	55915
758	399	55890
770	399	55891
783	399	55891
796	399	55876
810	399	55850
816	399	55827
820	399	55950
823	399	55898
826	399	55801
830	399	55871
833	399	55826
837	399	55806
841	399	55838
848	399	55851
856	399	55855
864	399	55842
880	399	55881
895	399	55882
910	399	55863
926	399	55882
942	399	55867
958	399	55856

LINE G1100

X	Y	Z
677	385	55922
692	385	55916
706	385	55917
720	385	55915
734	385	55867
748	385	55884
761	385	55886
768	385	55876
778	385	55855
788	385	55820
793	385	55823
798	385	55877
803	385	55990
808	385	56040
813	384	56200
818	384	56312
823	384	56057
828	384	55903
833	384	55776
838	384	55658
845	384	55782
853	384	55811
868	384	55842
883	384	55877
898	384	55894
913	383	55879
928	383	55871
943	383	55864
958	383	55882

LINE G1200

X	Y	Z
676	370	55906
685	370	55896
695	370	55889
704	369	55883
713	369	55884
723	369	55875
732	369	55875
742	369	55843
748	369	55849
755	369	55844
761	369	55836
768	369	55832
776	369	55802
784	369	55760
792	368	55764
800	368	55869
816	368	56557
824	368	56268
832	368	56253
840	368	56050
851	368	55726
863	367	55765
874	367	55857
886	367	55836
898	367	55847
909	367	55838
921	367	55858
933	367	55831

LINE G1300

X	Y	Z
677	356	55893
683	356	55878
690	367	55906

696	356	55900
702	356	55880
710	356	55872
718	356	55846
727	355	55855
735	355	55834
744	355	55835
752	355	55821
760	355	55807
769	355	55780
777	355	55756
785	355	55925
794	355	56396
802	355	56365
810	355	56251
819	355	56334
827	355	56254
835	354	56466
845	354	56017
855	354	55882
865	354	55830
875	354	55852
886	354	55854
896	354	55847
906	354	55860
915	354	55834
925	354	55847
936	354	55846
946	354	55845
956	354	55844

LINE G1400

X	Y	Z
679	341	55925
694	340	55915
709	340	55906
724	340	55901
739	340	55865
754	340	55877
770	339	55813
778	339	55792
787	339	55768
794	339	56191
799	339	56295
803	339	56532
807	339	56556
811	339	56370
814	339	56219
819	339	55774
823	339	56366
827	339	56633
831	339	56789
836	339	57196
840	339	57164
844	339	56224
848	339	55954
852	339	55909
861	339	55936
869	339	55926
886	339	55879
903	339	55883
919	339	55871
936	339	55873
952	339	55865

LINE G 1500

X	Y	Z
679	324	55930
695	324	55921
713	324	55913
730	324	55910
748	324	55904
766	324	55897
774	324	55888
783	324	55900
788	324	56568
792	324	56555
797	324	56533
801	324	56755
805	324	56596
810	324	56865
815	324	56675
819	324	56166
823	324	56494
828	324	56364
833	324	57318
837	324	56865
842	324	56383
851	324	56059
860	324	55986
878	324	55928
897	324	55897
915	324	55885
933	324	55877
952	324	55872

LINE G1600

X	Y	Z
679	304	55929
694	304	55929
711	304	55930
727	304	55917
743	304	55927
760	304	55946
776	304	56044
780	304	56221
784	304	56231
788	304	56327
792	304	56421
796	304	56515
801	304	56781
805	304	56399
810	304	56377
815	304	56374
819	304	56454
824	304	56492
828	304	56466
832	304	56381
836	304	56425
840	304	56530
845	304	56396
849	304	56194
853	304	56118
857	304	56061
861	304	56021
870	305	55969
878	305	55935
895	305	55902
912	305	55882
933	305	55890
953	306	55887

LINE G1700

X	Y	Z
692	284	55906
712	284	55903
727	284	55906
742	285	55912
749	285	55907
757	285	56009
764	285	55955
770	286	55955
780	286	55990
789	286	56031
797	286	56073
806	287	56159
810	287	56092
815	287	56108
819	287	56081
823	287	56081
827	287	56075
833	288	56161
839	288	56105
845	288	56089
851	288	56082
863	288	56020
875	289	55983
887	289	55957
899	289	55911
910	289	55894
925	290	55866
939	291	55856
952	292	55858

LINE G1800

X	Y	Z
695	270	55930
711	270	55945
727	270	55921
743	270	55932
759	270	55943
774	271	55968
791	271	55989
799	271	56002
806	272	55993
814	272	55982
822	272	55979
830	273	55976
837	273	55988
844	273	55981
851	273	55975
858	273	55968
865	273	55956
872	274	55936
886	274	55903
900	274	55877

LINE GX

X	Y	Z
793	506	55758
795	503	55733
797	500	55945
800	497	56061
801	494	56115
803	490	57273
805	487	56716
807	484	56202
809	481	56192
810	478	56201

LINE GY

X	Y	Z
787	476	56644
788	479	56592
790	482	56396
792	485	56428
793	488	56933
795	491	56296
797	494	55496
798	497	55877
800	501	56098
802	504	55996
804	507	55949

LINE GL

X	Y	Z
731	569	55863
745	559	55838
738	542	55807
734	534	55806
730	525	55786

LINE GT

X	Y	Z
832	275	55927
837	258	55882
845	242	55862

LINE P100

X	Y	Z
845	760	55813
860	758	55828
874	754	55808
889	751	55807
893	750	55810
907	747	55802
914	746	55779
921	745	55788
936	742	55772
943	740	55801
950	739	55792

LINE P150

X	Y	Z
853	705	55797
876	708	55764
883	710	55760
891	711	55744
899	712	55742
903	713	55744
906	713	55777
914	715	55728
918	715	55776
922	716	55665
925	717	55675
929	717	55674
933	718	55663
940	719	55718

LINE P200

X	Y	Z
870	687	55765
877	688	55761
884	689	55756
891	690	55790
895	691	55842
898	691	55974
902	692	56139
905	693	56253
909	693	56255
912	694	56227
915	694	56192
919	694	56137
922	695	56067
925	696	56000
929	696	55937
936	697	55870
943	698	55809
951	699	55785
958	700	55766
961	701	55775
964	702	55854
968	703	55945
971	704	56033
975	704	56005
982	706	55845
996	708	55786
1010	710	55794

LINE P250

X	Y	Z
934	675	55875
939	676	55847
947	677	55819
954	678	55787
961	679	55776
968	680	55806
974	681	56172
978	682	56055
981	683	55899
988	684	55857
1001	686	55810
1015	688	55822

LINE P300

X	Y	Z
846	676	55802
854	675	55778
857	675	55770
861	674	55825
865	574	55905
868	673	55929
875	672	55828
882	671	55896
885	670	55958
889	670	56002
892	669	56059
906	667	55931
913	666	55912
920	664	55886
934	662	55838
941	661	55833
944	660	55851
947	659	55728
951	659	55792
954	658	55986
958	658	56765
961	657	56412
965	657	56080
968	656	55985
982	654	55894
996	653	55869

LINE P400

X	Y	Z
832	647	55828
845	646	55844
858	645	55902
864	644	55947
870	643	55965
876	643	55961
882	642	55919
889	641	55896
895	640	55893
907	638	55916
920	637	55946
933	635	56033
945	634	56113
952	633	56147
954	632	56131
958	632	56040
964	631	55980
970	631	55950
982	629	55900
995	628	55872
1007	626	55848

LINE P500

X	Y	Z
831	616	55831
846	614	55846
860	612	55850
874	611	55851
889	609	55859
904	607	55876
907	606	55870
911	606	56021
914	605	56134
918	605	56100
922	605	56049
925	604	56042
932	603	55894
938	602	55909
943	601	55916
949	601	55931
954	600	55959
959	599	55987
964	599	56017
970	598	56051
975	597	56039
980	596	56007
990	595	55944
1000	594	55902
1010	593	55884

LINE P600

X	Y	Z
869	585	55857
884	584	55865
894	583	55879
914	582	55936
921	581	55896
928	580	55910
935	580	55907
949	579	55918
962	578	55925
976	577	55964
983	576	55943
990	575	55927
996	575	55918

1003 574 55915
1014 573 55892
1025 573 55885

LINE P700

X	Y	Z
869	557	55858
883	556	55850
898	554	55895
913	552	55861
920	552	55874
936	550	55878
951	549	55887
964	548	55887
976	547	55890
989	546	55852
1001	544	55871
1014	544	55854
1025	543	55843

LINE PA

X	Y	Z
943	677	55795
946	674	55777
950	670	55801
954	665	55872
957	661	55978
958	660	56037
960	659	56154
961	658	56752
963	655	56386
965	652	56086
967	650	56070
970	647	56052
974	643	56050
976	640	56062
978	638	55952
980	636	56108
982	633	56091
987	629	56008

LINE PB

X	Y	Z
956	634	56044
957	638	56189
958	641	56238
959	644	56267
960	647	56077
960	652	56139
961	654	56455
961	657	56574
962	660	56133
964	670	56008
966	680	55985

LINE PC

X	Y	Z
932	634	55850
937	638	55853
941	641	55869
945	644	55897
950	648	55918
954	651	55975
957	654	56146
960	656	56534
963	657	56352
967	661	55782
976	665	55808
986	672	55704
990	679	55759
999	685	55785

REGIONAL DATA

X	Y	Z
206	367	56093
186	276	56051
151	155	56040
266	130	55995
471	070	55950
512	080	55937
549	099	55956
579	130	55918
586	137	55885
583	142	55926
570	163	55915
558	184	55946
545	204	55944
539	214	55958
530	229	55977
521	244	56031
512	259	55983
483	357	55890
504	362	55947
524	368	55949
538	372	55954
551	376	55950
563	380	55939
576	384	55940
591	388	55926
475	508	55992
494	512	55863
514	516	55976
533	518	55971
552	522	55993
573	529	55922
588	540	56002
305	882	56116
350	894	56005
607	874	55926
702	856	55881
789	800	55829
604	551	55876
623	558	55875
643	559	55822
662	556	55871
682	553	55867
702	555	55850
717	567	55884
723	575	55866
742	630	55852
610	394	55906
626	399	55925
642	403	55922
653	406	55915
661	408	55909
611	152	55873
633	158	55897
660	169	55889
688	175	55872
716	184	55850
752	195	55857
779	205	55844
803	218	55845
830	230	55837
853	230	55782
860	231	55882
871	234	55885
880	240	55868
891	242	55855
901	243	55862
979	254	55797
833	768	55772
826	703	55826
868	734	55815
885	735	55823
898	735	55876
904	734	55711
908	734	55750
910	735	55746
914	735	55743
920	734	55742
927	734	55708
930	735	55729
934	735	55740
939	735	55757
946	735	55776
958	736	55794
970	741	55780
993	764	55795
1020	823	55739
1150	843	55731
1255	745	55722
1400	672	55673
1375	517	55702
1385	328	55708
1293	320	55721
1186	303	55732
1081	274	55771

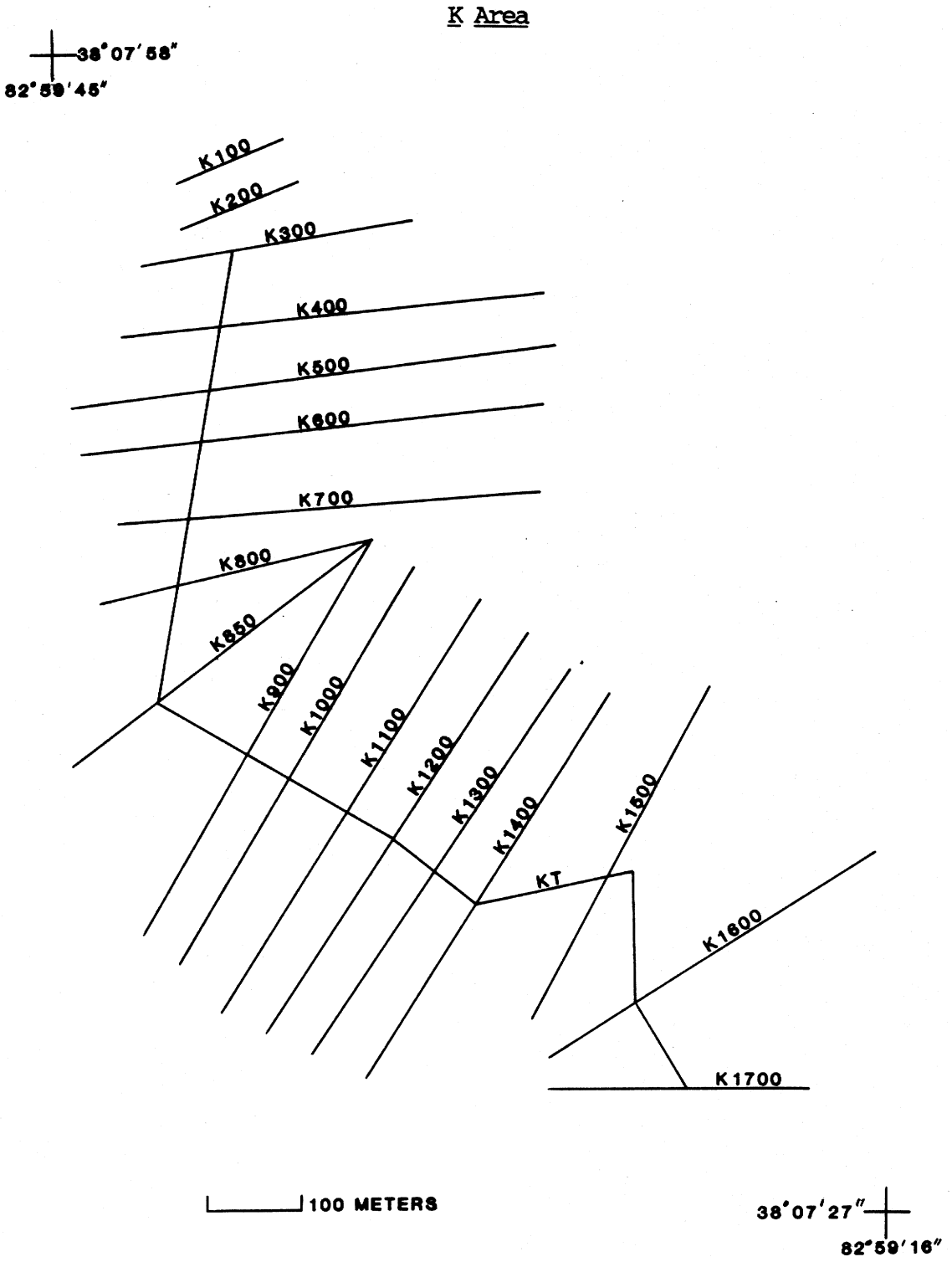
K Area
38°07'58"
82°59'45"
K100
K200
K300
K400
K500
K600
K700
K800
K850
K900
K1000
K1100
K1200
K1300
K1400
KT
K1500
K1600
K1700
100 METERS
38°07'27"
82°59'16"

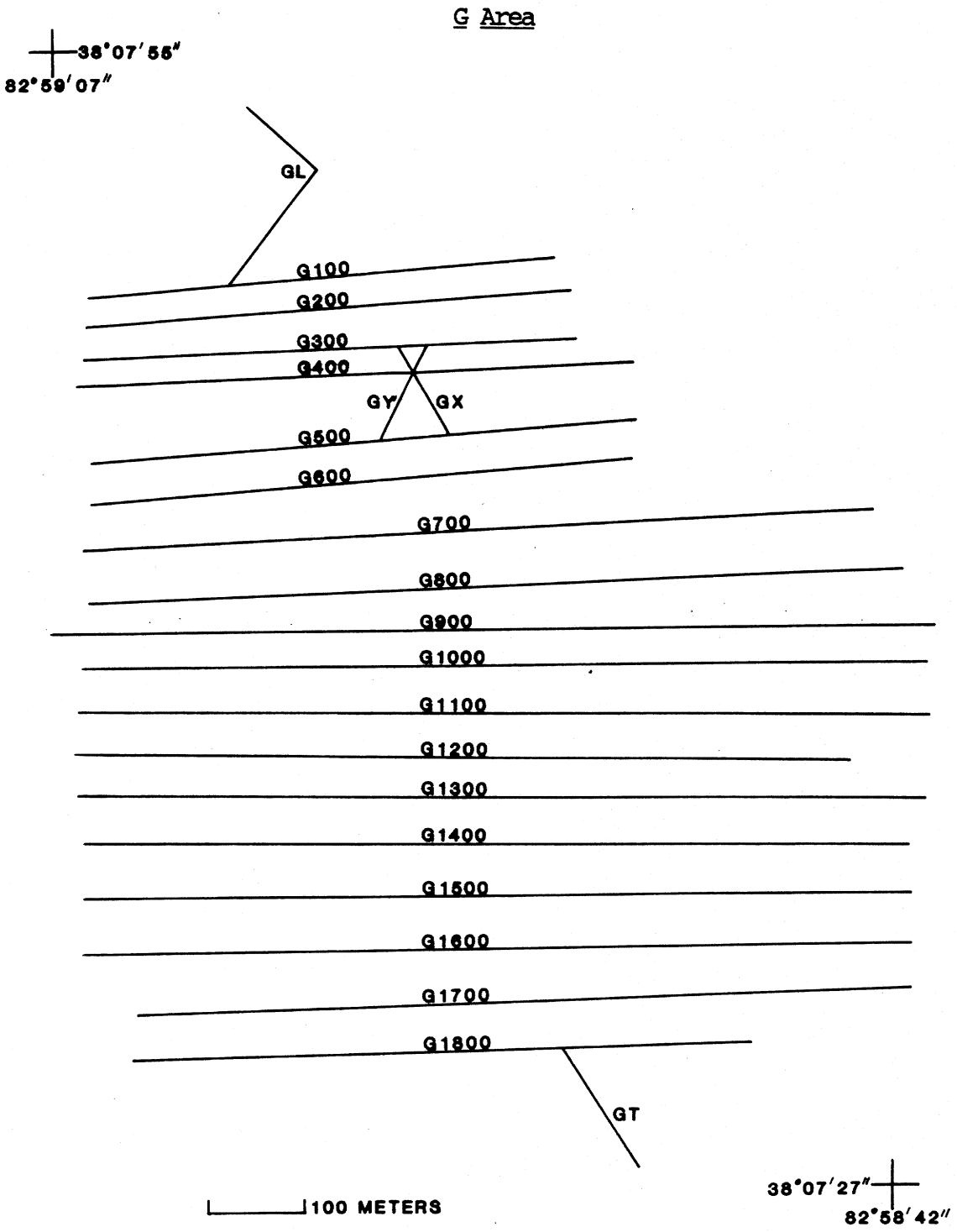
G Area
38°07′55″
82°59′07″
GL
G100
G200
G300
G400
GY
GX
G500
G600
G700
G800
G900
G1000
G1100
G1200
G1300
G1400
G1500
G1600
G1700
G1800
GT
100 METERS
38°07′27″
82°58′42″

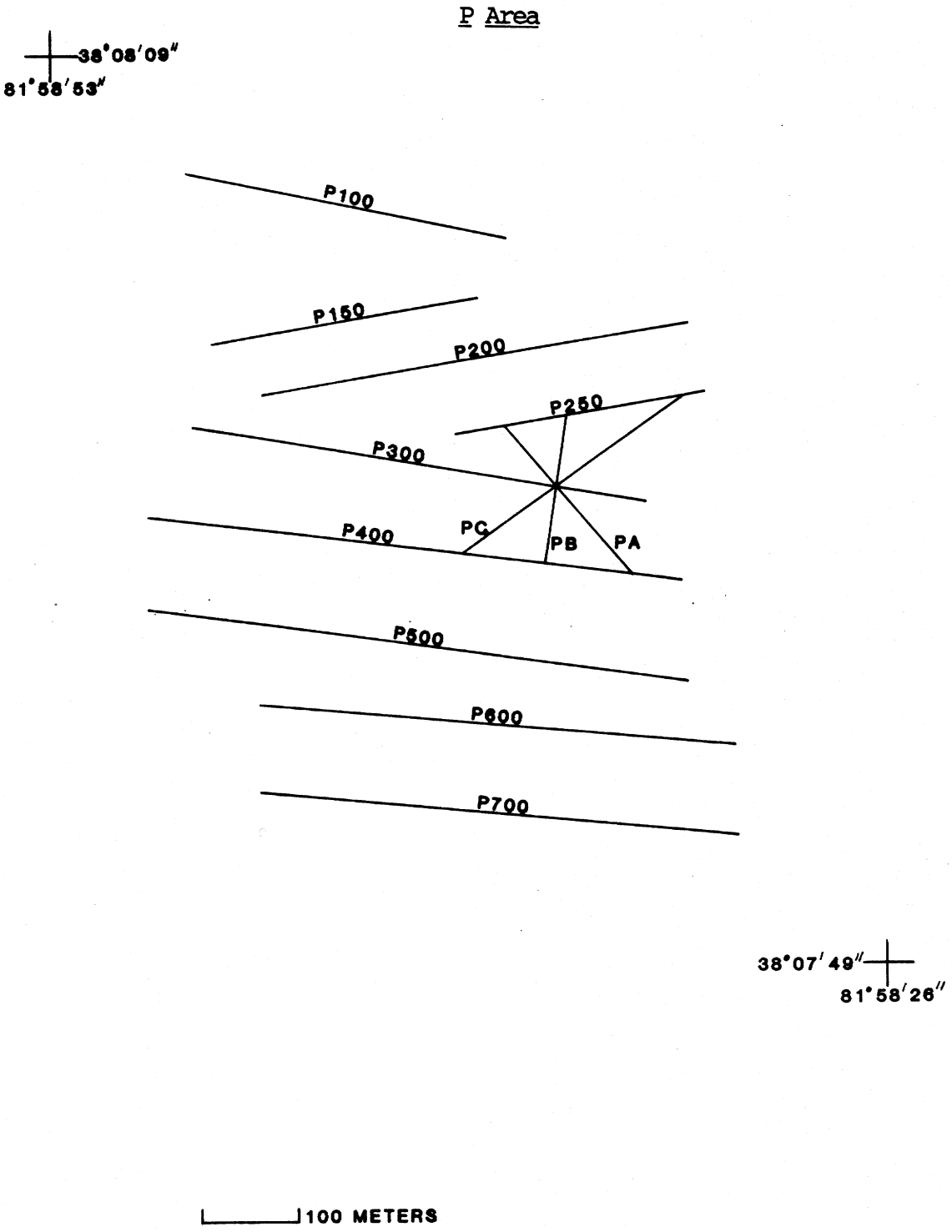
P Area
38°08′09″
81°58′53″
P100
P150
P200
P250
P300
P400
PC
PB
PA
P500
P600
P700
38°07′49″
81°58′26″
100 METERS

APPENDIX B: COMPUTER PROGRAMS USED IN STUDY

```
C     DIURNAL CORRECTIONS PROGRAM
C
C     THIS PROGRAM TAKES A LINE OF RAW MAGNETIC FIELD DATA, MAKES
C     THE DIURNAL CORRECTIONS ON IT, AND LISTS THE DATA BY STATION
C     NO., TIME DATA WAS TAKEN IN MILITARY TIME AND DECIMAL
C     SECONDS, THE RAW MAGNETIC READING (MAGRG), THE FRACTIONAL
C     DAY FROM THE BEGINNING OF THE SURVEY (DAY***), THE SPACING
C     FROM THE LAST DATA STATION (SPA), THE TOTAL DISTANCE ALONG
C     THE LINE AT THE PRESENT DATA STATION (T.D.), AND THE
C     MAGNETIC READING CORRECTED FOR DIURNAL VARIATION (DIURN).
C
      CHARACTER*8, END, LINE, DATE
      REAL STATN(99),HOUR(99),MIN(99),DAY(99),DIURN(99),T1,T2,DEC
      INTEGER MAGRG(99), SPA(99), TD(99), M1, M2, TUNE
      READ(88,10) M1,T1,M2,T2,TUNE,END,LINE,DATE,DEC
10    FORMAT(1X,T2,I5,T8,F3.2,T12,I5,T18,F3.2,T22,I5,T28,A8,T37,A5,
     1 T43,A8,T52,F4.0)
      WRITE(5,*) ' LINE ', LINE
      WRITE(5,*) ' ',DATE,' (=DAY ',DEC,') '
      WRITE(5,*) ' BASE CHECKS'
      WRITE(5,*) ' M1=', M1, ' T1=', T1
      WRITE(5,*) ' M2=', M2, ' T2=', T2
      WRITE(5,*) ' TUNE=', TUNE
      WRITE(5,*) ' THIS LINE BEGINS AT ', END
      WRITE(5,20) 'STATION','HOUR','MIN',MAGRG',DAY***','SPAC',
     1 'T.D.','DIURN'
20    FORMAT(' ',T2,A,T10,A,T15,A,T19,A,T25,A,T32,A,T37,A,T43,A)
C     READ LOOP IS CONTROLLED BY END OF FILE
      N=0
      DO 30, K=1,99
      READ(88,50,END=40) STATN(K),HOUR(K),MIN(K),MAGRG(K),DAY(K),
     1 SPA(K)
      N=N+1
30    CONTINUE
40    CONTINUE
      TD(1)=0
      DO 70,K=1,N
50    FORMAT(1X,T2,F7.2,T10,F4.1,T15,F3.2,T19,I5,T25,I4)
      MIN(K)=MIN(K)/.60
      DAY(K)=DEC+(HOUR(K)+MIN(K))/24.00
      DIURN(K)=MAGRG(K)+(TUNE-M1)+(((DAY(K)-DEC)-T1)/(T2-T1))*
     1 (M1-M2)+.5
      IF (K .GT. 1) TD(K)=TD(K-1)+SPA(K)
      WRITE(5,60) STATN(K),HOUR(K),MIN(K),MAGRG(K),DAY(K),SPA(K),
     1 TD(K),DIURN(K)
```

```
60    FORMAT('',T2,F7.2,T10,F4.1,T15,F3.2,T19,I5,T25,F6.2,
     1 T32,I4,T37,I5,T43,F6.0)
70    CONTINUE
      END
```

INPUT:

```
 55876 .52 55905 .68 55884 EAST END K 700 01/06/83 041.
 0700.01 13.0 .02 55962 0000
 0700.02 13.0 .07 55977 0159
 0700.03 13.0 .12 55974 0159
 0700.04 13.0 .18 56028 0318
 0700.05 13.0 .27 56029 0318
 0700.06 13.0 .32 56056 0318
 0700.07 13.0 .38 55997 0159
```

OUTPUT:

```
   LINE K 700
   1/06/83 (=DAY     41.00000)
   BASE CHECKS
   M1=       55876 T1=        0.5200000
   M2=       55905 T2=        0.6800000
   TUNE=       55884
   THIS LINE BEGINS AT EAST END
 STATION HOUR MIN MAGRG DAY*** SPA T.D. DIURN
 0700.01 13.0 .02 55962  41.54   0    0 55966
 0700.02 13.0 .07 55977  41.54 159  159 55981
 0700.03 13.0 .12 55974  41.55 159  318 55978
 0700.04 13.0 .18 56028  41.55 318  636 56031
 0700.05 13.0 .27 56029  41.55 318  954 56032
 0700.06 13.0 .32 56056  41.55 318 1272 56058
 0700.07 13.0 .38 55997  41.55 159 1431 55999
```

```
C     REGIONAL GRADIENTS REDUCTIONS PROGRAM
C
C     THIS PROGRAM SUBTRACTS OUT THE REGIONAL GRADIENT
C     IDENTIFIED FROM THE TOTAL MAGNETIC INTENSITY MAP,
C     AND REDEFINES ALL TOTAL INTENSITY MAGNETIC VALUES AS
C     EITHER A POSITIVE OR NEGATIVE VALUE RELATIVE TO A
C     COMMON BASE (THE BASE VALUE IS 55700 GAMMAS IN THIS
C     PROGRAM).
C
      INTEGER X(300), Y(300), MAGRG(300), RES(300), RG(300)
      WRITE(5,20) ' X=', ' Y=', ' MAGRG=', ' RG=', ' RES='
20    FORMAT(' ',T2,A,T7,A,T12,A,T20,A,T26,A)
C     READ LOOP IS CONTROLLED BY END OF FILE
      N=0
      DO 30, K=1,300
      READ(99,40,END=50) X(K), Y(K), MAGRG(K)
      N=N+1
30    CONTINUE
50    CONTINUE
      DO 70, K=1,N
      RG(K)=(9.1*(1200.00-X(K)))/25.00
      RES(K)=MAGRG(K)-RG(K)-55700
40    FORMAT(1X,T2,I3,T6,I3,T10,I5)
      WRITE(5,60) X(K), Y(K), MAGRG(K), RG(K), RES(K)
60    FORMAT(' ',T2,I3,T7,I3,T13,I5,T21,I3,T27,I4)
70    CONTINUE
      END
```

INPUT:

```
 334 574 56047
 346 579 56018
 369 589 56033
```

OUTPUT:

```
 X=   Y=   MAGRG=  RG=   RES=
 334  574  56047   315   32
 346  579  56018   311   7
 369  598  56033   302   31
```

All of the data refinement, modelling, and graphics for this study were performed on a Digital Equipment Corporation VAX-11/780 computer.

Plate 1. Kimberlite breccia hand samples. Notice the abundance of xenoliths (lighter material).

Plate 2. Massive kimberlite outcrop. Tag in center of photo is 4 inches long.

Plate 11. Sluice box used for trenching in G3 area.

MAP 1: TOTAL MAGNETIC INTENSITY MAP

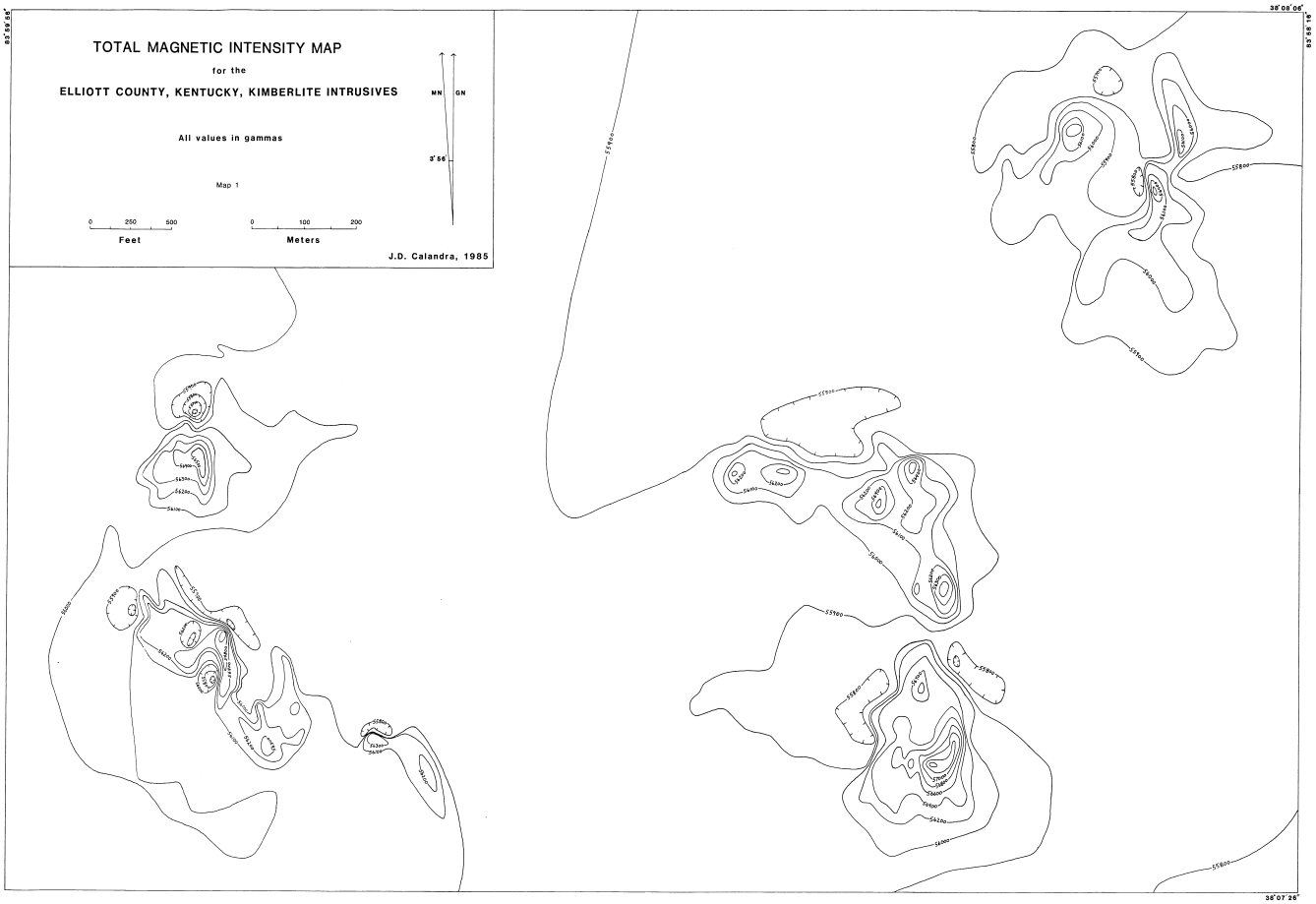

MAP 2: INDEX FOR ANOMALY MAPS AND DISTRIBUTION OF INTRUSIVE MODELS